USE OF REMOTE SENSING DATA FOR EVALUATING ELEVATION AND PLANT DISTRIBUTION IN A SOUTHEASTERN SALT MARSH

by

CHRISTINE MICHELLE HLADIK

(Under the Direction of Merryl Alber)

ABSTRACT

Salt marshes are valuable ecosystems that are susceptible to habitat loss due to changes in sea level and coastal flooding, and there is growing interest in obtaining accurate habitat and elevation maps for these areas. Remote sensing techniques such as Light Detection and Ranging (LIDAR) can produce digital elevation models (DEMs), but the accuracy of LIDAR in salt marshes is limited by a combination of sensor resolution, instrument errors, and poor laser penetration in dense vegetation. I assessed the accuracy of a LIDAR-derived DEM for the salt marshes surrounding Sapelo Island, GA using real time kinematic (RTK) GPS. These observations were used to develop and validate species-specific correction factors for ten marsh cover classes, which ranged from 0.03 to 0.25 m. In order to apply these corrections to the 13 km^2 study site, I classified hyperspectral imagery by cover class and combined this information with elevation in a decision tree. This produced both an accurate habitat classification (nine salt marsh habitat classes were mapped with a 90% overall accuracy) and a corrected DEM (overall mean error was reduced from 0.10 ± 0.12 (SD) to -0.003 ± 0.10 m (SD) and root mean squared error at the 68% confidence level decreased from 0.15 to 0.10 m) when validated with ground truth data. Finally, I evaluated the use of remote sensing-derived variables (DEM elevation, slope, distance metrics) versus field collected edaphic variables (soil organic matter, water content, salinity, redox) to develop predictive models of plant distributions with both linear discriminant analysis (LDA) and classification and regression trees (CART). Models that used remote sensing variables had accuracies of 0.78 and 0.79, whereas those for edaphic models were 0.63 and 0.72 for LDA and CART, respectively. Accuracies improved only slightly in the best models which combined remote sensing variables and soil organic matter (to 0.82 and 0.83 for LDA and CART, respectively), suggesting that remote sensing-derived variables alone can be effective predictors of marsh vegetation. Taken together, these findings show the potential for appropriately analyzed remote sensing data for evaluating elevation and habitat in marshes.

INDEX WORDS: Remote sensing; LIDAR; digital elevation model (DEM); hyperspectral imagery; salt marsh; habitat mapping; linear discriminant analysis (LDA); classification and regression trees (CART); Sapelo Island; LTER

USE OF REMOTE SENSING DATA FOR EVALUATING ELEVATION AND PLANT DISTRIBUTION IN A SOUTHEASTERN SALT MARSH

by

CHRISTINE MICHELLE HLADIK

BS, Creighton University, 2002

MS, Creighton University, 2004

A Dissertation Submitted to the Graduate Faculty of The University of Georgia in Partial Fulfillment of the Requirements for the Degree

DOCTOR OF PHILOSOPHY

ATHENS, GEORGIA

2012

USE OF REMOTE SENSING DATA FOR EVALUATING ELEVATION AND

PLANT DISTRIBUTION IN A SOUTHEASTERN SALT MARSH

by

CHRISTINE MICHELLE HLADIK

Major Professor:	Merryl Alber
Committee:	Clark Alexander
	Marguerite Madden
	James Morris
	Steve Pennings

Electronic Version Approved:

Maureen Grasso
Dean of the Graduate School
The University of Georgia
August 2012

DEDICATION

To my parents, Robert and Margaret, who have always loved, supported and inspired me.

ACKNOWLEDGEMENTS

This dissertation would not have been possible without the assistance of numerous individuals. First, I want to thank my advisor, Merryl Alber, who offered invaluable guidance and support, and provided me with the opportunity to explore the captivating salt marshes of Sapelo Island. I would also like to thank my committee members for all of their helpful suggestions and encouragement. I want to thank the staff of the University of Georgia Marine Institute, the Georgia Coastal Ecosystems Long Term Ecological Research Project and the Sapelo Island National Estuarine Research Reserve, who helped me with field sampling, logistics and who made my time at Sapelo memorable. I am particularly indebted to Kristen Anstead, Caitlyn Conner, Nick Scoville and Jacob Shalack for their assistance in the field and laboratory. I would also like to thank my lab mates, Caroline McFarlin, Sylvia Schaefer and Natalie McLenaghan who have provided me not only with knowledge and advice, but laughter and much needed breaks from data analysis and writing. To my other Marine Sciences friends, Heather Reader, Marcia Hsu, Vanessa Varaljay and Leanne Powers, thank-you for being my family away from home. Many other people contributed help: John Schalles, Wade and Joan Sheldon, Sharon Barnhart and Dale Bishop. Finally and most importantly, I’d like to thank my family for their infinite love, support and encouragement- without them this dissertation would not have been possible. I love you Mom, Dad, Bob, Jen, Greg, Katelin, Jay, R.J., Cooper, Baby Hladik-Weiderholt, the Stewarts and the Hladiks.

TABLE OF CONTENTS

APPENDIX

LIST OF TABLES

Page

LIST OF FIGURES

Chapter 1

INTRODUCTION AND LITERATURE REVIEW

1. Background

Salt marshes are valuable ecosystems. Positioned at the interface between aquatic and upland habitats, they provide critical habitat for both aquatic and terrestrial organisms, are sites of chemical transformations and detoxification, and protect developed coastal areas from shoreline erosion and storms (Chapman, 1974; Mitsch and Gosselink, 2000). Because they are situated in low-lying, intertidal areas with shallow slopes, small topographic differences affect water flow, sediment distribution, and the extent and frequency of tidal inundation in salt marshes, which in turn affect plant distributions (Gesch, 2009; Sanders, 2007). There is therefore growing interest in obtaining accurate elevation and vegetation maps for these areas in order to understand how marshes are affected by anthropogenic and natural perturbations such as sea level rise, changes in freshwater and sediment delivery and human activities.

Salt marsh macrophytes exhibit characteristic patterns of vertical zonation (Chapman, 1974; Sanchez et al., 1996; Silvestri et al., 2005). Zonation is typically described in terms of elevation relative to the tidal frame, separating the marsh into low, mid and high marsh zones based on flooding frequency. In salt marshes of the Southeastern United States *Spartina alterniflora* is the dominant plant in the low marsh, with taller plants found closest to the water. The mid-marsh zone is also dominated by *S. alterniflora,* with *Salicornia virginica* (more recently reclassified as as *Sarcocornia* sp., USDA, 2010), *Batis maritima* and *Distichlis spicata*, collectively termed marsh meadow or salt meadow, occurring at higher elevations in this zone. In high marsh areas along the upland fringe, where the marsh is inundated only at the highest tides, *Juncus roemerianus* and *Borrichia frutescens* become the dominant species (Weigert and Freeman, 1990).

Marsh plant distribution along the gradient from low to high marsh is generally explained by the stress-to-competition hypothesis: different species perform best in different portions of the marsh, and are generally restricted at low elevations due to physiological tolerances and at high elevations by competition (Pennings and Callaway, 1992; Snow and Vince, 1984). Elevation is related to the extent and frequency of tidal inundation, which in turn affects a number of abiotic parameters, including soil salinity and moisture (Adam, 1990; Adams, 1963; Chapman, 1974; Engels and Jensen, 2009; Sanderson et al., 2001), nutrient availability (Mitsch and Gosselink, 2000), soil aeration (Chapman, 1974; Patterson and Mendelssohn, 1991; Ursino et al., 2004), organic matter content (Morris and Haskin, 1990) and soil redox potential (Mendelssohn and Morris, 2000; Pezeshki, 2001). As a result of the topographic influence on these variables, even slight changes in elevation can affect both the overall extent of marshes and the patterns of vegetation within them (Zedler et al., 1999). Thus, elevation is a useful metric for predicting plant spatial patterns (Silvestri et al., 2003; Zedler et al., 1999) and productivity (Mendelssohn and Morris, 2000; Morris et al., 2002) in marshes.

This dissertation is focused on describing both elevation and plant distributions in a Southeastern salt marsh near Sapelo Island, Georgia. The site is located in the Georgia Coastal Ecosystems Long Term Ecological Research domain and the Sapelo Island National Estuarine Research Reserve. I had access to both Light Detection and Ranging (LIDAR) and hyperspectral imagery (HSI) of this region, which are remote sensing techniques that can be used to provide information on elevation and plant composition, respectively. I used field-collected observations of plant composition, real time kinematic (RTK) GPS elevation and edaphic conditions to process, classify and validate this imagery and to explore the potential for using remote sensing-derived variables to predict plant distributions. Below I provide an overview of remote sensing in salt marshes and the different analytical approaches utilized in this dissertation, and introduce my major objectives.

2. Remote sensing of salt marsh vegetation

2.1. LIDAR

Remote sensing is an ideal tool for studying salt marsh environments as it provides coverage for large areas that are often inaccessible. Over the past decade, many studies in forested ecosystems have used LIDAR to obtain information about ground elevation and vegetation structure (Brock and Purkis, 2009; Lefsky et al., 2002; MacMillan et al., 2003). LIDAR is a remote sensing technology that measures the distance between the sensor and a target surface by determining the time elapsed between the emission of a laser pulse and the arrival of the reflection of that pulse at the sensor's receiver (Wehr and Lohr, 1999). LIDAR can quickly collect dense point clouds of discrete point data with X, Y and Z coordinates over large areas, and can be used to describe surface topography and vertical structure of all features above the ground surface. LIDAR has been successfully used as an aid for mapping both vegetation and ground elevation in forest ecosystems where there is a large distance between the ground and canopy layers (Lefsky et al., 2002; Ritchie, 1996). LIDAR data is often filtered to produce a first surface or Digital Surface Model (DSM) (interpolated from the first return) and a bare earth digital elevation model (DEM) from the last return with vegetation and man-made features removed.

LIDAR has been used with mixed success in salt marsh environments, as it tends to overestimate marsh ground elevations and has required a correction factor (Montane and Torres, 2006; Rosso et al., 2006). Numerous investigators have found that LIDAR was unable to penetrate the dense marsh vegetation canopy and that accuracies vary for different species, making the calculation of vegetation height difficult (Rosso et al., 2006; Sadro et al., 2007). Moreover, the same studies found LIDAR errors increase as vegetation density and heights increase and are species-specific. The LIDAR systems used in these studies recorded only 2 returns (the first return is reflected from the top of the canopy, while the last return is from the ground) and had low pulse rates frequencies (PRF) of 16 kHz-30 kHz. PRF is the number of emitted pulses per second and is one of the LIDAR system parameters that determines the laser point density. As PRF increases, point density increases, thereby increasing the probability that a laser pulse will intercept a canopy gap and reach the ground. LIDAR-derived DEM errors could be reduced by increasing the LIDAR point density and PRF. A new generation of LIDAR systems has PRF of up to 167 kHz, making accurate measurements of ground elevations and vegetation height promising.

2.2. Hyperspectral Imagery

Although LIDAR can measure surface elevations and can be used to indicate different size categories of vegetation, it is unable to identify species. LIDAR only receives spectral information at one wavelength in the near infrared (NIR) and is therefore unable to sense pigment absorbance and reflectance properties of plants that occur in the visible portion of the electromagnetic spectrum. Therefore, to provide information on species composition LIDAR must be used in combination with visible wavelengths (Campbell, 2006). HSI in the visible and NIR portion of the electromagnetic spectrum has been shown to be suitable for the separation of marsh vegetation species by spectral signatures (Artigas and Yang, 2005; Schmidt and Skidmore, 2003). Hyperspectral sensors are ideal for this as they are able to collect a high number of continuous spectral bands (sometimes greater than 200 bands) with narrow bandwidths and at a fine spatial resolution. The increased dimensionality of hyperspectral data allows for better species differentiation based on subtle differences in leaf structure and pigment composition (Hardisky et al., 1986; Schmidt and Skidmore, 2003), when compared to multispectral imagery with only 3 to 7 spectral bands. HSI has been used extensively in salt marshes to map vegetation patterns (Belluco et al., 2006; Silvestri et al., 2003; Wang et al., 2007), monitor invasive species (Gilmore et al., 2008; Hirano et al., 2003; Rosso et al., 2006), document erosion and vegetation succession (Thomson et al., 2004), measure biomass and species abundance (Lucas and Carter, 2008; Wang et al., 2007) and detect vegetation change (Klemas, 2011), among other applications.

Two of the most commonly used pixel level HSI classification algorithms for vegetation mapping are the maximum likelihood classifier (MLC) and the spectral angle mapper classifier (SAM). MLC is a parametric classifier that assumes that the spectral band for each class is normally distributed and calculates the probability that a given pixel belongs to a specific class based on variance and covariance measures (Hoffbeck, 1995). SAM is a classification algorithm designed specifically for HSI. SAM measures the spectral similarity between each unknown pixel and endmember (training class) spectra by calculating the angle between the spectra, treating the spectra as vectors in n-dimensional space, with n equal to the number of image bands (Kruse et al., 1993). Overall, MLC has tended to perform better than SAM in salt marshes (Belluco et al., 2006; Hunter and Power, 2002), but SAM has been successfully applied in some studies (Marani et al., 2006; Marani et al., 2003; Sadro et al., 2007) and, therefore, both are evaluated here.

There are challenges to using HSI in salt marshes, particularly with respect to accurately classifying *S. alterniflora* of varying heights. First, there is persistent confusion within and between similar species. The different height classes of *S. alterniflora* (short, medium and tall), are commonly confused in HSI classification due to their spectral similarity in both the visible and NIR portions of the spectrum (Artigas and Yang, 2005; Schmidt and Skidmore, 2003). The spectral signature in the visible is largely controlled by pigment composition, which is the same for all *S. alterniflora* plants, and reflectance in the NIR is a function of air space configuration inside the leaf, which is genetically determined and invariant among the different height classes (Danson et al., 1992). Spectral confusion between classes of closely related species has been found in previous studies. Using HSI, Artigas and Yang (2005) were unable to separate *S. alterniflora* from *Spartina patens* in the visible and NIR in the New Jersey Meadowlands. Another source of error in HSI classifications results from mixed pixels that include more than one type of vegetation and/or mud. Both of these types of mixed pixels are observed with *S. alterniflora*: the different height classes represent a continuum and can therefore be found adjacent to one another, and *S. alterniflora's* erect structure and often sparse stem densities means that mud is spectrally mixed with vegetation

(Belluco et al., 2006; Silvestri et al., 2003; Thomson et al., 2003). Silvestri et al. (2003) found that *S. maritima* is often misclassified because it is found in low-lying areas where mud and water interfere with its spectral signature. Thomson et al. (2003) hypothesized that microphytobenthos on mud may also cause mud to resemble *Spartina* spectrally.

2.3. Data Fusion

One way to potentially overcome the individual limitations of LIDAR-derived DEMs and HSI, and to potentially address the difficulties associated with classifying *S. alterniflora*, is through data fusion. Data fusion combines data from different sources to obtain more information than could be derived from either independently (Pohl and van Genderen, 1998). It can be done at the pixel, feature or decision level. Pixel level fusion is the combination of raw data from multiple sources into a single image. At the pixel level, LIDAR-derived DEMs have been included as a component band with HSI to classify coastal habitats, resulting in improved classification accuracies (Chust et al., 2008; Collin et al., 2010). Feature level fusion requires the extraction of different features from the source data before features are merged together so that fusion takes place on features that match some selection criteria. At the feature level, LIDAR-derived DEMs have been used as data layers in object orientated classifications of marsh habitats (Brennan and Webster, 2006; Gilmore et al., 2008). Decision level fusion combines the independent results from multiple sources in a GIS to produce a final fused decision (Pohl and van Genderen, 1998). LIDAR-derived DEMs have been fused with land cover classifications post hoc to refine and improve classification products (Lu and Weng, 2007; Pal and Mather, 2003), to extract marsh species elevation ranges and distributions (Morris et al., 2005; Sadro et al., 2007), monitor the spread of invasive species (Rosso et al., 2006), model species habitat (Moeslund et al., 2011; Sellars and Jolls, 2007), and predict sea level rise impacts (Webster et al., 2006). The above studies have all used image fusion for classification purposes or for extracting additional elevation information. However, none have used elevation data to modify their existing classification of salt marshes or used an existing classification map to correct DEM elevations at the decision level.

3. Predictions of salt marsh plant distributions

3.1. Edaphic versus remote-sensing derived variables

As described above, numerous edaphic variables can influence where plants are found, with soil salinity and flooding (Adam, 1990; Pennings and Bertness, 2001; Pennings et al., 2005) being two of the most important. Since patterns of tidal inundation are the result of location in the marsh and topographical variations, elevation and distance metrics have both been used as proxies for inundation frequency and duration (Adams, 1963; Deleeuw et al., 1991; Earle and Kershaw, 1989). Elevation and distance to mean high water (MHW) are both related to flooding frequency and duration, and have been shown to influence species zonation patterns (Earle and Kershaw, 1989; Silvestri et al., 2005; Zedler et al., 1999), productivity (Mendelssohn and Morris, 2000; Morris et al., 2002) and sedimentation rates (Marion et al., 2009; Wijen et al., 2001) in salt marshes. However, simple correlations of elevation and/or distance metrics alone have been unable to fully explain zonation (Bockelmann et al., 2002; Silvestri et al., 2005; Zedler et al., 1999). A major advantage of using information on elevation and tidal inundation to predict plant distributions is that data can be collected synoptically at the landscape level via remote sensing.

3.2. Multivariate analytical approaches

Most previous studies of salt marsh plant distribution have used multivariate statistical approaches such as canonical correspondence analysis (CCA), which determines which linear combinations of multiple environmental variables best separate vegetation along environmental gradients (Ter Braak, 1987). CCA has been used in Northwestern Atlantic and Mediterranean Sea salt marshes (Batriu et al., 2011; Cacador et al., 2007; Rogel et al., 2000; Rogel et al., 2001) and in North Sea marshes (Engels and Jensen, 2009; Suchrow and Jensen, 2010). These studies have explained 23-95% of the variance in species percent cover based on edaphic variables. Although CCA can be used to better understand species relationships along ecological gradients, the technique cannot classify vegetation type or predict group membership of new datasets.

To classify and predict plant distributions, discriminant analysis is a commonly used parametric approach. Linear and quadratic discriminant analysis (LDA and QDA, respectively) use a priori knowledge of existing class membership to separate groups based on the linear or quadratic combination of predictor variables. Even though ecological data do not necessarily have a linear response along ecological gradients (Suchrow and Jensen, 2010), LDA has been applied in salt marshes with classification accuracies ranging from 57-70% to predict vegetation zonation in Southwestern Atlantic marshes (Isacch et al., 2006; Sanchez et al., 1998) and Southeastern U.S. salt marshes (Woerner and Hackney, 1997).

A nonparametric approach increasingly used as an alternative to discriminant analysis for the description and prediction of plant patterns using environmental data are classification and regression trees (CART). Tree based classification methods are valuable data exploration tools that provide straightforward visualization of the data structure through binary classification (categorical) or regression (continuous) trees. CART has numerous advantages: data do not need to be normally distributed or transformed, homogeneity of covariances is not assumed, missing data and combinations of categorical and continuous variables are permitted, it captures hierarchical and non-linear relationships as well as interactions between explanatory variables and is robust to outliers (Breiman et al., 1984; De'ath and Fabricius, 2000). In salt marshes, CART has been applied with accuracies that ranged from 54% to 90% to differentiate vegetation in relation to changes in upland sedimentation (Byrd and Kelly, 2006) and for invasive species habitat modeling (Andrew and Ustin, 2009). CART has been used to separate salt marsh vegetation based on landscape position (Dale et al., 2007) and edaphic variables (Lang et al., 2010).

CART can also be a valuable tool for data exploration and variable selection by reducing the number of explanatory variables before training a parametric classifier such as LDA, as linear models can become less effective as the complexity of the data increase (Breiman et al., 1984; De'ath and Fabricius, 2000; Maindonald and Braun, 2007); however, I was unable find any examples of this suggested workflow. Additionally, there are few comparative studies in which two classification methods are applied to the same data set. Although the utility of CART has been compared to linear models in other ecosystems (De'ath and Fabricius, 2000; Guisan and Zimmermann, 2000; Pino-Mejias et al., 2010; Vayssieres et al., 2000), no such assessment has been carried out for the classification of salt marsh vegetation using CART and LDA with the same data set.

4. Overview of Dissertation

The goal of this dissertation was to evaluate tools used to describe both elevation and plant distributions in salt marshes using remote sensing data. In Chapter 2, I evaluated high PRF LIDAR data with RTK elevations in order to test its accuracy for different vegetation classes. In Chapter 3, I developed an approach to fuse HSI of the salt marshes with the LIDAR-derived DEM to modify both habitat classification and elevation information and produced a high accuracy habitat map and corrected DEM of the study site. In Chapter 4, I compared the use of edaphic and remote sensing derived variables for the prediction of salt marsh plant distributions to determine which variables produce the most accurate classifications, and compared the use of discriminant analysis and CART to determine which classification technique is best suited for salt marsh data.

5. References

Adam, P. (1990). *Saltmarsh ecology*. Cambridge, UK: Cambridge University Press.

Adams, D.A. (1963). Factors Influencing Vascular Plant Zonation in North-Carolina Salt Marshes. *Ecology, 44*, 445-456.

Andrew, M.E., & Ustin, S.L. (2009). Habitat suitability modelling of an invasive plant with advanced remote sensing data. *Diversity and Distributions, 15*, 627-640.

Artigas, F.J., & Yang, J.S. (2005). Hyperspectral remote sensing of marsh species and plant vigour gradient in the New Jersey Meadowlands. *International Journal of Remote Sensing, 26*, 5209-5220.

Batriu, E., Pino, J., Rovira, P., & Ninot, J.M. (2011). Environmental control of plant species abundance in a microtidal Mediterranean saltmarsh. *Applied Vegetation Science, 14*, 358-366.

Belluco, E., Camuffo, M., Ferrari, S., Modenese, L., Silvestri, S., Marani, A., & Marani, M. (2006). Mapping salt-marsh vegetation by multispectral and hyperspectral remote sensing. *Remote Sensing of Environment, 105*, 54-67.

Bockelmann, A.C., Bakker, J.P., Neuhaus, R., & Lage, J. (2002). The relation between vegetation zonation, elevation and inundation frequency in a Wadden Sea salt marsh. *Aquatic Botany, 73*, 211-221.

Breiman, L., Feidman, J., Olshen, R., & Stone, C. (1984). *Classification and Regression Trees*. Belmont, CA: Wadsworth, Inc.

Brennan, R., & Webster, T.L. (2006). Object-oriented land cover classification of lidar-derived surfaces. *Canadian Journal of Remote Sensing, 32*, 162-172.

Brock, J.C., & Purkis, S.J. (2009). The Emerging Role of Lidar Remote Sensing in Coastal Research and Resource Management. *Journal of Coastal Research, 25*, 1-5.

Byrd, K.B., & Kelly, M. (2006). Salt marsh vegetation response to edaphic and topographic changes from upland sedimentation in a pacific estuary. *Wetlands, 26*, 813-829.

Cacador, I., Tiberio, S., & Cabral, H.N. (2007). Species zonation in Corroios salt marsh in the Tagus esturary (Portugal) and its dynamics in the past fifty years. *Hydrobiologia, 587*, 205-211.

Campbell, J.B. (2006). *Introduction to Remote Sensing, 4th Edition*. New York: The Guilford Press.

Chapman, V.J. (1974). *Salt marshes and salt deserts of the world*. Lehre, Germany: J. Cramer.

Chust, G., Galparsoro, I., Borja, A., Franco, J., & Uriarte, A. (2008). Coastal and estuarine habitat mapping, using LIDAR height and intensity and multi-spectral imagery. *Estuarine Coastal and Shelf Science, 78*, 633-643.

Collin, A., Long, B., & Archambault, P. (2010). Salt-marsh characterization, zonation assessment and mapping through a dual-wavelength LiDAR. *Remote Sensing of Environment, 114*, 520-530.

Dale, M.B., Dale, P.E.R., & Tan, P. (2007). Supervised clustering using decision trees and decision graphs: An ecological comparison. *Ecological Modelling, 204*, 70-78.

Danson, F.M., Steven, M.D., Malthus, T.J., & Clark, J.A. (1992). High-Spectral Resolution Data for Determining Leaf Water-Content. *International Journal of Remote Sensing, 13*, 461-470.

De'ath, G., & Fabricius, K.E. (2000). Classification and regression trees: A powerful yet simple technique for ecological data analysis. *Ecology, 81*, 3178-3192.

Deleeuw, J., Vandendool, A., Demunck, W., Nieuwenhuize, J., & Beeftink, W.G. (1991). Factors Influencing the Soil-Salinity Regime Along an Intertidal Gradient. *Estuarine Coastal and Shelf Science, 32*, 87-97.

Earle, J.C., & Kershaw, K.A. (1989). Vegetation patterns in James Bay (Canada) coastal marshes: III. Salinity and elevation as factors influencing plant zonations. *Canadian journal of Botany, 67*, 2967-2974.

Engels, J.G., & Jensen, K. (2009). Patterns of wetland plant diversity along estuarine stress gradients of the Elbe (Germany) and Connecticut (USA) Rivers. *Plant Ecology & Diversity, 2*, 301-311.

Gesch, D.B. (2009). Analysis of Lidar Elevation Data for Improved Identification and Delineation of Lands Vulnerable to Sea-Level Rise. *Journal of Coastal Research, 25*, 49-58.

Gilmore, M.S., Wilson, E.H., Barrett, N., Civco, D.L., Prisloe, S., Hurd, J.D., & Chadwick, C. (2008). Integrating multi-temporal spectral and structural information to map wetland vegetation in a lower Connecticut River tidal marsh. *Remote Sensing of Environment, 112*, 4048-4060.

Guisan, A., & Zimmermann, N.E. (2000). Predictive habitat distribution models in ecology. *Ecological Modelling, 135*, 147-186.

Hardisky, M.A., Gross, M.F., & Klemas, V. (1986). Remote-Sensing of Coastal Wetlands. *Bioscience, 36*, 453-460.

Hirano, A., Madden, M., Welch, R. (2003). Hyperspectral image data for mapping wetland vegetation, *Wetlands*, 23, 436-448.

Hoffbeck, J.P. (1995). Classification of high dimensional multispectral data. In. West Lafayette, Indiana: Purdue University.

Hunter, E.L., & Power, C.H. (2002). An assessment of two classification methods for mapping Thames Estuary intertidal habitats using CASI data. *International Journal of Remote Sensing, 23*, 2989-3008.

Isacch, J.P., Costa, C.S.B., Rodriguez-Gallego, L., Conde, D., Escapa, M., Gagliardini, D.A., & Iribarne, O.O. (2006). Distribution of saltmarsh plant communities associated with environmental factors along a latitudinal gradient on the south-west Atlantic coast. *Journal of Biogeography, 33*, 888-900.

Klemas, V. (2011). Remote Sensing of Wetlands: Case Studies Comparing Practical Techniques. *Journal of Coastal Research, 27*, 418-427.

Kruse, F.A., Lefkoff, A.B., Boardman, J.W., Heidebrecht, K.B., Shapiro, A.T., Barloon, P.J., & Goetz, A.F.H. (1993). The Spectral Image-Processing System (Sips) - Interactive Visualization and Analysis of Imaging Spectrometer Data. *Remote Sensing of Environment, 44*, 145-163.

Lang, F., von der Lippe, M., Schimpel, S., Scozzafava-Jaeger, T., & Straub, W. (2010). Topsoil morphology indicates bio-effective redox conditions in Venice salt marshes. *Estuarine Coastal and Shelf Science, 87*, 11-20.

Lefsky, M.A., Cohen, W.B., Parker, G.G., & Harding, D.J. (2002). Lidar remote sensing for ecosystem studies. *Bioscience, 52*, 19-30.

Lu, D., & Weng, Q. (2007). A survey of image classification methods and techniques for improving classification performance. *International Journal of Remote Sensing, 28*, 823-870.

Lucas, K.L., & Carter, G.A. (2008). The use of hyperspectral remote sensing to assess vascular plant species richness on Horn Island, Mississippi. *Remote Sensing of Environment, 112*, 3908-3915.

MacMillan, R.A., Martin, T.C., Earle, T.J., & McNabb, D.H. (2003). Automated analysis and classification of landforms using high-resolution digital elevation data: applications and issues. *Canadian Journal of Remote Sensing, 29*, 592-606.

Maindonald, J.H., & Braun, J. (2007). *Data analysis and graphics using R : an example-based approach*. Cambridge ; New York: Cambridge University Press.

Marani, M., Belluco, E., Ferrari, S., Silvestri, S., D'Alpaos, A., Lanzoni, S., Feola, A., & Rinaldo, A. (2006). Analysis, synthesis and modelling of high-resolution observations of salt-marsh eco-geomorphological patterns in the Venice lagoon. *Estuarine Coastal and Shelf Science, 69*, 414-426.

Marani, M., Silvestri, S., Belluco, E., Camuffo, M., DAlpaos, A., Defina, A., Lanzoni, S., Marani, A., Tortato, M., & Rinaldo, A. (2003). Patterns in tidal environments: salt-marsh channel networks and vegetation. In, *Proceedings of the IEEE International Geoscience and Remote Sensing Symposium*. Toulouse, France

Marion, C., Anthony, E.J., & Trentesaux, A. (2009). Short-term (<= 2 yrs) estuarine mudflat and saltmarsh sedimentation: High-resolution data from ultrasonic altimetery, rod surface-elevation table, and filter traps. *Estuarine Coastal and Shelf Science, 83*, 475-484.

Mendelssohn, I.A., & Morris, J.T. (2000). Eco-physiological controls on the productivity of Spartina Alterniflora Loisel In D.A. Kreeger (Ed.), *Concepts and Controversies in Tidal Marsh Ecology* (pp. 59-80). Dordrecht Kluwer Academic.

Mitsch, W.J., & Gosselink, J.G. (2000). *Wetlands*. New York: John Wiley.

Moeslund, J.E., Arge, L., Bocher, P.K., Nygaard, B., & Svenning, J.C. (2011). Geographically Comprehensive Assessment of Salt-Meadow Vegetation-Elevation Relations Using LiDAR. *Wetlands, 31*, 471-482.

Montane, J.M., & Torres, R. (2006). Accuracy assessment of lidar saltmarsh topographic data using RTK GPS. *Photogrammetric Engineering and Remote Sensing, 72*, 961-967.

Morris, J.T., & Haskin, B. (1990). A 5-Yr Record of Aerial Primary Production and Stand Characteristics of Spartina-Alterniflora. *Ecology, 71*, 2209-2217.

Morris, J.T., Porter, D., Neet, M., Noble, P.A., Schmidt, L., Lapine, L.A., & Jensen, J.R. (2005). Integrating LIDAR elevation data, multi-spectral imagery and neural network modelling for marsh characterization. *International Journal of Remote Sensing, 26*, 5221-5234.

Morris, J.T., Sundareshwar, P.V., Nietch, C.T., Kjerfve, B., & Cahoon, D.R. (2002). Responses of coastal wetlands to rising sea level. *Ecology, 83*, 2869-2877.

Pal, M., & Mather, P.M. (2003). An assessment of the effectiveness of decision tree methods for land cover classification. *Remote Sensing of Environment, 86*, 554-565.

Patterson, C.S., & Mendelssohn, I.A. (1991). A Comparison of Physicochemical Variables across Plant Zones in a Mangal Salt-Marsh Community in Louisiana. *Wetlands, 11*, 139-161.

Pennings, S.C., & Bertness, M.D. (2001). Salt marsh communities. In M.D. Bertness, S.D. Gaines & M.E. Hay (Eds.), *Marine Community ecology* (p. 550). Sunderland, MA: Sinauer Associates, Inc.

Pennings, S.C., & Callaway, R.M. (1992). Salt-Marsh Plant Zonation - the Relative Importance of Competition and Physical Factors. *Ecology, 73*, 681-690.

Pennings, S.C., Grant, M.B., & Bertness, M.D. (2005). Plant zonation in low-latitude salt marshes: disentangling the roles of flooding, salinity and competition. *Journal of Ecology, 93*, 159-167.

Pezeshki, S.R. (2001). Wetland plant responses to soil flooding. *Environmental and Experimental Botany, 46*, 299-312.

Pino-Mejias, R., Cubiles-de-la-Vega, M.D., Anaya-Romero, M., Pascual-Acosta, A., Jordan-Lopez, A., & Bellinfante-Crocci, N. (2010). Predicting the potential habitat of oaks with data mining models and the R system. *Environmental Modelling & Software, 25*, 826-836.

Pohl, C., & van Genderen, J.L. (1998). Multisensor image fusion in remote sensing: concepts, methods and applications. *International Journal of Remote Sensing, 19*, 823-854.

Ritchie, J.C. (1996). Remote sensing applications to hydrology: Airborne laser altimeters. *Hydrological Sciences Journal-Journal Des Sciences Hydrologiques, 41*, 625-636.

Rogel, J.A., Ariza, F.A., & Silla, R.O. (2000). Soil salinity and moisture gradients and plant zonation in Mediterranean salt marshes of southeast Spain. *Wetlands, 20,* 357-372.

Rogel, J.A., Silla, R.O., & Ariza, F.A. (2001). Edaphic characterization and soil ionic composition influencing plant zonation in a semiarid Mediterranean salt marsh. *Geoderma, 99*, 81-98.

Rosso, P.H., Ustin, S.L., & Hastings, A. (2006). Use of lidar to study changes associated with Spartina invasion in San Francisco Bay marshes. *Remote Sensing of Environment, 100*, 295-306.

Sadro, S., Gastil-Buhl, M., & Melack, J. (2007). Characterizing patterns of plant distribution in a southern California salt marsh using remotely sensed topographic and hyperspectral data and local tidal fluctuations. *Remote Sensing of Environment, 110,* 226-239.

Sanchez, J.M., Izco, J., & Medrano, M. (1996). Relationships between vegetation zonation and altitude in a salt-marsh system in northwest Spain. *Journal of Vegetation Science, 7*, 695-702.

Sanchez, J.M., Otero, X.L., & Izco, J. (1998). Relationships between vegetation and environmental characteristics in a saltmarsh system on the coast of Northwest Spain. *Plant Ecology, 136*, 1-8.

Sanders, B.F. (2007). Evaluation of on-line DEMs for flood inundation modeling. *Advances in Water Resources, 30*, 1831-1843.

Sanderson, E.W., Foin, T.C., & Ustin, S.L. (2001). A simple empirical model of salt marsh plant spatial distributions with respect to a tidal channel network. *Ecological Modelling, 139*, 293-307.

Schmidt, K.S., & Skidmore, A.K. (2003). Spectral discrimination of vegetation types in a coastal wetland. *Remote Sensing of Environment, 85*, 92-108.

Sellars, J.D., & Jolls, C.L. (2007). Habitat modeling for Amaranthus pumilus: An application of light detection and ranging (LIDAR) data. *Journal of Coastal Research, 23*, 1193-1202.

Silvestri, S., Defina, A., & Marani, M. (2005). Tidal regime, salinity and salt marsh plant zonation. *Estuarine Coastal and Shelf Science, 62*, 119-130.

Silvestri, S., Marani, M., & Marani, A. (2003). Hyperspectral remote sensing of salt marsh vegetation, morphology and soil topography. *Physics and Chemistry of the Earth, 28*, 15-25.

Snow, A.A., & Vince, S.W. (1984). Plant Zonation in an Alaskan Salt-Marsh .2. An Experimental-Study of the Role of Edaphic Conditions. *Journal of Ecology, 72*, 669-684.

Suchrow, S., & Jensen, K. (2010). Plant Species Responses to an Elevational Gradient in German North Sea Salt Marshes. *Wetlands, 30*, 735-746.

Ter Braak, C.J.F. (1987). The analysis of vegetation-environment relationships by canonical correspondence analysis. *Vegetatio, 69*, 69-77.

Thomson, A.G., Fuller, R.M., Yates, M.G., Brown, S.L., Cox, R., & Wadsworth, R.A. (2003). The use of airborne remote sensing for extensive mapping of intertidal sediments and saltmarshes in eastern England. *International Journal of Remote Sensing, 24*, 2717-2737.

Thomson, A.G., Huiskes, A., Cox, R., Wadsworth, R.A., & Boorman, L.A. (2004). Short-term vegetation succession and erosion identified by airborne remote sensing of Westerschelde salt marshes, The Netherlands. *International Journal of Remote Sensing, 25*, 4151-4176.

Ursino, N., Silvestri, S., & Marani, M. (2004). Subsurface flow and vegetation patterns in tidal environments. *Water Resources Research, 40*, 1-11.

USDA (2010). The PLANTS database. National Plant Data Center, Baton Rouge, Louisiana, USA. http://plants.usda.gov.

Vayssieres, M.P., Plant, R.E., & Allen-Diaz, B.H. (2000). Classification trees: An alternative non-parametric approach for predicting species distributions. *Journal of Vegetation Science, 11*, 679-694.

Wang, C., Menenti, M., Stoll, M.P., Belluco, E., & Marani, M. (2007). Mapping mixed vegetation communities in salt marshes using airborne spectral data. *Remote Sensing of Environment, 107*, 559-570.

Webster, T.L., Forbes, D.L., MacKinnon, E., & Roberts, D. (2006). Flood-risk mapping for storm-surge events and sea-level rise using lidar for southeast New Brunswick. *Canadian Journal of Remote Sensing, 32*, 194-211.

Wehr, A., & Lohr, U. (1999). Airborne laser scanning - an introduction and overview. *Isprs Journal of Photogrammetry and Remote Sensing, 54*, 68-82.

Weigert, R.G., & Freeman, B.J. (1990). Tidal Salt Marshes of the Southeast Atlantic Coast: a Community Profile In. Washington, DC: U.S. Department of the Interior, Fish and Wildlife Service.

Wijen, J.P.H., Nivard, M.J.V., & Vogel, E.W. (2001). Genetic damage by bifunctional agents in repair-active pre-meiotic stages of Drosophila males. *Mutation Research-Fundamental and Molecular Mechanisms of Mutagenesis, 478*, 107-117.

Woerner, L.S., & Hackney, C.T. (1997). Distribution of Juncus roemerianus in North Carolina tidal marshes: The importance of physical and biotic variables. *Wetlands, 17*, 284-291.

Zedler, J.B., Callaway, J.C., Desmond, J.S., Vivian-Smith, G., Williams, G.D., Sullivan, G., Brewster, A.E., & Bradshaw, B.K. (1999). Californian salt-marsh vegetation: An improved model of spatial pattern. *Ecosystems, 2*, 19-35.

CHAPTER 2

ACCURACY ASSESSMENT AND CORRECTION OF A LIDAR-DERIVED SALT MARSH DIGITAL ELEVATION MODEL[1]

[1] Hladik, C., & Alber, M. (2012). *Remote Sensing of Environment*, 121, 224-235. Reprinted here with permission of the publisher.

Abstract

Accurate habitat mapping in salt marshes is critical for both management and conservation goals. Information on marsh elevation is important to coastal managers, particularly for flood inundation mapping, coastal hazard assessments and modeling sea level rise. Elevation is also an important determinant of the frequency and duration of tidal flooding, which in turn affects species patterns in marshes: elevation differences of less than 10 cm can affect plant distributions and productivity. Light Detection and Ranging (LIDAR) can provide synoptic elevation information in many environments, but its accuracy in salt marshes is limited by a combination of sensor resolution (scan angle and frequency, pulse width, footprint size), instrument errors (GPS and inertial measurement unit errors), and poor laser penetration in dense vegetation. This means that uncorrected digital elevation models (DEM) are generally not accurate enough to distinguish elevation changes in salt marsh environments at the resolution that is used to determine tidal flooding or vegetation patterns. In this study, we used a LIDAR-derived DEM for the salt marshes surrounding Sapelo Island, GA obtained with a state-of- the-art Optech Gemini ALTM LIDAR system with a high laser pulse rate frequency of 125 kHz and advanced IMU/GPS technology, and evaluated its accuracy with elevations collected using real time kinematic (RTK) GPS. We found that DEM mean vertical errors for different cover classes ranged from 0.03 to 0.25 m in comparison to the RTK ground truth data, with the larger offsets for taller vegetation. We developed species-specific correction factors for ten cover classes and used these correction factors to modify the LIDAR-derived DEM in four areas of the study domain where vegetation boundaries were mapped directly in the field. Application of the derived correction

factors greatly improved the accuracy of the LIDAR-derived DEM within these areas, reducing the overall mean DEM error from 0.10 ± 0.12 (SD) to -0.01 ± 0.09 m (SD), and the Root Mean Square Error from 0.16 m to 0.10 m. In the corrected DEM, the ground elevations of all vegetation classes were no longer significantly different than the true RTK ground elevations. Our results suggest that these types of corrections can greatly improve the accuracy of LIDAR-derived DEMs in salt marshes and further emphasize the importance of accuracy assessments before DEM data are used, especially in environments such as salt marshes where small differences in elevation can have significant effects on inundation patterns and plant distributions.

1. Introduction

Salt marshes are valuable ecosystems. Positioned at the interface between aquatic and upland habitats, they provide critical habitat for both aquatic and terrestrial organisms; are sites of chemical transformations and detoxification; and protect developed coastal areas from shoreline erosion and storms (Chapman, 1976; Mitsch and Gosselink, 2000). Marshes are situated in low-lying, intertidal areas and have very little topographic relief. Even small topographic differences, however, can affect water flow, sediment distribution, and the extent and frequency of tidal inundation in this environment. These topographic variations affect the area and amount of water stored in intertidal areas and therefore detailed elevation data are also important for identifying and predicting areas vulnerable to storm surges and sea level rise (Blanton et al., 2006; Liu et al., 2007a; Sanders 2007). An incorrect Digital Elevation Model (DEM) can affect the output of hydraulic models and the predicted extent of flooding (Gesch, 2009; Raber et al., 2007).

Accurate elevation data is also important for salt marsh habitat mapping. Salt marsh plants are found within a narrow elevation range that is often less than 2 m (McKee and Patrick, 1988), but even subtle gradients in elevation are associated with changes in a range of factors including oxygen availability (Mitsch and Gosselink, 2000), soil moisture and porewater salinity (Adams, 1963), soil redox potential (Pezeshki, 2001), availability of nutrients (Gallagher, 1975), and concentrations of sulfide (Mendelssohn and Morris, 2000) and organic matter (Morris and Haskin, 1990), all of which contribute to the characteristic patterns of vertical zonation found in salt marsh macrophytes. As a result of the topographic influence on these variables, even slight changes in elevation can affect both the overall extent of marshes and the patterns of vegetation within them (Zedler et al., 1999). Topographic changes of less than 10 cm have been shown to significantly influence species patterns in marshes (Callaway et al., 1990; Silvestri et al., 2005; Suchrow and Jensen, 2010). Changes in plant distributions can alter erosion and accretion rates in marshes, and may serve as an early indicator of sea level rise (Kana et al., 1988; Vanderzee, 1988). There is therefore a need for accurate elevation mapping in salt marshes to identify sensitive habitat and predict how marshes will respond to perturbations that might alter plant distributions such as sea level rise or changes in sediment delivery (Gesch, 2009; Liu et al., 2007a; Sanders, 2007).

Over the past decade, many studies have used Light Detection and Ranging (LIDAR) to obtain information about ground elevation and vegetation structure (Brock and Purkis, 2009; Lefsky et al., 2002; MacMillan et al., 2003). LIDAR is a remote sensing technology that measures the distance between the sensor and a target surface by determining the time elapsed between the emission of a laser pulse and the arrival of the reflection of that pulse at the sensor's receiver (Wehr and Lohr, 1999). LIDAR can quickly collect dense elevation data over large areas which can be used to describe surface topography and vertical structure. LIDAR has been successfully used as an aid for mapping both vegetation and ground elevation in forest ecosystems where there is a large distance between the ground and canopy layers (Lefsky et al., 2002; Ritchie, 1996). Discrete return or pulsed LIDAR systems are able to discriminate multiple laser hits, or returns, for a target and assign each horizontal and vertical coordinates. In vegetated habitats, the first return is often assumed to be reflected from the top of the canopy, while the last return originates from the ground or from somewhere within the canopy (Shan and Toth, 2008). LIDAR data is often filtered to produce a first surface or Digital Surface Model (DSM) (interpolated from the first return) and a DEM with vegetation and man-made features removed (bare earth from the last return following point cloud classification and filtering routines).

Although LIDAR-derived DEMs can be effective at representing surface elevations in some environments, studies examining LIDAR-derived DEM accuracies in *Spartina alterniflora* marshes have reported errors: DEMs have been found to overestimate marsh ground elevations with a mean error of 0.07 to 0.17 m, and these errors have been found to increase with both increasing vegetation density and plant height (Montane and Torres, 2006; Morris et al., 2005; Rosso et al., 2006; Schmid et al., 2011). There are several reasons why these errors may occur. First, systematic instrument errors that are associated with sensor and GPS resolution in both the horizontal and vertical directions are relatively large compared to the small topographic variability in salt marshes, which makes it difficult to detect meaningful differences in elevation across the landscape (Hodgson and Bresnahan, 2004; Marani et al., 2006). If the magnitude of sensor error exceeds the elevation differences that are relevant for discerning where different plant species may be found, then the value of LIDAR is greatly reduced in salt marsh environments.

A second problem in using LIDAR to produce both DSMs and DEMs in salt marshes is related to vegetation structure. In areas where vegetation height is short, the time elapsed between subsequent returns can be too brief to be detected due to LIDAR system constraints (Brovelli et al., 2004; Wehr and Lohr, 1999). Most LIDAR systems have a "dead zone" of about 2 m (for a pulse length of 7 ns), meaning that if the vegetation is less than 2 m tall only one laser hit is recorded (Shan and Toth, 2008; Nayegandhi et al, 2006). The consequences of this "dead zone" in salt marshes, where all but the tallest plants are < 2 m, is the collection of only one LIDAR return and the inability to accurately measure vegetation heights in a DSM (Rosso et al., 2006; Sadro et al., 2007). Even with more than one return, predicted LIDAR-derived DEM elevations in marshes can be incorrect because the low, even stature of the vegetation has been found to limit laser pulse penetration in the canopy, resulting in the overestimation of marsh ground elevations in DEMs (Rosso et al., 2006; Sadro et al., 2007).

There have been several technological advancements in recent years that may allow for improved accuracies of LIDAR-derived elevations, as well as greater laser point density and penetration in salt marshes. First, advancements in onboard inertial measuring units (IMU) and kinematic GPS positioning systems minimize GPS errors, providing highly accurate laser point positions (X, Y, Z geographic coordinates) that can be used to rapidly collect ground truth observations (Ackermann, 1999; Maune et al., 2007). Second, within the last 5 years, a new generation of instruments has been developed that may have better capabilities for laser penetration due to higher pulse rate frequencies (PRF) as has been shown in forested ecosystems (Chasmer et al., 2006). PRF is the number of emitted pulses per second and is one of the LIDAR system parameters that determine the laser point density, in addition to flight altitude, flight line swath overlap, pulse width, scan rate and angle and laser footprint size (Shan and Toth, 2008). As PRF increases, point density increases, thereby increasing the probability that a laser pulse will intercept a canopy gap and reach the ground. The greater point density enables better spatial resolution and accuracy for DEMs (Hodgson and Bresnahan, 2004; Liu et al., 2007b). The salt marsh studies cited above used LIDAR systems with relatively low pulse PRFs (ranging from 25 to 83 kHz) and the ability of higher PRFs to penetrate dense canopies has not been rigorously tested in salt marshes.

Our overall goal for this project was to evaluate high PRF LIDAR data, obtained in combination with advanced IMU/GPS technology, in order to create accurate digital elevation models (DEMs) of low-lying salt marsh environments. We obtained a DEM of the salt marshes surrounding Sapelo Island, GA using a high PRF LIDAR system and evaluated its accuracy with elevations collected using real time kinematic (RTK) GPS. In contrast to earlier studies (Montane and Torres, 2006; Morris et al., 2005), which focused almost exclusively on *S. alterniflora* or high marsh species, we developed species-specific offsets from these data for ten cover classes that span the entire marsh vertical range. To assess the robustness of the correction factors, we selected four areas within the study domain where vegetation boundaries were mapped directly in the field, and used these as test sites to evaluate and validate our approach for DEM modification. Although it is beyond the scope of the current study, this approach can now be applied, in combination with a validated vegetation classification map, to the entire DEM domain.

2. Methods

2.1. Study Site

This study was conducted in the salt marshes surrounding Sapelo Island, Georgia, USA (UTM Zone 17 N, 471480 E 3473972 N, Figure 2.1). The site is located in the Georgia Coastal Ecosystems Long Term Ecological Research domain and the Sapelo Island National Estuarine Research Reserve. Tides are semi-diurnal with a mean tide range of 2.5 m. The Duplin River is a 13-km long tidal inlet that flows into Doboy Sound

(Blanton et al., 2006). The river forms the western boundary of Sapelo Island and is surrounded by a complex of salt marshes, tidal creeks and back barrier islands. This study included a total of 13.82 km^2 of salt marsh habitat in and around the Duplin River.

Salt marshes along the Eastern U.S. coast are often separated into low, mid and high marsh zones based on elevation and flooding frequency, with low marsh areas being inundated by the tide daily, high marsh areas being flooded at least every 15 days and mid marsh areas subjected to intermediate flooding regimes (Odum and Fanning, 1973; Teal, 1962). *S. alterniflora* is the dominant macrophyte in these marshes and is the primary plant found in the low marsh zone. For this study, *S. alterniflora* was classified as tall, medium or short, depending on its height (Figure 2.S1). *S. alterniflora* that was taller than 1 m was considered "tall". Tall *S. alterniflora* can grow up to 2 m tall and is found along the regularly flooded creek banks in the low marsh. *S. alterniflora* that ranged from 0.50 m to 1.0 m tall was considered "medium" and plants < 0.5 m were considered "short." Medium *S. alterniflora* dominates the mid-marsh and short *S. alterniflora* is found in the irregularly flooded high marsh. *S. alterniflora* typically has two canopy layers: a taller dead layer from the previous year, and a shorter, layer of new growth (Turner, 1976).

The high marsh contains a mixed community of *Salicornia virginica*, *Batis maritima, Distichlis spicata* and short *S. alterniflora* (Figure 2.S1), collectively termed marsh meadow or salt meadow (Wiegert and Freeman, 1990). Marsh meadow has dense canopies, generally less than 0.50 m tall. At the highest elevations along the upland fringe, *Juncus roemerianus* and *Borrichia frutescens* become the dominant species

(Figure 2.S1). Canopy heights of *J. roemerianus and B. frutescens* range from 0.50 m to over 2 m tall.

2.2. LIDAR Data

The National Center for Airborne Laser Mapping (NCALM) acquired 35 km^2 of LIDAR data for Duplin River marshes on March 9 and 10, 2009. Data were acquired when plant growth and biomass were seasonally low to maximize laser penetration of the vegetation canopy, and during a spring low tide (-1.6 m) to minimize the amount of water on the marsh surface. Water returns are considered unreliable since laser hits may be absorbed (due to the strong absorption of the 1047 wavelength by water) or scattered (due to specular reflectance) (Maune et al., 2007; Raber et al., 2007). Data were collected with an Optech GEMINI Airborne Laser Terrain Mapper (ALTM) mounted in a twin-engine Cessna Skymaster flown at an altitude of 800 m above ground level with a swath width of 370 m and 50% swath overlap between adjacent flight lines. The survey was conducted with a laser PRF of 125 kHz, a total field of view of 32 degrees and up to 4 returns. The high PRF was used to obtain a target point density of 9 laser points m^{-2} and test the ability of the LIDAR sensor to penetrate the vegetation canopy. Reported vertical and horizontal accuracies (root mean squared error (RMSE)) for the sensor are 0.05-0.10 m and 0.10-0.15 m, respectively (Optech Inc., 2011). Sensor and over-flight details can be found in Table 2.1.

Two GPS reference stations were used to process differential trajectories of the aircraft during the survey. After GPS processing, the trajectories were combined with IMU data to produce a final and complete navigation solution. In total, 21 flight lines were flown, in addition to three perpendicular crossing lines. Adjacent and crossing flight lines were classified individually to identify ground class points for each line using TerraSolid's TerraScan software (http://terrasolid.fi) and generate a bare earth data set using vegetation removal algorithms. A surface model was then created for each flight line using only the ground class points. To check for any misalignments and systematic errors, flight line to flight line calibration was performed by NCALM by analyzing swath overlaps and cross-lines using an algorithm in Terra Solid's TerraMatch software (http://terrasolid.fi) that employs a least-squares approach to find the best-fit values for system orientation parameters (roll angle, pitch angle, yaw (heading) and mirror-scale values) (i.e. bore-sight calibrations). After the best values for system orientation parameters were determined the flight strips were output again using the updated bore-sight values. The overlap areas of the flight lines were then checked for systematic height differences that can be largely attributed to the fact that LIDAR shot heights are directly correlated to the heights of the airplane trajectory, and the height error will vary as the GPS constellation changes during the flight. NCALM determined the height error between individual flight line surfaces ranged from 0.01 to 0.07 m. The height error values obtained for individual flight lines were averaged to get the final bore-sight correction values and were applied to the entire flight line as a final adjustment. Absolute calibration was done using 662 check points surveyed with a vehicle-mounted kinematic GPS over paved roads near the Brunswick, GA airport. These same road sections were surveyed with crossing flight lines using the ALTM and the heights of the check points were compared to the heights of the nearest neighbor LIDAR points within a radius of 20 cm. The RMSE of height differences was 0.11 m and RMSE at the 95% confidence level was 0.20 m.

A bare earth LIDAR-derived DEM was produced in SURFER Version 8 (http://www.goldensoftware.com) at 1.0 x 1.0 m resolution using a kriging algorithm with a maximum variance of 0.15 m. Elevations were all positioned in the NAD 83 reference frame and projected into UTM coordinate zone 17 N. Elevations are NAVD 88 orthometric heights (in meters) computed using the National Geodetic Survey GEOID 03, which is 0.203 m above mean sea level (MSL) based on the nearest NOAA tide gauge station at St. Simons Island, GA. The LIDAR-derived bare earth DEM product was used in the current analysis to determine vertical accuracy in salt marsh habitats.

2.3. RTK Survey

We conducted an initial ground survey of salt marsh ground control point (GCP) elevations and plant characteristics coincident with the LIDAR data collection in March 2009. We measured plant species presence, percent cover and height in 0.25 x 0.25 m quadrats at 50 locations; plots were marked with PVC poles and flagging so that they could be resurveyed as necessary. Plant percent cover in vegetated plots ranged from 30% to 100% and vegetation height ranged from 0.02 to 1.5 m. At these same locations we surveyed elevations using a Trimble R6 RTK GPS receiver with reported 0.0030 and 0.020 m vertical and horizontal RMSE at 68% percent confidence level (Trimble, 2009). Post-survey analysis of RTK data confirmed these accuracy values with an observed vertical RMSE of 0.0037 m, a mean vertical error of 0.010 and mean horizontal error of 0.012 m (all reported at 68% percent confidence level). RTK elevations are NAVD 88 orthometric heights (in meters) computed using the National Geodetic Survey GEOID 03. At each GCP location the RTK Rover foot was placed flush with the marsh surface and care was taken to leave the sediment and vegetation undisturbed. Although the tidal stage varied throughout this and subsequent sampling periods, elevations were only surveyed when the marsh surface was not inundated to avoid any elevation changes due to sediment swelling.

We carried out a more extensive RTK survey from June to August 2009 to collect additional GCPs for eight vegetation cover classes: *S. alterniflora* (short (SS), medium (SM) and tall (ST) height classes), *J. roemerianus* (JR), *B. maritima* (BM), *D. spicata* (DIST), *S. virginica* (SV) and *B. frutescens* (BF) and two non-vegetated classes (intertidal mud (MUD) and salt pan (SALT)). Intertidal mud consisted of patches of mud ≥ 1 m^2 within the vegetated portion of the salt marsh and did not include mud on creek banks at elevations below tall *S. alterniflora*. Salt pans were high marsh habitats with hypersaline sediments and less than 25% vegetation cover. The original 50 GCPs were re-surveyed to ensure that no change in elevation occurred between the March 2009 LIDAR acquisition and the summer 2009 RTK survey. Target RTK sampling locations were randomly selected using the ArcGIS 9.3 software program (http://www.esri.com) and a vegetation classification of the Duplin River salt marshes created using hyperspectral imagery collected in June 2006 (Hladik et al., Unpublished results). The vegetation map enabled us to identify sampling locations based on predicted vegetation class prior to the RTK survey.

We chose target sampling locations for each vegetation class based on the hyperspectral classification, which mapped the following marsh cover classes: tall *S. alterniflora*, medium *S. alterniflora*, short *S. alterniflora*, *S. virginica*, *B. maritima*, *J. roemerianus*, *B. frutescens*, salt pan and mud. Sampling locations were uploaded to the RTK GPS and in the field we navigated to each site to within 1 m of the target location insofar as that was possible. The number of RTK points sampled per cover class ranged from 35 (*D. spicata*) to 267 (medium *S. alterniflora*) (Table 2.2). This range in sampling was primarily due to the relative dominance of the various cover classes in the marsh. Additional GCPs were also collected opportunistically. In total, we collected over 1800 RTK ground elevations within the Duplin River marshes (Figure 2.1) and separated the data into training and validation data sets. 75% of the RTK GCPs (N = 1380) were used to assess the accuracy of the LIDAR-derived DEM and to calibrate the cover class-specific correction factors to be used for DEM modification in the four test areas (Section 2.4). 25% of the RTK GCPs were reserved for a subsequent assessment of the accuracy of the modified DEM of the entire domain (not presented here). Independent RTK validation data for the four test areas were collected and are described in Section 2.5.

We tested for differences in elevation between cover classes using one-way ANOVA followed by Tukey's honest significance test to compare means. Statistical results for all analyses in this study were considered significant when p-value < 0.05. All statistical analyses were done using the open source program R version 2.10.1 (http://cran.r-project.org/).

2.4. LIDAR-derived DEM Accuracy Assessment

We compared ground elevations from the RTK survey to the LIDAR-derived DEM elevation for each GCP location throughout the entire study domain (13.82 km^2) using various error metrics. For each GCP, the value of the corresponding 1 m^2 DEM grid cell was extracted using ArcGIS (Spatial Analyst toolbox). The RTK GCPs from the 2009 surveys were assumed to be the true observed ground elevations and the elevations extracted from the LIDAR-derived DEM were used as predicted elevations. We used these data to assess the accuracy of the DEM and compute a mean correction factor for each cover class.

To examine the scatter of the LIDAR-derived DEM elevation relative to the RTK ground survey elevation, we calculated the mean error, the RMSE, the fundamental vertical accuracy (FVA) and 95th percentile errors for each cover class following American Society for Photogrammetry and Remote Sensing guidelines (ASPRS Lidar Committee, 2004; Maune et al., 2007). The mean error, or vertical bias, has been used previously to quantify the accuracy of LIDAR-derived DEMs in wetland environments (Hodgson and Bresnahan, 2004; Montane and Torres, 2006; Morris et al., 2005; Sadro et al., 2007; Toyra et al., 2003; Wang et al., 2009) and is a good indicator of vertical offsets as compared to the RMSE which does not account for such offsets in the data (Populus et al., 2001). Both the RMSE and the FVA are representative errors for open terrain that are flat with no or sparse, low vegetation that conform to a normal distribution of errors. The 95th percentile errors are more appropriate for vegetated areas where the distribution of errors is non-normal, but are applicable to all cover classes (Maune et al., 2007). The mean error, RMSE, FVA and 95th percentile error are reported here.

The mean error for each GCP was calculated by subtracting the surveyed RTK elevation from the DEM elevation at the x/y coordinate of the GCP (ASPRS Lidar Committee, 2004; Maune et al., 2007). The mean error for each marsh cover class comprised the correction factors used in the subsequent DEM modification (Section 2.5). The RMSE, as described in Maune et al. (2007), is a common measure of vertical accuracy for LIDAR data and is calculated as:

$$\mathrm{RMSE} = \mathrm{sqrt}[\sum(z_{LIDARi} - z_{RTKi})^2/n] \qquad (2.1)$$

where z_{LIDARi} is the elevation of the i^{th} GCP in the LIDAR-derived DEM; z_{RTKi} is the i^{th} elevation of the i^{th} GCP in the RTK data set; n is the number of GCPs; and i is an integer from 1 to n. The FVA at a 95% confidence level was calculated as RMSE*1.96 (Maune et al., 2007). The 95th percentile errors are the interpolated absolute value of elevation errors obtained by dividing the distribution of errors into one hundred groups of equal frequency. The 95th percentile means that 95% of the elevation errors have a value equal to or less than the 95th percentile value (Maune et al., 2007). We compared the calculated RMSE for each cover class to the reported vertical RMSE of the LIDAR sensor (0.11 m based on vehicle mounted GPS absolute calibration) to determine whether or not the observed RMSE was within the range of instrument error.

2.5. DEM Correction – Test application

To evaluate the utility of modifying the LIDAR-derived DEM using the species-specific correction factors obtained from the field survey, we selected four small marsh areas as test sites where we mapped individual plant communities, representing nine cover classes (mud was not included) (Figure 2.2). Vegetation stands were mapped using a high-resolution, differential GPS (Trimble Geo-XH DGPS; http://www.trimble.com) with a horizontal RMSE of less than 0.20 m (Figure 2.2). To enable validation of the modified DEM, a new dataset of RTK GCP elevations were collected in the vegetation polygons coincident with DGPS mapping. These RTK data were independent of the RTK data used to perform the initial DEM accuracy assessment and to derive the correction factors (Section 2.4).

The DGPS mapped polygons were brought into ArcGIS 9.3 as shapefiles where vegetation areas were edited to smooth boundaries and remove any obviously anomalous data points. The data table for each polygon shapefile identified the dominant marsh cover and its corresponding correction factor quantified from the 2009 RTK survey. The correction factors were the mean error computed for each marsh cover type (see Section 2.4) and represented the average difference between the DEM and RTK GCP elevations. In ArcGIS, the vegetation polygons were converted to raster format using the Polygon to Raster tool (Conversion toolbox). Each polygon was assigned a numeric value as part of the rasterization. For our purpose of DEM modification, each vegetation polygon was assigned the corresponding species-specific correction factor. The end product of the Polygon to Raster step was four “correction factor” DEMs, one for each test location, with values corresponding to the species-specific correction factors. The DEM of the larger domain was clipped to include only the test location areas, resulting in four “unmodified” DEMs. The “correction factor” DEMs were subtracted from the four “unmodified” DEMs using the Raster Math tool in ArcGIS (Spatial Analyst toolbox) to produce four “modified” DEMs.

We performed accuracy assessments on both the “modified” DEMs and the “unmodified” DEMs, using the new RTK elevation validation data set as ground truth. Data from the four test sites were aggregated (total area of 0.107 km^2) to ensure all vegetation classes were represented, and analyzed as one summed unit in all statistical analyses (N = 350). The mean error, RMSE, FVA and 95th percentile errors were calculated for each cover class as described above. The effectiveness of the correction factors were determined by comparing mean error, RMSE errors, FVA and 95th percentile errors in the modified and unmodified DEMs. We compared the calculated RMSE for each cover class to the reported vertical RMSE of the LIDAR sensor (0.11 m based on vehicle mounted GPS absolute calibration) to determine whether or not the observed RMSE was within the range of instrument error.

3. Results

3.1. LIDAR Data

This study employed a new high PRF LIDAR sensor designed to more accurately measure salt marsh elevations. Even with the high point density (obtained point density of 9 points m^{-2}) and PRF, the sensor was unable to discriminate ground from vegetation and differentially map them for all cover classes. The majority of the salt marsh only had one LIDAR return. Based on our analyses for the entire domain (N = 1380), a LIDAR-derived DEM can accurately measure elevations for non-vegetated and vegetated classes with a short stature. The RMSE for *D. spicata*, short *S. alterniflora*, intertidal mud, *B. maritima*, *S. virginica* and salt pan were within the reported vertical RMSE of the LIDAR sensor (0.11 m), however, tall *S. alterniflora*, *J. roemerianus*, *B. frutescens* and medium *S. alterniflora* all had RMSEs that exceeded instrument error (see section 3.3). The fact that the mean errors for salt pan and mud flat cover classes were within instrument error suggests that the overall LIDAR sensor system calibration and standard LIDAR survey corrections were effective.

3.2. RTK survey

RTK ground elevations from the 2009 survey of plant species followed the expected zonation from the low marsh to the high marsh (Table 2.2). The species mean elevations occurred within a vertical range of 0.87 m, between 0.36 m (tall *S. alterniflora*) and 1.23 m (*B. frutescens*), with zero being relative to NAVD 88 (0.203 m above mean sea level), while elevation differences between adjacent cover classes (RTK

Elevation Difference) ranged from < 0.01 m to 0.42 m (Table 2.3). The three height classes of *S. alterniflora* had significantly ($p < 0.05$) different elevations from each other, within a mean elevation range of only 0.51 m (Table 2.2). Tall *S. alterniflora*, medium *S. alterniflora* and *B. frutescens* were significantly different from all other classes (Tables 2.2 and 2.3). However, the elevations of high marsh species overlapped considerably and were not significantly different, spanning an elevation range of only 0.15 m (from short *S. alterniflora* to *J. roemerianus*) (Tables 2.2 and 2.3).

3.3. LIDAR-derived DEM Accuracy Assessment

The LIDAR-derived DEM for the entire study domain over-predicted ground elevations for all cover classes, in comparison to the RTK ground elevation data, with mean errors up to 0.25 m and an overall mean error (Mean) of 0.10 ± 0.11 m (SD) (Table 2.4). The LIDAR-derived DEM elevations were significantly different than the RTK ground elevations for all cover classes (Table 2.4). DEM mean overestimation error increased with plant height ($R^2 = 0.44$, $p < 0.001$, Figure 2.S2), ranging from 0.03 m (salt pan) to 0.25 m (tall *S. alterniflora*). RMSE ranged from 0.05 m (salt pan) to 0.30 m (tall *S. alterniflora*) (Table 2.4). The RMSE for *D. spicata*, short *S. alterniflora*, intertidal mud, *B. maritima*, *S. virginica* and salt pan were within the reported vertical RMSE of the LIDAR sensor (0.11 m), however, the overall RMSE, and the RMSE for tall *S. alterniflora*, *J. roemerianus*, *B. frutescens* and medium *S. alterniflora* all exceeded instrument error.

LIDAR-derived DEM errors were greater than the elevation differences between many vegetation classes (see Section 3.2). Mean DEM errors for adjacent cover classes (Domain DEM Error (Unmodified)) ranged from 0.03 to 0.25 m, whereas mean elevation differences (RTK Elevation Difference) were < 0.01 to 0.41 m (Table 2.3). A consequence of this is that DEM errors would prevent differentiation among some cover classes. For example, mean errors were equal to, or exceeded, the elevation differences between medium *S. alterniflora* and short *S. alterniflora* and between *J. roemerianus* and *B. frutescens.* These two pairs of cover classes have significantly different elevations based on the RTK ground truth data (Table 2.2). As there was greater overlap in cover class elevations in the high marsh (*S. virginica*, *B. maritima*, *D. spicata*) and smaller associated errors (Table 2.4), these classes were less affected by LIDAR-derived DEM errors.

3.4. *DEM Correction – Test application*

3.4.1. Unmodified DEM

The LIDAR-derived DEM elevations in the four test sites over-predicted elevations and had the same overall mean error (Mean) in comparison to the RTK ground elevations as was previously quantified for the larger domain (mean error of 0.10 ± 0.12 m (SD)), with the amount of overestimation varying by cover class (Table 2.5, Figure 2.3A). The unmodified DEM elevations were significantly different than the RTK ground elevations for all cover classes except short *S. alterniflora* and salt pan (Table 2.5). Again, tall *S. alterniflora* had the greatest mean error (0.27 m) and salt pan had the smallest mean error (0.01 m, Table 2.5). RMSE ranged from 0.04 m (salt pan) to 0.31 m (tall *S. alterniflora*) (Table 2.5). The RMSE for *D. spicata*, short *S. alterniflora*, intertidal mud, *B. maritima, S. virginica* and salt pan were within the reported RMSE of the LIDAR sensor (0.11 m). The overall RMSE, as well as the RMSEs for tall *S. alterniflora*, medium *S. alterniflora*, *J. roemerianus* and *B. frutescens* all exceeded instrument error, which is again similar to the results obtained for the larger domain (Section 3.3).

As was found in the larger accuracy assessment (Section 3.3), LIDAR-derived DEM errors exceeded differences in elevation between many cover classes. Mean DEM errors for adjacent cover classes (Test Site DEM Error (Unmodified)) ranged from 0.01 to 0.27 m (Table 2.3). For example, mean errors were again larger than the elevation difference between medium *S. alterniflora* and short *S. alterniflora* and the combined errors for *J. roemerianus* and *B. frutescens* overwhelmed the elevation difference between the two classes. DEM errors had less impact on the differentiation of high marsh cover classes compared to cover classes with larger error values.

3.4.2. Corrected DEM

We modified the LIDAR-derived DEM elevations in the four test sites by applying the correction factors derived for each cover class (Section 3.3; Table 2.4 ('Mean'), Figures 2.3B and 2.4). DEM modification considerably reduced the overall mean error in comparison to RTK elevations across the four sites (-0.01 ± 0.10 m (SD) from 0.10 ± 0.12 m (SD), Table 2.5, Figure 2.3B). Elevation errors associated with the taller, dense vegetation classes were greatly decreased: tall *S. alterniflora* mean error averaged 0.05 m in the modified DEMs as compared to 0.27 m in the unmodified DEMs and *B. frutescens* mean error averaged -0.01 m as compared to 0.12 m. Elevations of the remaining cover classes were all slightly under-predicted (< -0.01 to -0.06 m) in the modified DEMs, but were not significantly different in comparison to RTK GCPs (Table 2.5).

The overall RMSE and RMSE for all cover classes in the modified DEMs, except tall *S. alterniflora* (RMSE = 0.18), fell within the reported instrument vertical RMSE (0.11 m). In contrast to the unmodified DEM (Section 3.4.1), mean errors for cover classes (Test Site DEM Error (Modified)) ranged from < 0.01 to 0.05 m, which is less than or equal to the elevation differences observed between cover classes (RTK Elevation Difference, < 0.01 to 0.42 m) (Table 2.3).

4. Discussion

4.1. LIDAR Data

In salt marshes, a few centimeters of elevation are critical in determining flooding frequency, and hence accurate elevation data is vital for the modeling of coastal hydrology and the potential impacts of sea level rise, as well as the distribution and productivity of the marsh plants. If LIDAR-derived DEMs are to be of use in salt marsh studies, they must be capable of detecting these small variations in topography against the background of the error signal. The high PRF LIDAR system used in this study overestimated salt marsh ground elevations at our study site at Sapelo Island, GA. Although the system performed quite well for most cover classes, it was unable to penetrate thick canopy and the unmodified DEM required corrections based on our RTK survey data. Even though the PRF contributed to attaining the high point density (9 points m^{-2}), the laser hits did not penetrate the canopy or the lower signal-to-noise-ratio may have obscured the separation of low vegetation from the ground surface (Hopkinson, 2006; Shan and Toth, 2008). There is also a tradeoff between PRF and the energy of the emitted pulse: an increase in PRF reduces pulse energy depending on the laser output power and could decrease accuracy due to the lower signal-to-noise ratio (Hopkinson, 2006; Shan and Toth, 2008). High PRF LIDAR alone is therefore not a solution for deriving accurate DEMs for salt marshes and more attention should be given to narrowing FOV and pulse width to better detect closely space returns, decreasing footprint size, or improving filtering to minimize misclassification of low vegetation as ground.

There are multiple sources of elevation errors in LIDAR-derived DEMs in addition to sensor errors. Elevation errors can be introduced from the processing of raw LIDAR LAS point cloud data. Classification and filtering routines could introduce LIDAR point labeling errors by misclassifying low vegetation as ground points: with short, even vegetation, the laser hits may resemble the flat ground surface and be classified as such (Gopfert and Heipke, 2006; Hodgson and Bresnahan, 2004). This was likely the case here, as our examination of the raw LAS point clouds showed that the laser did not completely penetrate the vegetation canopy and reach the marsh ground surface (data not shown). The interpolation of point clouds to generate a gridded DEM may introduce additional elevation error and the various methods (deterministic and geostatistical) can produce significantly different representations of a surface (Bater and Coops, 2009; Liu, 2008; Maune et al., 2007; Su and Bork, 2006). In this study the interpolation process (geostatistical kriging) actually created a marsh ground surface that was lower than the point cloud and reduced the mean error and RMSE based on RTK GCPs (data not shown). Even though the LIDAR-derived DEM marsh ground surface was more accurate than the point cloud, there were still substantial errors when compared to RTK GCPs. It is possible that other interpolation techniques, such as the minimum bin method (deterministic), may produce a more accurate surface representation (Rosso et al., 2003; Schmid et al., 2011), however, an analysis of DEM interpolation methods was beyond the scope of this study .

Full waveform-resolving LIDAR is an advancement in LIDAR technology which may produce higher accuracy salt marsh LIDAR-derived DEMs (Doran et al., 2010; Nayegandhi et al., 2006; Nayegandhi et al., 2009). As opposed to discrete return LIDAR that only records individual pulse returns, full waveform sensors detect and digitize the complete backscattered return waveform and have been shown to be very sensitive to variations in vegetation structure (Mallet and Bretar, 2009; Nayegandhi et al., 2006). The absence of a "dead zone" with full waveform LIDAR can produce a better representation of vegetation vertical complexity and has been shown to be effective at characterizing the ground surface (RMSE = 0.24 m; mean error = -0.05 m) and canopy height (RMSE = 1.64 m; mean error = -0.22 m) in coastal vegetation communities (Nayegandhi et al., 2006).

4.2. RTK Survey

As in other marshes, we found that vegetation species followed a general zonation pattern across the topographical gradient from low to high marsh (Table 2.2). Observed plant distributions corresponded to those described in Weigert and Freeman (1990) for Southeastern salt marshes with tall *S. alterniflora* at lower elevations and *J. roemerianus* and *B. frutescens* at higher elevations. The RTK data show that there are subtle, but significant, differences in species elevation distributions. These distributions indicate the vertical resolution needed to discriminate amongst vegetation zones (RTK Elevation Difference), which ranged from < 0.01 to 0.42 m (Table 2.3).

McKee and Patrick (1988) have found that species elevations can vary widely among salt marshes. In a survey of marshes along the Atlantic and Gulf coasts they found the mean upper limit of *S. alterniflora* was 0.17 m and the mean lower limit was -0.72 m, both in relation to mean high water (MHW). When expressed in relation to MHW, *S. alterniflora* at our site occupied a higher elevation and broader range, with an upper limit of 0.34 m and lower limit of -1.46. In North Inlet, SC, which is a similar setting to the marshes examined here, Morris et al. (2005) reported median elevations (in relation to NAVD 88) for short *S. alterniflora* of 0.349 m, with a range of 0.22 to 0.481 m. The elevations in this study (in relation to NAVD 88 which is 0.203 m above MSL) were again higher: median elevation of short *S. alterniflora* averaged 0.87 m (range of 0.59 to 1.14 m), medium *S. alterniflora* averaged 0.78 m (range of 0.24 to 1.09 m) and tall *S. alterniflora* averaged 0.38 m (range of -0.67 to 0.85 m in relation to NAVD 88).

Morris and his collaborators (2002, 2005) have shown that the elevation distribution of *S. alterniflora* in relation to mean sea level can be used to assess marsh stability. Morris et al. (2002) found that each *S. alterniflora* marsh has an optimal elevation for primary production, below which productivity is reduced due to hypoxia and above which productivity is reduced by desiccation and salt stress (see Mendelssohn and Morris, 2000). When elevations are greater than the optimum (up to a point), marshes are stable against changes in relative sea level, whereas marshes at lower elevations are unstable. The observed elevation range of *S. alterniflora* in this study (mean values of 0.56 to 1.07 m in relation to MSL) suggests that the marshes near Sapelo Island will be relatively stable with respect to sea level rise in comparison to marshes where the plants are located at lower elevations. This finding is in agreement with a previous study by Craft (2007), who suggested that Georgia salt marshes are stable based on sediment accretion data.

4.3. LIDAR Accuracy Assessment

The LIDAR-derived DEM (1 m grid size) for the entire study domain in this study over-predicted the ground elevation for every cover class when validated with the RTK ground truth data, with an average overall mean error of 0.10 m (RMSE = 0.15 m) (Table 2.4). We found that LIDAR-derived DEM overestimation is greatest for the tallest plant species (tall *S. alterniflora*, *J. roemerianus*, and *B. frutescens*) and the mean error decreases as plant height decreases (Table 2.4). To determine the cause of DEM error, we examined the relationship between plant height and DEM mean error in a separate analysis. Vegetation height had a statistically significant but not strong relationship with DEM mean error, explaining 44% of the variation (Figure 2.S2). Sadro et al. (2007) also found a significant, but weak correlation (R^2 = 0.18) between vegetation height and DEM error. As plant height could not fully explain DEM error, this suggests that other factors, such as stem density, leaf orientation, and biomass are also prohibiting laser penetration and contributing to DEM error, in addition to height (Schmid et al., 2011).

Our results are consistent with previous evaluations of LIDAR-derived DEMs in salt marsh ecosystems, which have all found that DEMs consistently overestimate salt marsh ground elevations. In South Carolina *S. alterniflora* marshes (in areas primarily dominated by short and medium *S. alterniflora*), LIDAR-derived DEMs have been shown to overestimate marsh ground elevations with a mean error of 0.07 m (Montane and Torres, 2006), 0.11 m (Schmid et al., 2011), and 0.13 m (Morris et al., 2005). Although we found that tall *S. alterniflora* had substantially greater mean errors (0.25 m) than these previous studies, our results (Table 2.4) conform well with these findings for short and medium *S. alterniflora*. Our RMSE reported for short *S. alterniflora* is comparable to those identified by Morris et al. (2005) and Rosso et al. (2006). RMSE for medium *S. alterniflora* are in agreement with the RMSE reported by Schmid et al. (2011) (0.16 m) and Rosso et al. (2006) (0.17 m). The RMSE for tall *S. alterniflora* (0.30 m), however, exceeded all previously reported values.

Relatively few studies have examined LIDAR-derived DEM errors for the other marsh species considered here, but in general the RMSE values we found for non-vegetated and short, high marsh vegetation were considerably less than in other studies (Rosso et al., 2006; Sadro et al., 2007; Toyra et al., 2003). In the high marsh, Schmid and others (2011) reported a mean error of 0.30 m (RMSE of 0.37 m) for *J. roemerianus*, 0.11 m (RMSE of 0.15 m) for *B. frutescens* and 0.02 m (RMSE of 0.12 m) for *S. virginica*. Although the errors reported in this study for *B. frutescens* and *S. virginica* were comparable, our errors associated with *J. roemerianus* were considerably less (mean error of 0.17 m, RMSE of 0.20 m) than those in the Schmid et al. (2011) study. The RMSE errors reported here for *D. spicata* and *S. virginica*, (0.09 and 0.06 m, respectively, Table 2.4) are also substantially less than those reported by Sadro et al. (2007) (0.18 and 0.17 m) for a California salt marsh. The differences in quantified errors between our study and others is most likely due to differences in sensor characteristics (PRF, FOV, pulse width, footprint size) and site specific variations in plant height and density.

Overall, the species-specific errors observed here are larger than the elevation variation found between significantly different adjacent vegetation zones (Tables 2.3, 2.4

and 2.5). In particular, LIDAR-derived DEM errors exceeded the elevation differences between medium *S. alterniflora* and short *S. alterniflora* and between *J. roemerianus and B. frutescens.* As medium and short *S. alterniflora* constitute almost 80% of the Duplin River marshes (Hladik et al., Unpublished results), the inability of LIDAR-derived DEMs to distinguish between the two vegetation classes is noteworthy. This is important because medium and short *S. alterniflora* can have significantly different biomass and productivity values (Morris and Haskin, 1990; Turner, 1976). Additionally, corrected elevations are required for accurate hydrological modeling of flooding frequency and coastal hazard assessments (Gesch, 2009; Raber et al., 2007).

4.4. DEM Correction-Test Application

The application of the derived correction factors and subsequent DEM modification in the four test areas were successful and greatly improved the accuracy of the LIDAR-derived DEM in those locations, reducing the overall mean DEM error from 0.10 to -0.01 m and the RMSE from 0.16 to 0.10 m. Applying the species-specific correction factors (ranging from 0.03 to 0.25 m) brought all DEM elevations in agreement with their true RTK elevations (Table 2.5, Figures 2.3B and 2.4). DEM correction was particularly visible in areas surrounding creek banks and creek heads (Figure 2.4), where medium and tall *S. alterniflora* are typically found. The slight negative value for the overall mean error means that the correction factors produced a DEM surface that was slightly lower than RTK elevations, but well within the instrument error, for all classes except tall *S. alterniflora*. Notably, the reduced errors in the modified DEM are less than the elevation differences between vegetation classes, making the corrected DEM appropriate for use in salt marsh studies.

Using a similar approach in a salt marsh in California composed mostly of high marsh plants, Sadro et al. (2007) reported improved LIDAR-derived DEM accuracies for extracted elevation values following a species-specific correction in combination with an AVIRIS classification and found no mean difference between survey and extracted LIDAR-derived DEM elevations after correction and an overall RMSE of 0.06 m. It should be noted that Sadro et al. (2007) did not modify the actual DEM, but rather adjusted extracted elevations according to species-specific offsets. Another approach to correcting DEMs is custom classification (analysis of LIDAR LAS point clouds) and generation of a new LIDAR-derived bare earth DEM surface. Although custom classification requires more advanced software and expertise, it has been successfully applied in salt marshes. Wang et al. (2009) used statistical techniques to better differentiate ground and canopy returns in marsh vegetation. Other authors have experimented with various DEM interpolation algorithms to produce the most representative ground surface (Schmid et al., 2011; Toyra et al., 2003). The errors in these efforts, however, were generally greater than, or comparable to, those reported here.

5. Conclusion

This study demonstrates that, despite advancements in LIDAR sensor technology, state-of-the-art high PRF LIDAR as applied here, does not produce accurate DEMs of salt marsh habitats and is of limited utility without correction. The magnitude of LIDAR-derived DEM error was greatest for taller vegetation, however, plant height could not fully explain errors and suggests that the relationship between DEM error and other vegetation characteristics, such as stem density, leaf orientation and biomass should be investigated. We were successfully able to correct the LIDAR-derived DEM in four test areas based on high accuracy RTK observations. We achieved large reductions in mean error, which ranged from 0.01 to 0.27 m for ten cover classes, spanning the entire marsh elevation gradient, which allowed us to produce improved DEM elevations for four test sites within our study area. Post-correction accuracy assessments showed that our corrections were robust, with errors ranging from -0.03 to 0.05 m, and are appropriate for the correction of DEM elevations in these salt marshes. Based on these results, we can now correct the larger DEM of the whole Sapelo study area using a high accuracy hyperspectral classification to delineate cover classes. This research underscores the importance of undertaking accuracy assessments before LIDAR-derived DEM data are used, particularly for low-lying habitats such as salt marshes where small differences in elevation are important for assessments of flood inundation, modeling sea level rise and habitat mapping.

6. Acknowledgements

We thank Kristen Anstead, Caitlyn Connor, Nick Scoville and Jacob Shalack for all of their assistance with this project as well as Michael Santori at NCALM and Mark White at Duncan Parnell for technical support. The Sapelo Island National Estuarine Research Reserve and the University of Georgia Marine Institute also provided logistical support. This research was supported by the Georgia Coastal Ecosystems LTER Project (NSF Award OCE-0620959) and a National Estuarine Research Reserve System Graduate Research Fellowship (NOAA Award NA09NOS4200046). We thank Steve Pennings, Clark Alexander and three anonymous reviewers for helpful comments on the manuscript.

7. References

Ackermann, F. (1999). Airborne laser scanning-present status and future expectations. *ISPRS Journal of Photogrammetry and Remote Sensing*, 54, 115-122.

Adams, D. A. (1963). Factors influencing vascular plant zonation in North Carolina salt marshes. *Ecology*, 44, 445– 456.

ASPRS Lidar Committee (2004). ASPRS Lidar guidelines: Vertical accuracy reporting for Lidar data. Retrieved November 16, 2011, from http://www.asprs.org/a/society/committees/lidar/Downloads/Vertical_Accuracy_Reporting_for_Lidar_Data.pdf

Bater, C.W., and Coops, N.C. (2009). Evaluating error associated with lidar-derived DEM interpolation. *Computers and Geosciences*, 35, 289-300.

Blanton, J., Andrade, F., and Ferreira, M. A. (2006). The relationship of hydrodynamics and morphology in tidal-creek and salt-marsh systems in South Carolina and Georgia. In: Kleppel, G., DeVoe, M., and M.V. Rawson, J. (ed.), *Implications of Changing Land Use Patterns to Coastal Ecosystems* (pg. 93-107). New York, NY: Springer-Verlag.

Brock, J.C., and Purkis, S.J. (2009). The emerging role of Lidar remote sensing in coastal research and resource management. *Journal of Coastal Research*, 53, 1-5.

Brovelli, M. A., Cannata, M., and Longoni, U. M. (2004). LIDAR data filtering and DTM interpolation within GRASS. *Transactions in GIS*, 8(2),155–174.

Callaway, R. M., Jones, S., Ferren, W. R., and Parikh, A. (1990). Ecology of a Mediterranean-climate estuarine wetland at Carpinteria, California – plant distributions and soil-salinity in the upper marsh. *Canadian Journal of Botany*, 68, 1139−1146.

Chapman, V.J. (1976). *Coastal Vegetation*, second ed. Oxford : Pergamon Press.

Chasmer, L., Hopkinson, C., Smith, B., and Treitz, P. (2006). Examining the influence of changing laser pulse repetition frequencies on conifer forest canopy returns. *Photogrammetric Engineering and Remote Sensing*, 17, 1359-1367.

Craft, C. (2007). Freshwater input structures soil properties, vertical accretion, and nutrient accumulation of Georgia and U.S. tidal marshes. *Limnology and Oceanography*, 52, 1220-1230.

Doran, K.J., Sallenger, A.H., Reynolds, B.J., and Wright, C.W. (2010). Accuracy of EAARL lidar ground elevations using a bare-earth algorithm in marsh and beach grasses on the Chandeleur Islands, Louisiana, U.S. Geological Survey Open-File Report 2010-1163, 9 p.

Gallagher, J.L. (1975). Effects of an ammonium nitrate pulse on the growth and elemental composition of natural strands of *Spartina alterniflora* and *Juncus roemerianus*. *American Journal of Botany*, 62, 644–648.

Gesch, D.B. (2009). Analysis of Lidar elevation data for improved identification and delineation of lands vulnerable to sea-level rise. *Journal of Coastal Research,* 53, 49-58.

Gopfert, J., and Heipke C. (2006). Assessment of LIDAR DTM in coastal vegetated areas. *International Archives of Photogrammetry, Remote Sensing, and Spatial Information Sciences*, 36, 79–85.

Hodgson, M. E., and Bresnahan, P. (2004). Accuracy of airborne lidar-derived elevation: Empirical assessment and error budget. *Photogrammetric Engineering and Remote Sensing*, 70, 331−339.

Hopkinson, C. (2006). The influence of LIDAR acquisition settings on canopy penetration and laser pulse return characteristics. In *IGARSS 2006: International Conference on Geoscience and Remote Sensing Symposium* (IEEE, Denver, Colorado), pp. 2420-2424.

Kana, T. W., Baca, B. J. and Williams, M. L. (1988). Charleston case study. In: Titus, J. G. (ed.). *Greenhouse Effect, Sea Level Rise, and Coastal Wetlands* (pp. 37-59). Washington, DC: U.S. Environmental Protection Agency.

Lefsky, M. A., Cohen, W. B., Parker, G. G., and Harding, D. J. (2002). Lidar remote sensing for ecosystem studies. *Bioscience*, 52, 19−30.

Liu, H., Sherman, D., and Gu, S. (2007a). Automated extraction of shorelines from airborne light detection and ranging data and accuracy assessment based on Monte Carlo simulation. *Journal of Coastal Research*, 23, 1359-1369.

Liu, X., Zhang, Z., Peterson, J., and Chandra, S. (2007b). The effect of lidar data density on DEM accuracy, In *Proceedings of the International Congress on Modelling and Simulation (MODSIM07)*,Christchurch, New Zealand.

Liu, X. (2008). Airborne LIDAR for DEM generation: some critical issues. *Processes in Physical Geography*, 32, 31-49.

MacMillan, R.A., Martin, T.C., Earle, T.J., and McNabb, D.H. (2003). Automated analysis and classification of landforms using high-resolution digital elevation data: applications and issues. *Canadian Journal of Remote Sensing*, 29, 592-606.

Mallet, C., Bretar, F. (2009). Full-waveform topographic Lidar: State-of-the-art. *ISPRS Journal of Photogrammetry and Remote Sensing*, 64, 1-16.

Marani, M., Belluco, E., Ferrari, S., Silvestri, S., D'Alpaos, A., and Lanzoni, S. (2006). Analysis, synthesis and modeling of high-resolution observations of salt-marsh eco-geomorphological patterns in the Venice lagoon. *Estuarine, Coastal and Shelf Science*, 69, 414−426.

Maune, D.F.; Maitra, J.B., and McKay, E.J. (2007). Accuracy standards and guidelines. In: Maune, D. (ed.), *Digital Elevation Model Technologies and Applications: The DEM Users Manual, 2nd Edition* (pp. 65-97). Bethesda, Maryland: American Society for Photogrammetry and Remote Sensing.

McKee, K.L., and Patrick, W.H., Jr. (1988). The relationship of smooth cordgrass (*Spartina alterniflora*) to tidal datums: A review. *Estuaries*, 11, 143-151.

Mendelssohn, I.A., and Morris, J.T. (2000). Eco-physiological controls on the productivity of *Spartina Alterniflora* Loisel. In: Kreeger, D.A. (ed.) *Concepts and Controversies in Tidal Marsh Ecology* (pp. 59-80). Dordrecht : Kluwer Academic.

Mitsch, W. J., and Gosselink, J. G. (2000). *Wetlands*, third edition. New Jersey: John Wiley and Sons.

Montane, J.M., and Torres, R.T. (2006). Accuracy assessment of Lidar salt marsh topographic data using RTK GPS. *Photogrammetric Engineering and Remote Sensing*, 72, 961-967.

Morris, J.T., and Haskin, B. (1990). A 5-yr record of aerial primary production and stand characteristics of *Spartina alterniflora*. *Ecology*, 7, 2209-2217.

Morris, J. T., Sundareshwar, P. V., Nietch, C. T., Kjerfve, B., and Cahoon, D. R. (2002). Responses of coastal wetlands to rising sea level. *Ecology*, 83, 2869−2877.

Morris, J. T., Porter, D., Neet, M., Noble, P. A., Schmidt, L., and Lapine, L.A. (2005). Integrating LIDAR elevation data, multi-spectral imagery and neural network modeling for marsh characterization. *International Journal of Remote Sensing*, 26, 5221−5234.

Nayegandhi, A., Brock, J.C., Wright, C.W., and O'Connell, M.J. (2006). Evaluating a small footprint, waveform-resolving LIDAR over coastal vegetation communities. *Photogrammetric Engineering and Remote Sensing*, 72, 1407-1417.

Nayegandhi, A., Brock, J.C., and Wright, C.W. (2009). Small-footprint, waveform resolving lidar estimation of submerged and sub-canopy topography in coastal environments. *International Journal of Remote Sensing*, 30, 861-878.

Odum, E.P., and Fanning, M.E. (1973). Comparisons of the productivity of *Spartina alterniflora* and *Spartina cynosuroides* in Georgia coastal marshes. *Bulletin of the Georgia Academy of Sciences*, 31, 1-12.

Optech (2011). Gemini summary specification sheet. Retrieved August 11, 2011, from http://www.optech.ca/pdf/ALTM_Gemini_SpecSheet_110309_Web.pdf.

Pezeshki, S. R. (2001). Wetland plant responses to flooding. *Environmental and Experimental Botany*, 46, 299-312.

Populus, J., Barreau, G., Fazilleau, J., Kerdreux, M., and L'Yavanc, J. (2001). Assessment of the LIDAR topographic technique over a coastal area. In *Proceedings of CoastGIS'01: 4th International Symposium on GIS and Computer Mapping for Coastal Zone Management*, Halifax, Nova Scotia, 11p.

Ritchie, J.C. (1996). Remote sensing applications to hydrology: airborne laser altimeters. *Hydrological Sciences Journal*, 41, 625-636.

Raber, G.T., Jensen, J.R., Hodgson, M.E., Tullis, J.A., Davis, B.A., and Berglund, J. (2007). Impact of Lidar nominal post-spacing on DEM accuracy and flood zone delineation. *Photogrammetric Engineering and Remote Sensing*, 73, 793-804.

Rosso, P. H., Ustin, S.L., and Hastings, A. (2003). Use of LIDAR to produce high resolution marsh vegetation and terrain maps. Presentation at The Three Dimensional Mapping from InSAR and LIDAR Workshop, ISPRS, Portland, Oregon.

Rosso, P. H., Ustin, S. L., and Hastings, A. (2006). Use of lidar to study changes associated with Spartina invasion in San Francisco Bay marshes. *Remote Sensing of Environment*, 100, 295−306.

Sadro, S., Gastil-Buhl, M., and Melack, J. (2007). Characterizing patterns of plant distribution in a southern California salt marsh using remotely sensed topographic and hyperspectral data and local tidal fluctuations. *Remote Sensing of Environment*, 110, 226-239.

Sanders, B.F. (2007). Evaluation of on-line DEMs for flood inundation modeling. *Advances in Water Resources*, 30, 1831-1843.

Schmid, K.A., Hadley, B.C., and Wijekoon, N. (2011). Vertical accuracy and use of topographic LIDAR data in coastal marshes. *Journal of Coastal Research*, 27, 116-132.

Shan, J., and Toth, C. (ed). (2008). Topographic Laser Ranging and Scanning, Principles and Processing. Boca Raton, FL: Taylor and Francis Group.

Silvestri, S., Defina, A., and Marani, M. (2005). Tidal regime, salinity and salt marsh plant zonation. *Estuarine, Coastal and Shelf Science*, 62, 119-130.

Su, J.G., Bork, E.W. (2006). Characterization of diverse plant communities in Aspen Parkland rangeland using LiDAR data. *Applied Vegetation Science*, 10, 407-416.

Suchrow, S., and Jensen, K. (2010). Plant species responses to an elevational gradient in German North Sea salt marshes. *Wetlands*, 30, 735-746.

Teal, J.M. (1962). Energy flow in the salt marsh ecosystem of Georgia. *Ecology*, 43, 614-624.

Trimble (2009). Trimble R6 GPS receiver datasheet. Retrieved August 11, 2011, from http://trl.trimble.com/docushare/dsweb/Get/Document-333155/022543-259D_Trimble_R6_DS_1109_LR.pdf.

Turner, R.E. (1976). Geographic variations in salt marsh macrophyte productions: A review. *Contributions to Marine Sciences*, 20, 47-68.

Toyra, J., Pietroniro, A., Hopkinson, C., and Kalbfleisch, W. (2003). Assessment of airborne scanning laser altimetry (lidar) in a deltaic wetland environment. *Canadian Journal of Remote Sensing*, 29, 718-728.

Vanderzee, M.P. (1988). Changes in saltmarsh vegetation as an early indication of sea-level rise. In: Pearman, G.I. (ed.), *Greenhouse: Planning for Climatic Change* (pp.147-160). Melbourne: CSIRO.

Wang, C., Menenti, M., Stoll, M., Feola, A., Belluco, E., and Marani, M. (2009). Separation of ground and low vegetation signatures in LIDAR measurements of salt-marsh environments. *IEEE Transactions on Geoscience and Remote Sensing*, 47, 2014-2023.

Wehr, A., and Lohr, U. (1999). Airborne laser scanning: An introduction and overview. *ISPRS Journal of Photogrammetry and Remote Sensing*, 54, 68–82

Wiegert, R.G., and Freeman, B.J. (1990). *Tidal Salt Marshes of the Southeast Atlantic Coast: a Community Profile*. Washington, DC: U.S. Department of the Interior, Fish and Wildlife Service.

Zedler, J.B., Callaway, J. C., Desmond, J. S., Vivian-Smith, G., Williams, G. D., and Sullivan, G. (1999). Californian salt-marsh vegetation: An improved model of spatial pattern. *Ecosystems*, 2, 19−35.

Table 2.1. LIDAR sensor system specifications for the Optech Gemini ALTM used by the National Center for Airborne Laser Mapping (NCALM) to acquire LIDAR data for this study.

Altitude (m)	800
Swath Width (m)	370
Swath Overlap (%)	50
Laser PRF (kHz)	125
Scan Freq (Hz)	40
Field of View (degrees)	32
Scan Angle (degrees)	16
Scan Cutoff (degrees)	3
Footprint (cm)	60
Wavelength (nm)	1047
Pulse Length (ns)	7
DEM grid size (m)	1

Table 2.2. Summary of RTK survey mean elevation (Mean), sample size (N), standard deviation (SD), standard error (SE), salt marsh zone(s) where each cover class is typically found (Marsh Zone(s)) and statistical significance grouping (Grouping) for each cover class evaluated in this study based on RTK data for the entire domain. To determine the 'Grouping' we tested for differences in elevation between cover classes using one-way ANOVA followed by Tukey's honest significance test to compare means. Mean elevations for each cover class was considered to be significantly different if the *p*-value < 0.05. Zero elevation (in relation to NAVD 88) corresponds to 0.203 m below mean sea level. All units are in meters (m).

Cover Class	Mean (m)	N	SD (m)	Grouping	Marsh Zone(s)
Tall *S. alterniflora*	0.36	152	0.27	a	low
Medium *S. alterniflora*	0.77	267	0.13	b	low, mid
Short *S. alterniflora*	0.87	214	0.10	c	mid, high
Intertidal Mud	0.89	53	0.10	cd	low, mid, high
S. virginica	0.95	227	0.07	de	high
D. spicata	0.96	35	0.07	de	high
B. maritima	0.99	160	0.07	de	high
Salt Pan	1.01	62	0.06	e	high
J. roemerianus	1.02	117	0.20	e	mid, high
B. frutescens	1.23	78	0.10	f	high

Table 2.3. Summary of RTK elevations for each cover class in comparison to DEM errors for the DEM accuracy assessment of the larger domain and the subset of four areas used as test sites for the DEM test modification. The column 'RTK Elevation' contains mean ground elevations for each cover class quantified in the 2009 RTK survey and subsequently used in the accuracy assessment of the larger domain (N = 1380, Table 2.2). The column 'RTK Elevation Difference' represents the difference in mean elevation between sequential cover classes from low to high elevation. For example, the elevation difference between tall *S. alterniflora* and medium *S. alterniflora* was calculated as the absolute value of 0.36-0.77 m. 'Domain DEM Error (unmodified)' is the mean error for each cover class in the DEM of the entire domain based on the accuracy assessment (N = 1380, Table 2.4). 'Test site DEM Error (unmodified)' and 'Test site DEM Error (modified)' are the mean errors for each cover class based on the four DEM test modification sites (N = 350, Table 2.5). RTK grouping shows significant (p-value < 0.05) differences in elevation among cover classes based on post hoc ANOVA multiple comparison of means using Tukey's HSD and are presented in the 'Grouping' column. All units are in meters (m).

Cover Class	RTK Elevation (m)	RTK Elevation Difference (m)	Domain DEM Error (m) (Unmodified)	Test Site DEM Error (m) (Unmodified)	Test Site DEM Error (m) (Modified)	RTK Grouping
Tall *S. alterniflora*	0.36		0.25	0.27	0.05	a
Medium *S. alterniflora*	0.77	0.42	0.11	0.09	-0.03	b
Short *S. alterniflora*	0.87	0.09	0.05	0.03	-0.03	c
Intertidal Mud	0.89	0.03	0.04	--	--	cd
S. virginica	0.95	0.05	0.04	0.04	-0.01	de
D. spicata	0.96	0.01	0.08	0.05	-0.02	de
B. maritima	0.99	0.04	0.04	0.04	< 0.01	de
Salt Pan	1.01	0.02	0.03	0.01	-0.03	e
J. roemerianus	1.02	< 0.01	0.17	0.10	-0.06	e
B. frutescens	1.23	0.21	0.12	0.12	-0.01	f

Table 2.4. LIDAR-derived DEM accuracies for each cover class relative to RTK ground survey elevations measured in this study for the larger domain. Table lists mean LIDAR-derived DEM error (Mean), number of observations (N), standard deviation (SD), standard error (SE), root mean square error (RMSE), fundamental vertical accuracy (FVA) and 95th percentile error (95th Percentile). See Section 2.4 for details on specific error calculations. *p*-values are from a paired t-test between the RTK elevations and the predicted DEM elevations for each cover class. The 'Mean' values are the species-specific correction factors that were used for DEM modification. All units are in meters (m).

Cover Class	Mean (m)	N	SD (m)	SE (m)	RMSE (m)	FVA (m)	95th Percentile (m)	*p*-value
Tall *S. alterniflora*	0.25	152	0.17	0.01	0.30	0.59	0.49	< 0.001
Medium *S. alterniflora*	0.11	267	0.07	0.00	0.13	0.26	0.24	< 0.001
Short *S. alterniflora*	0.05	214	0.05	0.00	0.07	0.14	0.11	< 0.001
Intertidal Mud	0.04	53	0.06	0.01	0.08	0.15	0.14	0.032
S. virginica	0.04	227	0.05	0.00	0.06	0.12	0.11	< 0.001
D. spicata	0.08	35	0.04	0.01	0.09	0.17	0.14	< 0.001
B. maritima	0.04	160	0.04	0.00	0.06	0.12	0.11	< 0.001
Salt Pan	0.03	62	0.04	0.01	0.05	0.10	0.10	0.012
J. roemerianus	0.17	117	0.09	0.01	0.19	0.38	0.32	< 0.001
B. frutescens	0.12	78	0.07	0.01	0.14	0.27	0.23	< 0.001
Overall	0.10	1380	0.11	0.00	0.15	0.29	0.32	< 0.001

Table 2.5. Summary of LIDAR-derived DEM accuracies in the four areas used as test sites for DEM modification. Accuracies for each cover class are presented for both the unmodified and modified DEM relative to the RTK ground survey elevation. Table lists mean LIDAR error (Mean), number of observations (N), standard deviation (SD), standard error (SE), root mean square error (RMSE), fundamental vertical accuracy (FVA) and 95th percentile error (95th Percentile). See Section 2.4 for details on specific error calculations. *p*-values are from a paired t-test between the RTK elevations and the predicted DEM elevations for each cover class. All units are in meters (m).

Cover Class	Mean (m)	N	SD (m)	SE (m)	RMSE (m)	FVA (m)	95th Percentile (m)	*p*-value
Unmodified DEM								
Tall *S. alterniflora*	0.27	66	0.15	0.02	0.31	0.61	0.52	< 0.001
Medium *S. alterniflora*	0.09	62	0.06	0.01	0.11	0.22	0.18	0.007
Short *S. alterniflora*	0.03	72	0.04	0.01	0.05	0.10	0.10	0.073
S. virginica	0.04	49	0.05	0.01	0.07	0.13	0.14	0.024
D. spicata	0.05	10	0.03	0.01	0.06	0.11	0.09	0.001
B. maritima	0.04	15	0.04	0.01	0.05	0.10	0.10	0.032
Salt Pan	0.01	26	0.04	0.01	0.04	0.07	0.06	0.815
J. roemerianus	0.10	35	0.08	0.01	0.13	0.25	0.24	0.007
B. frutescens	0.12	15	0.09	0.02	0.15	0.29	0.24	0.001
Overall	0.10	350	0.12	0.01	0.16	0.31	0.37	< 0.001

Table 2.5 (continued).

Cover Class	Mean (m)	N	SD (m)	SE (m)	RMSE (m)	FVA (m)	95th Percentile (m)	*p*-value
<u>*Modified DEM*</u>								
Tall *S. alterniflora*	0.05	66	0.18	0.02	0.18	0.36	0.33	0.691
Medium *S. alterniflora*	-0.03	62	0.06	0.01	0.07	0.13	0.06	0.068
Short *S. alterniflora*	-0.03	72	0.04	0.01	0.05	0.10	0.04	0.131
S. virginica	-0.01	49	0.05	0.01	0.05	0.10	0.08	0.515
D. spicata	-0.02	10	0.03	0.01	0.03	0.07	0.02	0.168
B. maritima	0.00	15	0.03	0.01	0.03	0.06	0.04	0.981
Salt Pan	< -0.01	26	0.04	0.01	0.05	0.10	0.02	0.416
J. roemerianus	-0.06	35	0.08	0.01	0.10	0.19	0.07	0.125
B. frutescens	-0.01	15	0.09	0.02	0.08	0.17	0.12	0.799
Overall	-0.01	350	0.10	0.01	0.10	0.19	0.17	0.494

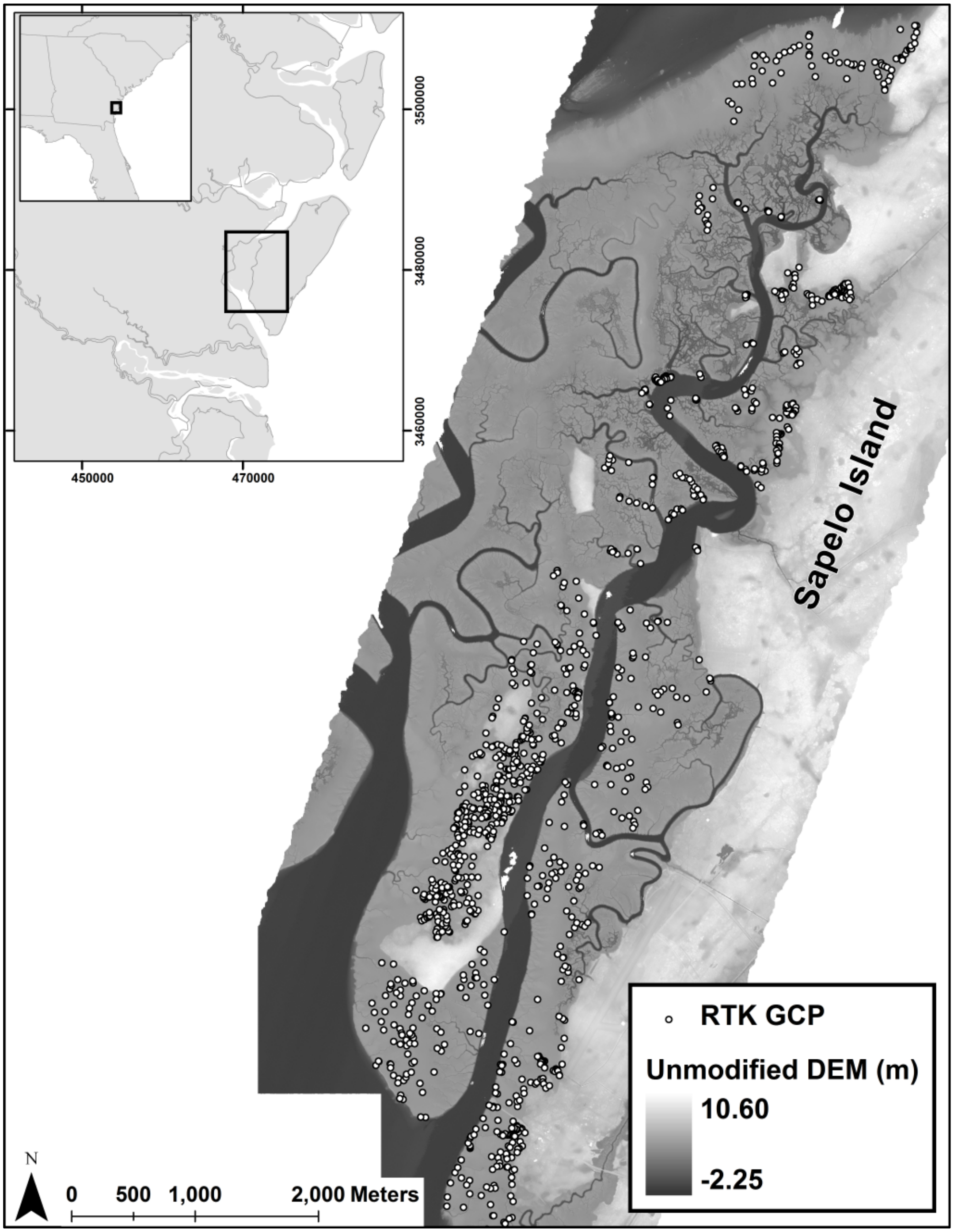

Figure 2.1. The unmodified LIDAR-derived bare earth DEM showing the location of the study area surrounding the Duplin River adjacent to Sapelo Island, GA. White dots indicate RTK ground control points (GCPs) used to assess DEM elevation accuracy and calibrate species-specific correction factors.

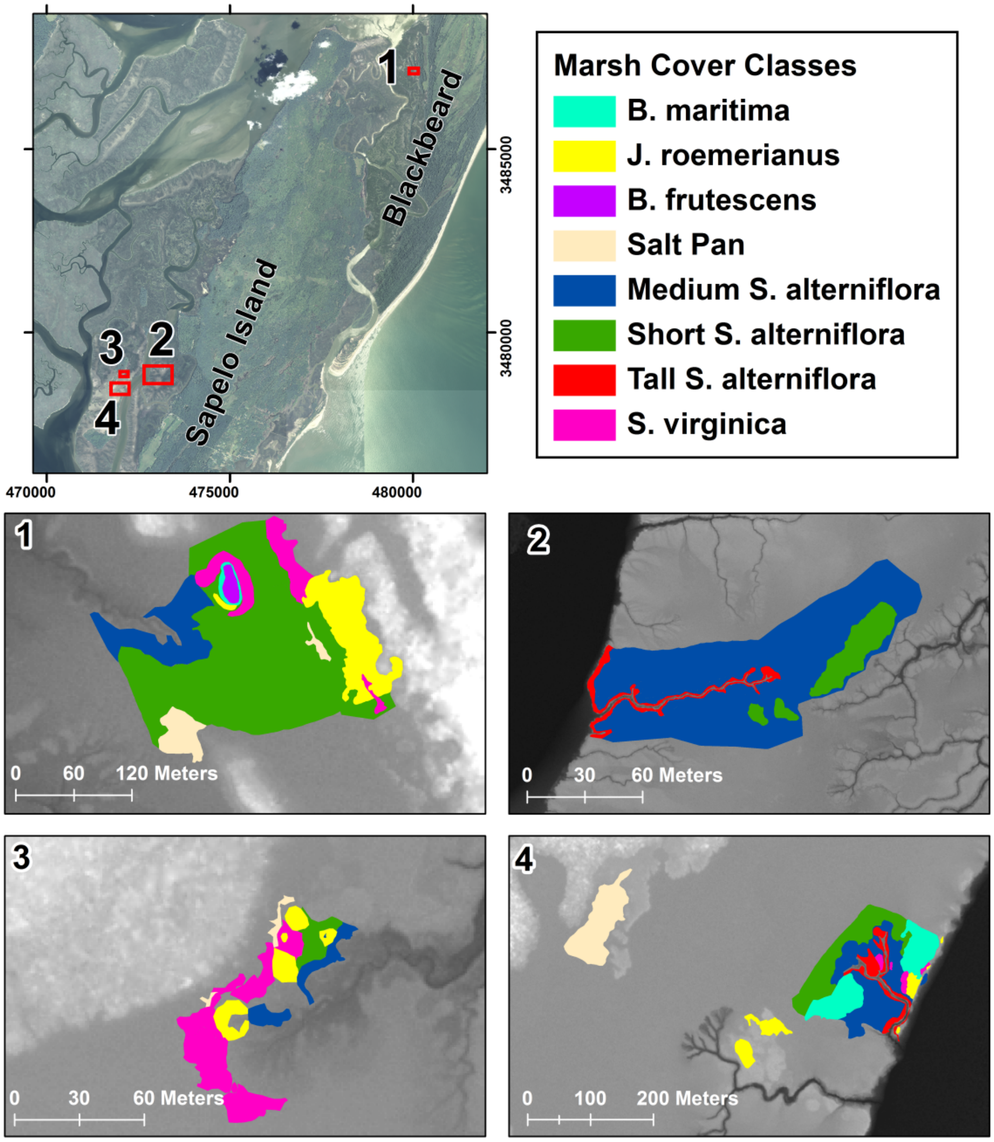

Figure 2.2. Overview map and vegetation polygons for the four areas used as test sites for DEM corrections. A decimeter DGPS unit was used to delineate the boundaries of the various salt marsh cover types in these locations. These areas were modified using the correction factors derived for the entire domain (see Figure 2.4). Data from all test sites were aggregated for statistical analyses and together covered a total area of 0.107 km^2.

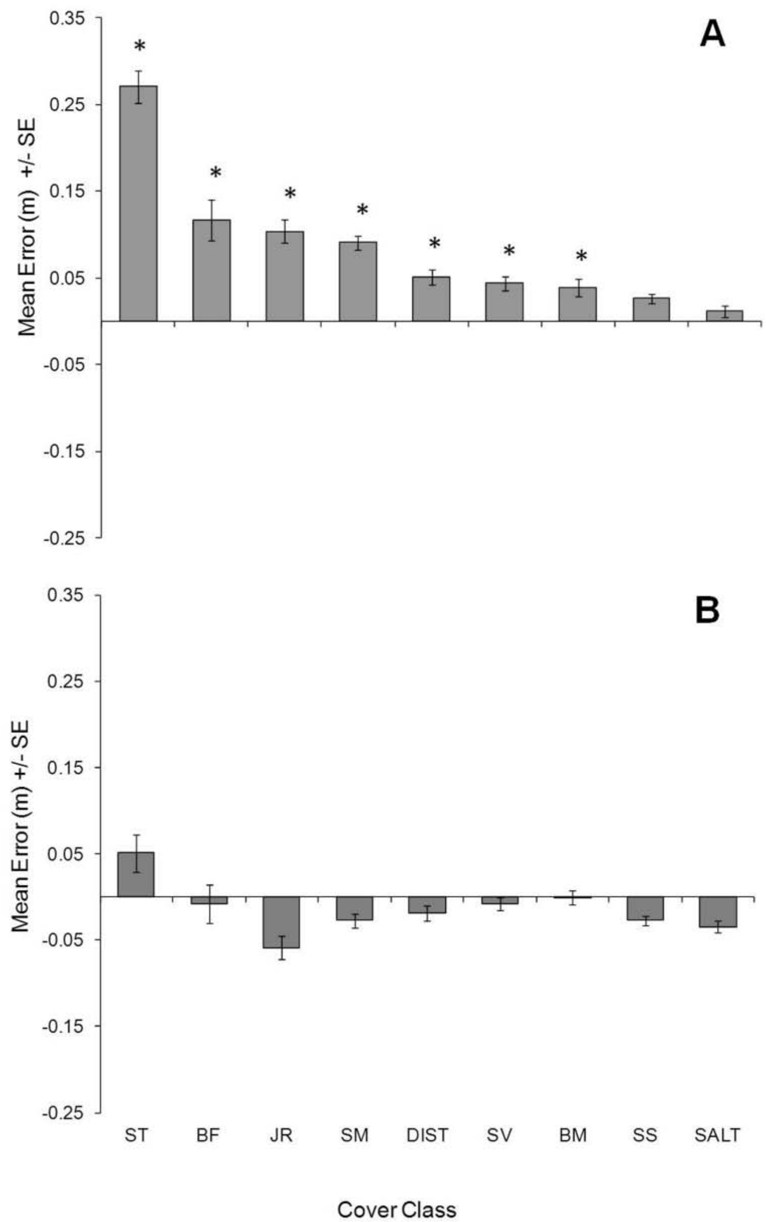

Figure 2.3. LIDAR-derived DEM mean elevation errors from the four test locations (N = 350) for each cover class before (A) and after (B) correction. Bars represent mean errors in meters (m) +/- standard error. Asterisks (*) above bars indicate significant *p*-values ($p < 0.05$) from a paired t-test between the RTK elevations and the predicted DEM elevations for each cover class (see Table 2.5). Cover class abbreviations are as follows: ST: tall *S. alterniflora*; BF: *B. frutescens*; JR: *J. roemerianus*; SM: medium *S. alterniflora*; DIST: *D. spicata*; SV: *S. virginica*; BM: *B. maritima*; SS: short *S. alterniflora*; and SALT: salt pan.

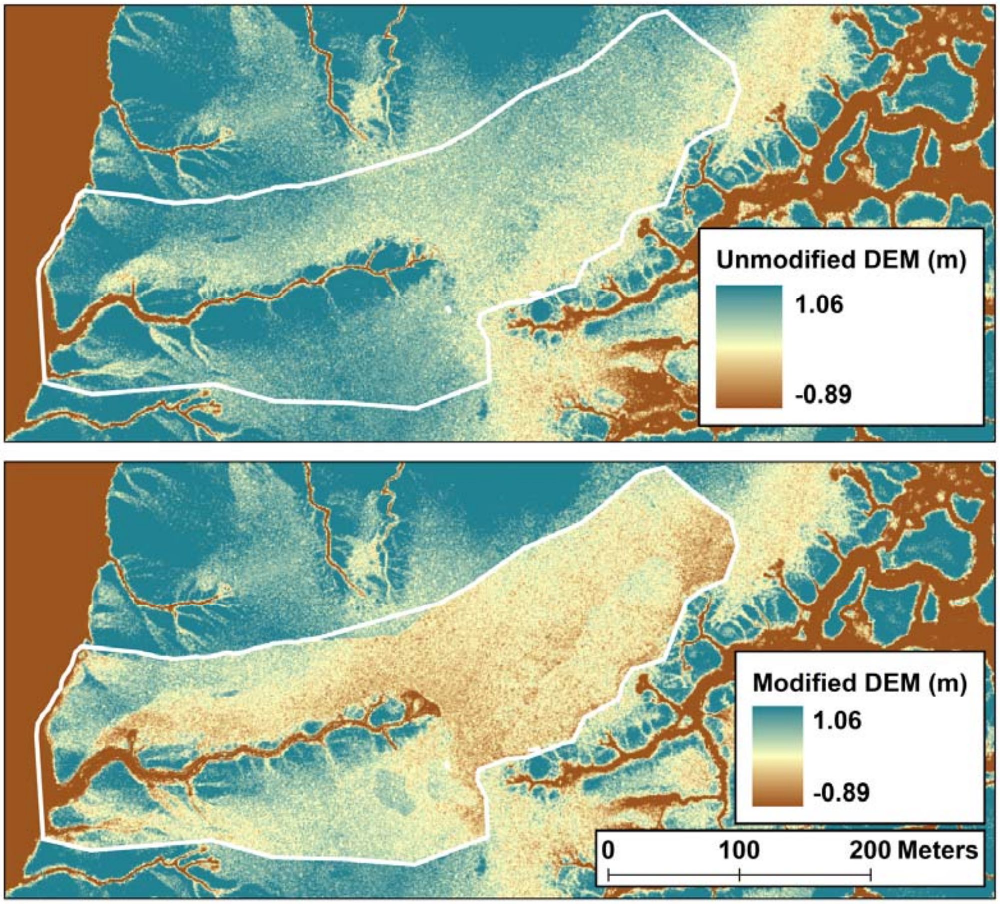

Figure 2.4. Map of one of the four areas (location 2, Figure 2.2) used as a test site for LIDAR-derived DEM corrections showing unmodified (top) and modified (bottom) DEM elevations (m). Cooler blue colors indicate higher elevations and warmer dark browns indicate lower elevations. Note the decrease in elevation associated with creek heads surrounded by tall and medium *S. alterniflora* in the modified DEM. Total area mapped and modified at location 2 was 0.078 km^2 (outlined in white).

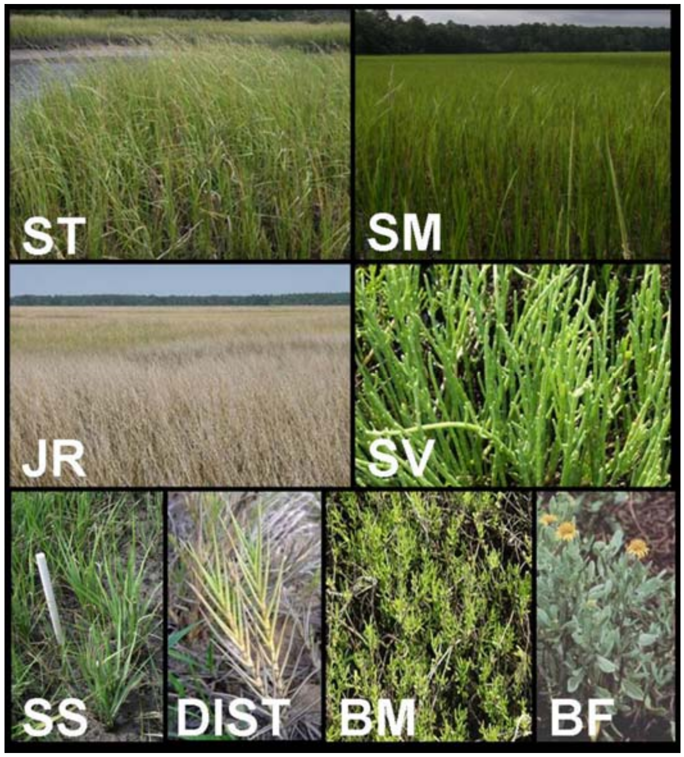

Figure 2.S1. Vegetated cover classes examined in this study. ST: *Spartina alterniflora* tall height, SM: *Spartina alterniflora* medium height; JR: *Juncus roemerianus*; SV: *Salicornia virginica*; SS: *Spartina alterniflora* short height; DIST: *Distichlis spicata*; BM: *Batis maritima*; and BF: *Borrichia frutescens*. The two non-vegetated cover classes (intertidal mud (MUD) and salt pan (SALT)) are not depicted.

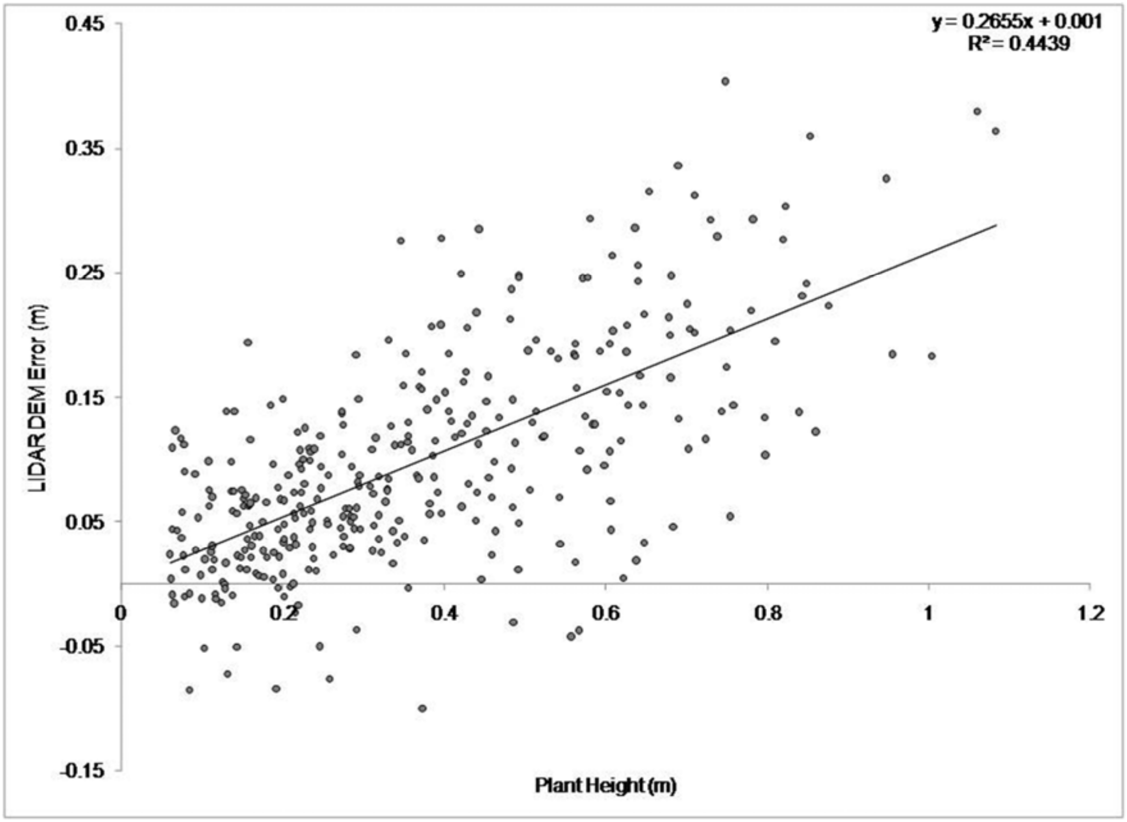

Figure 2.S2. Measured plant stem height (m) versus LIDAR-derived DEM error (m) (R^2 = 0.44, p < 0.001). During the RTK survey (section 2.3), heights of all stems in a 0.25 m x 0.25 m quadrat were measured to the closest centimeter at a subset of locations (N = 342) representing the eight vegetated cover classes considered in this study. Shown here are average plant height values for each quadrat plotted against LIDAR-derived DEM error for that location, which was calculated by subtracting the observed RTK elevation from the extracted LIDAR-derived DEM elevation (see section 2.4 for details).

CHAPTER 3

DATA FUSION OF HYPERSPECTRAL AND LIDAR IMAGERY FOR SALT MARSH ELEVATION AND PLANT COMMUNITY MAPPING[2]

[2] Hladik, C., Alber, M., and Schalles, J. To be submitted to *Remote Sensing of Environment*.

Abstract

Accurate mapping of both elevation and plant distributions in salt marshes is important for management and conservation goals. Although Light Detection and Ranging (LIDAR) is effective at measuring surface elevations, laser penetration is limited in dense salt marsh vegetation. In a previous study, we found that LIDAR-derived DEM error varied with vegetation cover and derived cover class-specific correction factors to reduce these errors, including separate corrections for three different height classes of *Spartina alterniflora*, the dominant macrophyte in Southeastern salt marshes. In order to apply these species-specific corrections, it is necessary to have information on the distribution of cover classes in a LIDAR-derived DEM. Hyperspectral imagery (HSI) has been shown to be suitable for the separation of marsh vegetation species by spectral signatures, and can be used to determine cover classes; however, there is persistent confusion between the different height classes of *S. alterniflora* and mud (the *Spartina* problem). This paper presents a method to overcome the respective limitations of LIDAR and HSI through data fusion. HSI was combined with a LIDAR-derived DEM through a decision tree, to map nine salt marsh habitat classes with a 90% overall accuracy. The decision tree appreciably reduced the *Spartina* problem and demonstrated the utility of this approach for improving salt marsh classifications. Further, fusing the HSI classification with the DEM to apply class-specific elevation correction factors for elevation mapping resulted in large reductions in overall mean error from 0.10 ± 0.12 (SD) to -0.003 ± 0.10 m (SD) and root mean squared error at the 68% confidence level from 0.15 to 0.10 m. Our results suggest that the use of decision trees to fuse elevation and spectral information can aid both HSI classification and DEM elevation mapping.

1. Introduction

Salt marshes are intertidal wetlands typically found in association with estuaries in temperate coastal areas. Marshes are susceptible to habitat loss due to changes in sea level and coastal flooding, and there is growing interest in obtaining accurate elevation maps for these areas in order to understand how small topographic differences affect water flow, sediment distribution, and the extent and frequency of tidal inundation (Gesch, 2009; Sanders, 2007). Differences in elevation also affect plant distributions, as salt marsh macrophytes exhibit characteristic patterns of vertical zonation. In Southeastern Atlantic U.S. salt marshes, the height of *Spartina alterniflora,* the dominant plant, is affected by elevation, with taller plants found growing in low areas closest to the water's edge and medium and shorter plants at higher elevations (Wiegert and Freeman, 1990). A variety of other plants, including *Juncus roemerianus*, *Salicornia virginica*, *Batis maritima*, *Distichlis spicata* and *Borrichia frutescens*, are typically found in the highest parts of the marsh. Gradients in elevation are also associated with a range of changes in soil characteristics, including oxygen availability and redox potential (Mitsch and Gosselink, 2000; Pezeshki, 2001), soil moisture and porewater salinity (Adam, 1990), and concentrations of sulfides and nutrients (Gallagher, 1975; Mendelssohn and Morris, 2000). Accurate elevation maps are therefore important not only for understanding flooding and inundation patterns but also for determining habitat characteristics of marshes (Adam, 1990; Silvestri et al., 2003; Zedler et al., 1999).

Many coastal researchers use light detection and ranging (LIDAR) to produce digital elevation models (DEMs) of salt marshes, as it provides broad coverage for areas that are large and sometimes difficult to access on the ground. However, there are several drawbacks to this approach. First, LIDAR tends to overestimate salt marsh elevations due to poor laser penetration of the dense canopy (Montane and Torres, 2006;

Rosso et al., 2006; Sadro et al., 2007; Schmid et al., 2011). The majority of prior studies have focused on improving techniques to separate LIDAR returns (Wang et al., 2009) and optimizing DEM interpolation methods (Schmid et al., 2011; Toyra et al., 2003), both of which can help to reduce error. These corrections have been applied without taking plant species into account, and have had accuracies (mean error) ranging from -0.02 to 0.12 m. In a previous study (Hladik and Alber, 2012), we found that LIDAR-derived DEM mean error varied with vegetation cover but could be reduced to -0.01 m by applying cover class-specific correction factors to four test areas (total area of 0.107 km^2). For example, ground elevations for tall *S. alterniflora* were severely overestimated and required a 0.25 m correction factor, whereas those for short *S. alterniflora* were only overestimated by 0.05 m. Because correction factors vary, it is necessary to have information on the distributions of cover classes to use this approach to correct the entire DEM, which was the limiting factor in the earlier study. A second, related limitation of LIDAR is that it only receives spectral information at one wavelength in the near infrared (NIR). It therefore cannot be used to distinguish among plant species, which requires information from the visible portion of the electromagnetic spectrum. To provide information on species composition for habitat maps LIDAR-derived DEMs can be used in combination with visible wavelengths (Campbell, 2007; Sadro et al., 2007).

Hyperspectral imagery (HSI) in the visible and NIR portion of the electromagnetic spectrum has been shown to be suitable for the separation of marsh vegetation species by spectral signatures (Artigas and Yang, 2005; Schmidt and Skidmore, 2003). Hyperspectral sensors are ideal for this as they are able to collect a high number of continuous spectral bands (sometimes greater than 200 bands) with narrow bandwidths and at a fine spatial resolution. The increased dimensionality of hyperspectral data allows for better species differentiation based on subtle differences in leaf structure and pigment composition (Hardisky, 1986; Schmidt and Skidmore, 2003), when compared to multispectral imagery with only 3 to 7 spectral bands. HSI has been used extensively in salt marshes to map vegetation patterns (Belluco et al., 2006; Silvestri et al., 2003; Wang et al., 2007), monitor invasive species (Gilmore et al., 2008; Rosso et al., 2006), document erosion and vegetation succession (Thomson et al., 2004), measure biomass and species abundance (Lucas and Carter, 2008; Wang et al., 2007) and detect vegetation change (Klemas, 2011), among other applications. These studies employed a variety of supervised classification techniques to process HSI including both subpixel and whole pixel algorithms.

The current study focuses on the pixel level analysis of salt marshes with HSI. Two of the most commonly used pixel level HSI classification algorithms for vegetation mapping are the maximum likelihood classifier (MLC) and the spectral angle mapper classifier (SAM). MLC is a parametric classifier that assumes each spectral band for each class is normally distributed and calculates the probability that a given pixel belongs to a specific class based on variance and covariance measures (Hoffbeck, 1995). A drawback to MLC is that it performs poorly when there are a large number of spectral bands due to the large covariances that need to be calculated (i.e. the Hughes' effect, Hughes, 1968). As a result, very large training data sets are needed for successful MLC classifications, or spectral data must be reduced using statistical techniques (principle components analysis or minimum noise fractionation) (Lillesand et al., 2004). SAM is a classification algorithm designed specifically for HSI. SAM measures the spectral similarity between each unknown pixel and endmember (training class) spectra by calculating the angle between the spectra, treating the spectra as vectors in n-dimensional space, with n equal to the number of image bands (Kruse et al., 1993). Two advantages to SAM are that not all endmembers need to be identified and the spectral angle is insensitive to variations in illumination (Leckie et al., 2005) and albedo effects (Kruse et al., 1993). A significant limitation is that SAM is unable to differentiate cover classes having the same spectral angle, a particular concern for salt marsh vegetation classes that have small, but significant, reflectance differences (Schmidt and Skidmore, 2003). Overall, MLC has tended to perform better than SAM in salt marshes (Belluco et al., 2006; Hunter and Power, 2002), but SAM has been successfully applied in some studies (Marani et al., 2003; Marani et al., 2006; Merani, 2007; Sadro et al., 2007) and, therefore, both are evaluated here.

Regardless of how imagery is processed, there are several challenges to using HSI in salt marshes, particularly with respect to accurately classifying *Spartina* species. First, there is persistent confusion within and between similar species. The different height classes of *S. alterniflora* (short, medium and tall), are commonly confused in HSI classification due to their spectral similarity in both the visible and NIR portions of the spectrum (Artigas and Yang, 2005; Schmidt and Skidmore, 2003). The spectral signature in the visible is largely controlled by pigment composition, which is the same for all *S. alterniflora* plants, and reflectance in the NIR is a function of air space configuration inside the leaf, which is genetically determined and invariant among the different height classes (Danson et al., 1992). In addition, a number of studies have also found spectral confusion between classes of closely related species. Using HSI, Artigas and Yang (2005) were unable to separate *S. alterniflora* from *Spartina patens* in the visible and NIR in the New Jersey Meadowlands. Another source of error in HSI classifications results from mixed pixels that include more than one type of vegetation and/or mud. Both of these types of mixed pixels are observed with *S. alterniflora*: the different height classes represent a continuum and can therefore be found adjacent to one another, and *S. alterniflora's* erect structure and often sparse stem densities means that mud is spectrally mixed with vegetation (Belluco et al., 2006; Silvestri et al., 2003; Thomson et al., 2003). Silvestri et al. (2003) found that *S. maritima* is often misclassified because it is found in low-lying areas where mud and water interfere with its spectral signature. Thomson and others (2003) hypothesized that microphytobenthos on mud may also cause mud to resemble *Spartina* spectrally. The inability to accurately classify the three height classes of *S. alterniflora,* compounded by the presence of mud in mixed pixels, is what we term the *Spartina* problem.

One way to potentially overcome the individual limitations of LIDAR-derived DEMs and HSI, and to potentially address the *Spartina* problem, is through data fusion. Data fusion combines data from different sources to obtain more information than could be derived from either independently (see review by Pohl and Van Genderen, 1998). It can be done at the pixel, feature or decision level. Pixel level fusion is the combination of raw data from multiple sources into a single image. At the pixel level, LIDAR-derived DEMs have been included as a component band with HSI to classify coastal habitats, resulting in improved classification accuracies (Chust et al., 2008; Collin et al., 2010). Feature level fusion requires the extraction of different features from the source data before features are merged together so that fusion takes place on features that match some selection criteria. At the feature level, LIDAR-derived DEMs have been used as data layers in object orientated classifications of marsh habitats (Brennan and Webster, 2006; Gilmore et al., 2008). Decision level fusion combines the independent results from multiple sources in a GIS to produce a final fused decision (Pohl and Van Genderen, 1998). LIDAR-derived DEMs have been fused with land cover classifications *post hoc* to refine and improve classification products (Lu and Weng, 2004; Pahl and Mather, 2003), to extract marsh species elevation ranges and distributions (Morris et al., 2005; Sadro et al., 2007), monitor the spread of invasive species (Rosso et al., 2006), model species habitat (Moselund et al., 2011; Sellars and Jolls, 2007), and predict sea level rise impacts (Webster et al., 2006).

The above studies have all used image fusion for classification purposes or for extracting additional elevation information. However, none have used elevation data to modify their existing classification of salt marshes. In the case of *S. alterniflora*, the three height classes are spectrally similar but they occupy different elevations in salt marshes and require significantly different correction factors (ranging from 0.05 to 0.25 m, Hladik and Alber, 2012). We therefore expect that the *Spartina* problem could potentially be reduced through the use of a decision tree that incorporates both spectral and elevation data. A decision tree is a nonparametric multistage or hierarchical classifier that can be applied to a single image or multiple co-registered images (Breiman et al., 1984). Using a multistage approach, a decision tree breaks down a complex decision into a series of nodes, or branches, where binary decisions are made to sequentially subdivide the data into classes. In a top-down approach, the process continues moving down the tree until the final node is reached. Data sources that can be used in decision trees include classified images (such as products from MLC and SAM), DEMs and vegetation indices.

This paper describes our approach to fusing HSI of the salt marshes surrounding Sapelo Island, GA with a LIDAR-derived DEM at the decision level, combined with a decision tree, to modify habitat classification and elevation information to produce both an accurate habitat classification and DEM for the study area. Our objectives were: (1) to compare the accuracy of MLC and SAM to determine the optimal classification routine for mapping salt marsh habitats with HSI; (2) to improve vegetation classification accuracy and address the Spartina problem by incorporating elevation information in vegetation mapping through a decision tree; and (3) to fuse the final vegetation classification with a LIDAR-derived DEM to produce corrected DEM elevations. The method we outline is of specific use to those interested in developing accurate maps of salt marshes, but is also more broadly applicable as a demonstration of the combined power of LIDAR and HSI through an iterative data decision level fusion process.

2. Methods

2.1. Study site

This study included a total of 13.82 km^2 of salt marsh habitat in and around the Duplin River, a 13-km long tidal inlet that flows into Doboy Sound and forms the western boundary of Sapelo Island, Georgia, USA (UTM Zone 17 N, 471480 E 3473972 N, Figure 3.1). The river is surrounded by a complex of salt marshes, tidal creeks and back barrier islands. *S. alterniflora* is the dominant macrophyte in these marshes. For this study, *S. alterniflora* that was taller than 1 m was considered “tall”. Tall *S. alterniflora* can grow up to 2 m tall and is the dominant plant found along the regularly flooded creek banks in the low marsh. *S. alterniflora* that ranged from 0.50 m to 1.0 m tall was considered “medium” and plants < 0.5 m were considered “short” (Reimold et al., 1973; Figure 3.S1). Medium *S. alterniflora* dominates the mid-marsh and short *S. alterniflora* is found in the irregularly flooded high marsh. The high marsh contains a mixed community of *S. virginica*, *B. maritima, D. spicata* and short *S. alterniflora,* collectively termed marsh meadow or salt meadow (Wiegert and Freeman, 1990). Marsh meadow has dense canopies, generally less than 0.50 m tall. At the highest elevations along the upland fringe, *J. roemerianus* and *B. frutescens* become the dominant species. Canopy heights of *J. roemerianus and B. frutescens* range from 0.50 m to over 2 m tall.

2.2. Hyperspectral imagery

Airborne Imaging Spectrometer for Applications (AISA) Eagle hyperspectral imagery were acquired on June 20, 2006, by the Center for Advanced Land Management Information Technologies (CALMIT) (Figure 3.1, Table 3.1). AISA is a push-broom sensor with a 1000 pixel swath width (1 km swath width when flown at 1 m spatial resolution). The AISA sensor calculates the apparent at-platform reflectance by simultaneously measuring both downwelling and upwelling radiance (Specim Imaging LTD, 2011). The AISA sensor was mounted in a Piper Saratoga plane flown at 1650 m above ground level. It collected spectral data in 63 bands in the visible and NIR portion of the electromagnetic spectrum from 400-980 nm (9 nm average bandwidth, 2.3 nm Full Width Half Maximum spectral resolution). The high spectral resolution was selected to obtain continuous spectral data for better discrimination among the dominant marsh species, and the fine spatial resolution (1 m) was selected to minimize the number of mixed pixels. The AISA Eagle system includes an imaging unit mounted in the rear of the passenger compartment to allow a nadir view collection of upwelling radiance. A Specim FODIS diffuse light collector measured the downwelling irradiance signal and was used for percent reflectance estimates (at aircraft level) for each spectral band.

Imagery, solar downwelling data, and flight positional data (altitude, GPS coordinates, pitch, roll, and yaw) were simultaneously collected for each flight line (see http://calmit.unl.edu/champ for more detailed information). Four parallel flight lines of data were captured in a northeast to southwest alignment, for a total area of over 25 km^2. (Two of these were used in the current study.) The flight lines were acquired in mid-morning, to coincide with low tide (-0.09 m) and captured extensive areas of exposed intertidal mud. The aircraft was flown in a "racetrack" path, meaning that the plane turned around to refly parallel swaths at the same downtrack orientation and with approximately 30% overlap of adjacent swaths. Trimble AgGPS 132 receiver (Trimble, http://www.trimble.com) and Flightbar instruments allowed precise parallel swathing guidance for accurate navigation of specified flight line coordinates.

Initial post-processing of data was performed by CALMIT using the CaliGeo (Specim Imaging LTD) and Environment for Visualizing Imagery (ENVI) (EXELIS, www.exelisvis.com) software programs. The processing sequence for each flight line consisted of (1) radiometric corrections applied to raw imagery; (2) GPS and altitude data used to calculate and apply static geometric correction factors; (3) image rectification and geocorrection; and (4) image data produced with pixel values as normalized percent reflectance using the FODIS downwelling solar information. Imagery was atmospherically corrected using FLAASH (Fast-Line-of-sight Atmospheric Analysis of Spectral Hypercube), an atmospheric correction module for ENVI (Adler-Golden et al., 1999; Berk et al., 1998). Sensor and over-flight details can be found in Table 3.1. An initial product of the HSI was a normalized difference vegetation index (NDVI) image, which was used in the subsequent decision tree classification (section 2.7). NDVI uses the ratio of reflectance in the red and NIR wavelengths ($NDVI = (NIR_{799} - RED_{675}) / (NIR_{799} + RED_{675})$) to derive an index of plant vigour (Rouse et al., 1974). The subscript values are the wavelength band centers used to calculate NDVI for these HSI data.

2.3. LIDAR data

The National Center for Airborne Laser Mapping (NCALM) acquired 35 km^2 of LIDAR data for Duplin River marshes on March 9 and 10, 2009. Data were acquired when plant growth and biomass were seasonally low and during a spring low tide (-0.33 m) to maximize laser penetration of the vegetation canopy and minimize the amount of standing water on the marsh surface. Data were collected with an Optech GEMINI Airborne Laser Terrain Mapper (ALTM) mounted in a twin-engine Cessna Skymaster flown at an altitude of 800 m above ground level. The survey was conducted with a laser pulse rate frequency (PRF) of 125 kHz and up to 4 returns. The high PRF was used to obtain a target point density of 9 hits m^{-2}. Reported vertical and horizontal accuracies (root mean squared error (RMSE)) for the sensor are 0.05-0.10 m and 0.10-0.20 m, respectively (Optech, 2011). Absolute calibration was done using 662 ground control points (GCPs) surveyed with a vehicle-mounted kinematic GPS over paved roads near the Brunswick, GA airport. These same road sections were surveyed with crossing flight lines using the ALTM and the heights of the check points were compared to the heights of the nearest neighbor LIDAR points within a radius of 20 cm. The RMSE of height differences was 0.11 m, with a RMSE at the 95% confidence level of 0.20 m. LIDAR processing routines are described in Hladik and Alber (2012); sensor and over-flight details can be found in Table 3.1.

A bare earth LIDAR-derived DEM was produced in SURFER Version 8 (Golden Software, http://www.goldensoftware.com) at 1.0 x 1.0 m resolution using a kriging algorithm that calculated the mean elevation value of all laser hits within each grid cell with a maximum variance of 0.15 m. Elevations were all positioned in the NAD 83 reference frame and projected into UTM coordinate zone 17 N. Elevations are NAVD 88 orthometric heights (in meters) computed using the National Geodetic Survey GEOID 03. The LIDAR-derived bare earth DEM product was used in the current analysis.

The LIDAR-derived DEM covered the same area as the HSI data; however, there was an almost 3 year lag between HSI (2006) and LIDAR (2009) acquisition dates. An RGB composite image of the HSI was compared to a 2009 aerial photograph of the same area to assess whether plant community boundaries or ground survey data locations had shifted during this interval. We found no discrepancies or shifts in the dominant salt marsh vegetation between these images and do not think the difference in HSI and LIDAR acquisition dates affected the results of this study.

2.4 Supporting field surveys

2.4.1 HSI field survey

We carried out an extensive field survey of 373 plots with horizontal submeter differential GPS (DGPS) positions (Trimble Geo-XH DGPS) coincident with the AISA hyperspectral flyover. Plots were positioned along 24 transects that spanned the marsh elevation gradient from low marsh to high marsh. Within each plot, all species present within a 1 x 1 m quadrat were documented and a dominant habitat type was assigned based on percent cover (Schalles et al., Unpublished Data). Seven vegetation cover classes were included in the classification: *S. alterniflora* (short (SS), medium (SM) and tall (ST) height classes), *J. roemerianus* (JR), *B. maritima* (BM), *S. virginica* (SV) and *B. frutescens* (BF) and two non-vegetated classes (intertidal mud (MUD) and salt pan (SALT)) (Figure 3.S1). The *S. virginica* class generally represented a mixture of high marsh plants, including *B. maritima, D. spicata* and short *S. alterniflora*, and as such, was rarely composed of only *S. virginica*. Intertidal mud consisted of patches of mud ≥ 1 m^2 within the vegetated portion of the salt marsh as well as mud on creek banks at elevations below tall *S. alterniflora*. Salt pans were high marsh habitats with hypersaline sediments and less than 25% vegetation cover. An additional 468 plots were surveyed in a similar manner in June and July 2007.

Vegetation stand polygons were delineated in the field for HSI training and validation purposes between September 2006 and August 2007. Relatively homogenous stands of each vegetation class were selected and mapped using a DGPS by walking a polygon area within respective stands, taking care to avoid boundaries between vegetation classes. These polygon data were brought into ENVI as Regions of Interest (ROIs) and included in the training and validation data sets. These field-based polygons were augmented with user-defined ROIs selected based on our knowledge of plant distributions and image interpretation. These additional ROIs were necessary to attain a range of 10 n to 100 n training pixels for each cover class (n = number of bands), to improve estimates of class means and covariance matrices (Lillesand et al., 2004). Note that although some user-defined training locations were a heterogeneous mix of cover classes, the dominant habitat class (based on percent cover) was assigned to each pixel. This was done to include training data that represented the full range of spectral variability for each cover class throughout the entire image, recognizing that in reality most pixels are not pure.

All data (plot points, field-based polygons and user-defined ROIs) were randomly divided into training (33923 m^2 pixels) and validation data sets (10701 m^2 pixels) using the ArcGIS version 9.3 software program (http://www.esri.com), with approximately 75% of the data reserved for supervised classifier training and 25% for validation of the classification results.

2.4.2 RTK field survey

To ground truth the LIDAR-derived DEM, a high-accuracy real time kinematic (RTK) survey was conducted using a Trimble R6 RTK GPS receiver (Trimble, 2009) with an observed vertical RMSE of 0.0037 m, a mean vertical error of 0.010 and mean horizontal error of 0.012 m (all reported at 68% percent confidence level). RTK elevations are NAVD 88 orthometric heights (in meters) computed using the National Geodetic Survey GEOID 03 (see Appendix A for elevations in relation to tidal datums). As reported previously (Hladik and Alber, 2012), RTK GCPs were collected throughout the Duplin River marshes in a survey that encompassed all of the vegetation cover classes considered in the HSI classification (section 2.4.1, Figure 3.S1). RTK Data were collected in March 2009 coincident with LIDAR data acquisition and additional data were collected from June to August 2009. Sampling locations were randomly selected using the ArcGIS 9.3 software program and a preliminary HSI vegetation classification of the Duplin River salt marshes (although if an area was misclassified it was corrected). At each GCP location the RTK Rover foot was placed flush with the marsh surface without disturbing the sediment and vegetation. The number of RTK points sampled per cover class ranged from 53 (intertidal mud) to 267 (medium *S. alterniflora*) (Table 3.2). This range in sampling was primarily due to the relative dominance of the various cover classes in the marsh. Additional GCPs were also collected opportunistically. In total, 1830 RTK GCPs were acquired and were used for two purposes: to determine the elevation range of each marsh cover type for use in the decision tree analysis (section 2.7), and to derive correction factors for DEM modification (section 2.9). The data were randomly divided into training and validation data sets using ArcGIS. Seventy-five percent (N = 1380) of the RTK GCPs were used to calibrate the elevation ranges and correction factors (Table 3.2) and 25% (N = 450, Figure 3.1) data were reserved as validation data for the modified DEM accuracy assessment (section 2.9).

2.5. Overview of work flow

The work flow employed in this study used a two-step classification routine followed by DEM modification (Figure 3.2). In the first step, two standard supervised classification algorithms (MLC and SAM) were used to classify the HSI based on spectral reflectance characteristics in the visible and NIR. The second step combined the classification results from step 1 with both the LIDAR-derived DEM and HSI-derived NDVI to modify classifications. NDVI has been shown to aid in the separation of vegetated (*S. alterniflora*) versus non-vegetated pixels (mud) since vegetation has a high NDVI value and mud has a low NDVI value (Yang and Artigas, 2010). This second classification iteration was used to correct misclassifications between the various cover classes, especially between the three height classes of *S. alterniflora* and mud pixels (the *Spartina* problem). Following the second classification, the accuracy of both the final MLC and SAM classifications were assessed. Finally, the best classification was fused with the LIDAR-derived DEM at the decision level, and cover class-specific correction factors were applied for DEM modification. The end products of this work flow were both a final habitat map (product of the first data fusion) and a corrected DEM of the study area (product of the second data fusion).

2.6 Initial hyperspectral supervised classification

All image analyses were conducted using ENVI version 4.8. Each of the two flight lines were processed and classified independently and then mosaiced together for the final classified habitat map. Prior to classification, a water and upland mask were applied to the data so that only the salt marsh areas of interest were classified. During the initial stages of HSI preprocessing, data masking of surface water pixels was accomplished using wavelength-specific reflectance differences in a NIR band (858 nm), with reflectance values lower than 6.5% identified as water. Remaining marsh and non-marsh upland areas were separated manually using analyst image interpretation and a digitizing tablet. This manual technique was used because non-salt marsh herbaceous vegetation in adjacent upland areas was confused with marsh vegetation in automated masking attempts.

To carry out the supervised classifications, the mean spectra (Figure 3.S2) for each cover class was calculated from training pixels (section 2.4.1). The success of the classifier is dependent on using unique spectral signatures for each cover class identified in the training data. To evaluate this, we computed the Jeffries-Matusita distance and Transformed Divergence separability measures for each cover class. Larger values (greater than 1.9, on a scale of 0 to 2) indicate good separability (Richards and Jia, 2006). In our data, training data pairs had values greater than 1.9 for both measures except the short *S. alterniflora* and medium *S. alterniflora* pair, which had a value of 1.62 for the Jeffries-Matusita distance measure (Table 3.S1). However, short and medium *S. alterniflora* were kept as two distinct classes in this analysis as it is recommended that only pairs with values less than one be combined (Richards and Jia, 2006).

Both SAM and MLC routines were used to classify salt marsh habitats. Both classifiers require the user to specify thresholds for class membership, and then pixels are assigned to the class that has the greatest probability of membership. The MLC probability threshold was set to 0.95, which means that each pixel must have a 95% probability of belonging to a specific cover class or it remains unclassified. The spectral angle threshold for the SAM classification was set at 0.15 radians, which means that if angles are smaller than this in comparison to an endmember spectra, then it is considered a match. Pixels with angles larger than the specified threshold remain unclassified.

2.7. Data fusion: Decision tree classification

The results of both the MLC and SAM classifications were fused with the LIDAR-derived DEM and classifications were refined through a decision tree that evaluated both spectral and elevation information. Note that both the HSI and DEM had the same grid cell size (1 m) and were spatially aligned by forced co-location whereby HSI coordinates were "snapped" to the DEM raster coordinates. We used three input bands in the decision tree classification: the initial MLC or SAM classification, the DEM image and a NDVI image. The expected elevation ranges for each cover class were informed by the ranges obtained in our RTK ground survey data (section 2.4.2), extended using ± one standard deviation to account for the possibility that the RTK survey did not sample the entire range of habitat class elevations. All elevations in the decision tree are NAVD 88 orthometric heights (in meters). Following the decision tree classification, a majority filter (ENVI Majority/Minority Analysis module within Post-Classification routines) was applied to each SAM and MLC classification output to remove isolated pixels with a 5x5 moving window and create a more coherent classified image by removing the "salt and pepper" appearance.

The decision tree was straightforward for all classes except the three height classes of *S. alterniflora*. For all vegetation classes and areas classified as mud, the decision tree reassigned all pixels with an elevation less than -1.2 m as unclassified. This was done because -1.2 m was the lowest elevation for exposed creek bank areas based on RTK survey data and, as such, any areas lower than -1.2 m would have been inundated at the time of LIDAR data acquisition. LIDAR-derived DEM elevations in areas with standing water are assumed to be unreliable (Maune et al., 2007; Raber et al., 2007), so these areas were effectively masked out using the decision tree, in addition to those areas already masked during HSI preprocessing (section 2.6). For areas initially classified as salt pan, the decision tree reassigned pixels with an elevation less than 0.8 m into a new shell class. This was done because salt pan and shell have similar spectral characteristics, but 0.8 m was the minimum observed RTK elevation for salt pans. Our knowledge of habitat distributions in the marsh supports this separation as oyster reefs are found in low-lying areas in the study site.

More complicated decision tree nodes were created for areas between -0.26 and 1.25 m elevation initially classified as tall, medium or short *S. alterniflora* (Figure 3.3). Pixels initially classified as tall *S. alterniflora* in the MLC (or SAM) classification were reassigned to the medium *S. alterniflora* class if they had a corresponding DEM elevation greater than tall *S. alterniflora's* maximum elevation (plus 1 standard deviation) observed in the RTK survey. Pixels with elevations less than the maximum were then evaluated based on whether or not their elevation was greater than the minimum observed elevation (minus 1 standard deviation). If so, they were kept in the tall *S. alterniflora* class. If not (which means they were at lower elevations), they were assessed based on NDVI. An NDVI cutoff of 0.30 was used to distinguish between mud and vegetated areas because tall S. *alterniflora* has a high NDVI value and mud has a very low index value. Pixels with an NDVI value greater than 0.30 remained classified as tall *S. alterniflora* and those less than 0.30 were classified as either mud or unclassified based on the minimum DEM elevation cutoff of -1.2 m.

At the medium *S. alterniflora* node, pixels initially classified as such were first evaluated based on medium *S. alterniflora's* minimum DEM elevation (minus 1 standard deviation). Pixels with elevations greater than the minimum remained classified as medium *S. alterniflora* class. Note that the RTK survey did not support the separation of medium and short *S. alterniflora* based on medium *S. alterniflora's* maximum observed elevation, and therefore maximum elevation was not included in the decision tree. Pixels with elevations less than the medium *S. alterniflora* minimum elevation were then assessed based on whether or not their elevations were greater than the minimum tall *S. alterniflora* elevation (minus 1 standard deviation). In either case, pixels were evaluated by NDVI. If elevations were greater than the minimum for tall *S. alterniflora* and NDVI was greater than 0.30, plants were classified as tall *S. alterniflora* whereas if the NDVI was less than 0.30 they were reassigned to mud. If pixel elevations were lower than had previously been observed for tall *S. alterniflora* but their NDVI was greater than 0.30, they were classified as tall *S. alterniflora*, whereas if NDVI was less than 0.30 they were assigned to either mud or unclassified (based on the minimum of -1.2 m).

Short *S. alterniflora* class membership was first assessed based on whether or not corresponding pixel elevations were greater than the minimum short *S. alterniflora* elevation observed in the field (minus 1 standard deviation). If so, they remained classified as short *S. alterniflora*. If not, they were assessed based on medium *S. alterniflora's* minimum elevation. If they met this criterion, they were reclassified as medium *S. alterniflora*. If not, they were assessed based on tall *S. alterniflora's* minimum elevation and reclassified as tall *S. alterniflora* if they met this criterion. Otherwise they were reassigned to either mud or unclassified based on the minimum of -1.2 m.

2.8. Hyperspectral classification accuracy assessment

Classification accuracy of the decision tree output was evaluated by constructing a confusion matrix using the reserved validation data (section 2.4.1) and calculating the overall accuracy and kappa coefficient (Congalton, 1991). The overall accuracy is the ratio of the number of validation pixels that are correctly classified to the total number of validation pixels regardless of their class (Foody, 2002). The kappa coefficient is the proportion of correctly classified validation pixels and is considered more robust than overall percent accuracy because it takes into account chance agreement (Rosenfield and Fitzpatrick-Lins, 1986). The producer's and user's accuracies, as well as the errors of commission and omission for individual classes, were also used to evaluate classifier performance. The producer's accuracy is the probability that a ground truth pixel for a cover class is correctly identified as that class in the classified image. The user's accuracy is the probability that a pixel in the classified image really belongs to the assigned class on the ground. Errors of commission represent the percentage of pixels that belong to another class but which are classified as belonging to the target cover class, whereas errors of omission indicate the percentage of pixels that belong to the ground truth class but which the classifier has failed to classify as such. A good classification should have high producer's and user's accuracies and low errors of commission and omission. We also evaluated accuracy qualitatively based on user knowledge of the study area.

2.9. Data fusion: DEM modification and accuracy assessment

The classification with the highest overall accuracy and kappa coefficient was fused at the decision level with the unmodified LIDAR-derived DEM and the DEM correction factors for the purpose of correcting the DEM (on a HSI classification polygon-to-polygon basis). The HSI classification and the DEM were aligned by forced co-location (see section 2.7) prior to DEM modification. As described in Hladik and Alber (2012), class-specific correction factors were derived for the same area as this study from the RTK training data set (N = 1380, section 2.4.2) by subtracting the surveyed RTK elevation from the DEM elevation at the corresponding x/y coordinate of each GCP. Corrections represented the mean error for each cover class (Table 3.2). To modify the DEM, the final HSI classification was exported as a polygon shapefile from ENVI and brought into ArcGIS. Next, the classification vegetation polygons were converted to raster format using the Polygon to Raster tool (Conversion toolbox), by assigning a cover class-specific correction factor to each polygon. The end product of the Polygon to Raster step was a "Correction Factor" DEM with values corresponding to the cover class-specific correction factors. The "Correction Factor" DEM was then subtracted from the original, "Unmodified" DEM using the Raster Math tool in ArcGIS (Spatial Analyst toolbox) to produce a "Modified" DEM. It should be noted that since the method used here applied different corrections to discrete portions of the marsh, it did create unrealistic "steps" in the surface of the marsh (for example, when going from short to medium *S. alterniflora*) which would require smoothing at class boundaries prior to some modeling applications.

We performed accuracy assessments on both the "Modified" and "Unmodified" DEMs using the reserved RTK survey validation data (N = 450), which had not been used to derive the correction factors. For each GCP location, the RTK elevations were assumed to be the true observed ground elevations and the elevations extracted from the DEM were used as predicted elevations. To examine the accuracy of the DEM elevation, we calculated the mean error, RMSE, the fundamental vertical accuracy (FVA) with a 95% confidence level and 95th percentile errors for each cover class following American Society for Photogrammetry and Remote Sensing guidelines (ASPRS Lidar Committee, 2004). The vertical RMSE, as described in Maune et al. (2007), is a common measure of vertical accuracy for LIDAR-derived DEM and is calculated as:

$$\text{RMSE} = \text{sqrt}\,[\textstyle\sum (\, z_{LIDARi} - z_{RTKi})^2/n] \qquad (3.1)$$

where z_{LIDARi} is the elevation of the i^{th} RTK GCP in the LIDAR-derived DEM; z_{RTKi} is the i^{th} elevation of the i^{th} GCP in the RTK data set; n is the number of GCP; and i is an integer from 1 to n. The FVA at a 95% confidence level was calculated as RMSE*1.96. The 95th percentile errors are the interpolated absolute value of elevation errors obtained by dividing the distribution of errors into one hundred groups of equal frequency. The 95th percentile means that 95% of the elevation errors have a value equal to or less than the 95th percentile value (Maune et al., 2007).

Modified DEM elevations from each cover class were compared to RTK elevations using paired t-tests. The calculated RMSE for each cover class in the DEM was also compared to the reported vertical RMSE of the LIDAR sensor (0.11 m based on vehicle mounted GPS absolute calibration) to determine whether it was within the range of instrument error. Statistical results for all analyses in this study were considered significant when $p \leq 0.05$. All statistical analyses were done using the open source program R version 2.10.1 (http://cran.r-project.org/).

3. Results

3.1. Overview of results

As described below, the MLC classification performed significantly better than SAM. Most vegetation classifications were only slightly improved by the fusion of the HSI and DEM and the application of the decision tree, but there was clear improvement in the identification and separation of mud and tall *S. alterniflora* at creek edges as well as better separation of mud and medium *S. alterniflora* pixels. When fused with the best decision tree classification, the overall mean error of the modified DEM decreased from 0.10 m to -0.003 m.

3.2. Objective 1: Comparison of MLC and SAM

Our initial classification of the HSI showed that MLC had a higher overall accuracy than SAM (89% versus 59%, Tables 3.S2 and 3.S3). These accuracies changed only slightly after the application of the decision tree (MLC improved from 89% to 90% and SAM from 59% to 61%, Tables 3.S2, 3.S3, 3.3 and 3.4) and only the final classifications (post-decision tree application) are presented here.

3.2.1 Maximum likelihood classification

Class cover distributions in the MLC results were consistent with the typical zonation patterns for Southeastern salt marshes with tall *S. alterniflora* at lower elevations and *J. roemerianus* and *B. frutescens* at higher elevations (Figure 3.4). In terms of areal extent, medium *S. alterniflora* was the dominant habitat class, covering 47% of the classified marsh area (Table 3.5). Together, the three *S. alterniflora* height classes represented 82% of the Duplin River marshes (when Unclassified areas were excluded). Mud covered 9% of the marsh area, *J. roemerianus* and *S. virginica* were 5% each and *B. frutescens*, *B. maritima* and salt pan each covered less than 2%.

The MLC performed well, as seen in the confusion matrix results (Tables 3.3 and 3.4). Overall accuracy was 90% and the kappa coefficient was 0.88. There were no unclassified pixels, and producer's and user's accuracies ranged from 80 to 99% for all cover classes. Areas classified as salt pan (99%) and *B. frutescens* (96%) had the highest producer's accuracies, whereas *S. virginica* (80%) and short *S. alterniflora* (86%) had the lowest. The largest error of commission was *B. maritima* (14%) and the greatest error of omission was *S. virginica* (20%), indicating that *B. maritima* was over-classified whereas *S. virginica* was under-represented in the final MLC classification.

Seven percent of validation pixels were misclassified, ranging from 0% to 12% for each cover class pairing (Table 3.3). The confusion matrix revealed notable misclassifications among the three height classes of *S. alterniflora*: 6% of medium *S. alterniflora* validation pixels were misclassified as short *S. alterniflora*; 12% of short *S. alterniflora* pixels were misclassified as medium *S. alterniflora;* and 5% of tall *S. alterniflora* pixels were misclassified as medium *S. alterniflora*. *S. virginica* had the lowest classification accuracies and was most often spectrally confused with other classes, most notably as *B. maritima* (7%), medium *S. alterniflora* (7%) and salt pan (5%). Additionally, 6% of *B. maritima* pixels were classified as *B. frutescens* and 11% of mud pixels were classified as short *S. alterniflora.*

3.2.2. Spectral angle mapper classification

In contrast to MLC, spatial distributions in the SAM classification were not consistent with typical spatial patterns, largely due to the over-representation of *S. virginica* and *B. frutescens* at the expense of medium and tall *S. alterniflora* (Figures 3. 3 and 3.4). SAM performed poorly with a low overall accuracy of 61% and kappa coefficient of 0.55. Unlike MLC, 1% of validation pixels were unclassified, the majority belonging to the mud class. This indicates that the SAM angle for those pixels exceeded the specified threshold whereas the MLC threshold was not surpassed and could classify the same pixels. SAM class producer's and user's accuracies ranged from 35% to 89%. Mud and *J. roemerianus* had the highest producer's accuracies (89% and 88%, respectively), whereas the lowest producer's accuracies were for medium *S. alterniflora* and tall *S. alterniflora* (43% and 58%, respectively). Of note, the user's accuracy for tall *S. alterniflora* was 90%, and represented the highest accuracy value for the entire SAM classification. The errors of commission and omission confirmed the over-classification of *S. virginica* and *B. frutescens* and the under-representation of medium and tall *S. alterniflora*.

The poor performance by SAM is also evidenced by the percentage of validation pixels misclassified, which had an overall error rate of 39% and ranged from 0% to 27% per cover class pairing in the confusion matrix (Table 3.3). Like MLC, there was confusion between the three *S. alterniflora* height classes; however the percent of SAM pixels misclassified are much larger than MLC. Additionally, tall and medium *S. alterniflora* was misclassified as *S. virginica* and *B. frutescens* in the SAM classification.

3.3. Objective 2: Data fusion of elevation data with decision tree results

The application of the -1.2 m minimum elevation mask had little effect on the four non *S. alterniflora* classes with only 0.002% of all *B. frutescens*, *B. maritima*, *J. roemerianus* and *S. virginica* pixels reclassified as unclassified (Table 3.5). However, application of the mask had a greater effect on the mud class as 38% of those pixels were reassigned to unclassified. The majority of the reclassified mud pixels were exposed creek bank areas. Seventeen percent of salt pan pixels were reclassified as shell, as they had corresponding elevations less than 0.8 m.

The individual elevation-based decision trees for tall, medium and short *S. alterniflora* show the percent of pixels that were assigned to each class (Figure 3.3). Of the pixels initially classified as tall *S. alterniflora*, 1.4% were reassigned to medium *S. alterniflora*, 0.5 % to mud and less than 0.1% to unclassified. Of the pixels initially classified as medium *S. alterniflora*, 7% were reclassified as tall *S. alterniflora*, 3% as mud and 0.05% as unclassified. Only 1% of short *S. alterniflora* pixels were reassigned as medium *S. alterniflora*, 0.4% as tall *S. alterniflora*, 0.3% as mud and 0.9% as unclassified. Taken together, these reclassifications of *S. alterniflora* and mud only affected 10% of all pixels, thus it did not have a large effect on the overall accuracy of the habitat classification (e.g. MLC accuracy improved from 89% to 90%).

The majority of the reclassified pixels occurred in the upper portion of the Duplin River, and it is instructive to focus on this area, which has a high density of small creeks and is predominately classified as tall or medium *S. alterniflora* or mud. We selected three locations within this portion of the marsh, each with an area of 0.15 km^2, which exemplified the effects of the decision tree on class distributions (Figures 3.4 and 3.5). In these example areas, there were 8 to 14% gains in tall *S. alterniflora* pixels, 12 to 22% losses in medium *S. alterniflora* pixels, and 0.004 to 5% changes in pixels classified as mud following use of the decision tree (Table 3.5, ‘Change in Total Proportion’ column). When expressed as a proportionate change per class, however, there were substantial increases in areas classified as both tall *S. alterniflora* (50-300%) and mud (2-29%) and corresponding losses in areas classified as short (32-70%) and medium *S. alterniflora* (20-33%) (Table 3.6, ‘Change in Proportion Per Class’ column) The majority of the reclassification involved medium *S. alterniflora* being reclassified as tall because the pixels occurred in low elevation areas where medium *S. alterniflora* is not observed, and mud pixels changed to unclassified because they occurred in areas less than -1.2 m.

3.4. Objective 3: DEM modification and accuracy assessment

In keeping with our previous observations (Hladik and Alber, 2012), elevations in the unmodified LIDAR-derived DEM were over-predicted in comparison to RTK validation data. The amount of overestimation varied by cover class, but taller and denser vegetated cover classes had larger errors. Elevations in the unmodified DEM were significantly different than the RTK ground elevations for all cover classes except for mud and salt pan (Table 3.6, Figure 3.6A). The RMSE for short *S. alterniflora*, intertidal mud, *B. maritima, S. virginica* and salt pan, were all within the reported vertical accuracy of the LIDAR sensor (0.11 m). However, the overall RMSE of the unmodified DEM (0.15 m), as well as those for tall and medium *S. alterniflora*, *J. roemerianus* and *B. frutescens* all had RMSE that exceeded instrument error, with the greatest RMSE for tall *S. alterniflora* (0.34 m).

The overall mean error in the modified DEM, calculated using the RTK validation data, was substantially reduced to -0.003 ± 0.10 m (SD) (Table 3.6, Figures 3.6B and 3.7) compared to the unmodified DEM. The largest error reduction was for tall *S. alterniflora,* where mean error decreased from 0.28 to 0.08 m. Similarly, *J. roemerianus* error was reduced from 0.16 to -0.005 m in the modified DEM. Elevations were slightly under-predicted (-0.0001 to -0.05 m) for all cover classes except tall *S. alterniflora* and *B. maritima* in the modified DEMs, but no classes were significantly different in comparison to RTK GCPs (Table 3.6, Figure 3.6B). Overall RMSE (0.10 m) and RMSE for all cover classes, except tall *S. alterniflora* (0.22 m), fell within the reported instrument vertical RMSE in the modified DEM.

4. Discussion

4.1. Objective 1: Classifier performance

The integration of the LIDAR-derived DEM with the MLC classification of the HSI produced a habitat map of the Duplin River salt marshes with an overall accuracy of 90%, as compared to 61% when the SAM classifier was used (Figure 3.4). The MLC had higher kappa coefficient values, and greater class producer's and user's accuracies. As demonstrated in the confusion matrices (Tables 3.3 and 3.4), MLC more accurately classified each of the nine cover classes compared to SAM. In particular, SAM had substantially greater misclassifications for medium and tall *S. alterniflora,* largely due to greater confusion between those classes and *S. virginica, J. roemerianus* and *B. frutescens*. Indeed, some of the largest discrepancies in the SAM classification were related to the over-classification of *S. virginica* and *B. frutescens* in areas where medium and tall *S. alterniflora* are typically found.

Although a few studies have successfully used SAM in salt marshes (Marani et al., 2003; Marani et al., 2006; Merani, 2007), our findings support the results of previous studies that compared SAM and MLC classification performance (Belluco et al., 2006; Rosso et al., 2006). In heterogeneous salt marshes, SAM is generally unable to handle under-represented classes and mixed pixels, as well as variations in vegetation density, cover, height, and leaf orientation (Belluco et al., 2006; Jollineau and Howarth, 2008). Belluco et al. (2006), in their classification of Lagoon of Venice salt marsh vegetation, attributed MLC's superior results to the high quantity and quality of the training data and to the high spatial and spectral resolution of the sensor, which enabled spectral separation of heterogeneous areas. MLC calculates the within- and between-class variability (variance and covariance) of the training sites and as a result, assuming a large enough sample size, can better separate mixed assemblages. Belluco et al. (2006) also note the over-classification of *J. roemerianus* in SAM classifications and suggest that because *J. roemerianus* training pixels were typically mixed, SAM interpreted any mixed pixel whose spectra did not match any other class as *J. roemerianus*. This reasoning could explain the large percent of pixels erroneously assigned to *J. roemerianus* in the SAM classification in this study, as well. Similar reasoning might explain *S. virginica* since it also represented a mixed cover class.

The highest overall MLC accuracy attained in this study was 90%, with a kappa coefficient of 0.88 and class producer's accuracies ranging from 80 to 99% (Table 3.4). These results are quite good and suggest that our approach is robust. Previous studies classifying salt marsh habitats have attained a range of accuracies, from 59 to 99% (Rosso et al., 2006; Sadro et al., 2007; Wang et al., 2007). The highest reported accuracies were in the Lagoon of Venice, where Belluco et al. (2006) and Marani et al. (2006) had class producer's accuracies ranging from 75 to 99% using SAM and MLC. Those studies classified four salt marsh species (*Spartina maritima*; *Limonium*, *Salicornia* and *J. roemerianus*), in addition to mud and water. Belluco et al. (2006) used data from a variety of airborne sensors to test numerous classification algorithms, including MLC and SAM, and achieved the highest class accuracies for *S. maritima* (98%) and *Limonium* (98%) using MLC. Marani et al. (2006) found that SAM classified *Limonium* (98.5 %) and *S. maritima* (97.9%) with the greatest accuracies.

4.2. Objective 2: Data fusion and application of decision tree

This study tested a hybrid approach that combined MLC and decision tree algorithms to fuse LIDAR-derived topographic and spectral information. A high accuracy vegetation classification map was essential for performing the final DEM correction as the classification determined the boundaries by which correction factors were applied for each pixel of the map. Moreover, accurate classification of the creek-marsh interface was necessary for the proper representation of topography. The greatest challenge in classifying the salt marsh vegetation was to separate the different height classes of a single species, *S. alterniflora*, which is something that previous studies have not done. Given that the height classes of *S. alterniflora* are continuous rather than trimodal, it not unreasonable for them to be spectrally confused or misclassified. Although the decision tree did not appreciably improve overall classification accuracies, it did produce small gains in separating the three height classes of *S. alterniflora* and mud (Tables 3.3, 3.S2 and 3.S3). The majority of changes were seen in the upper part of the study area where tall and medium *S. alterniflora* are highly mixed with mud areas (Table 3.5, Figure 3.5). In these areas the decision tree produced a more accurate representation of the marsh: low-lying areas on the edges of creeks, which were classified as medium *S. alterniflora* in the initial classification (darker blue areas in Figure 3.5), were reassigned to mud with a border of tall *S. alterniflora*, which meets our expectations. Unfortunately, we did not have many GCPs in the areas that showed the most change due to the difficulty of assessing these low-lying parts of the marsh, so we do not have validation pixels to quantify accuracy in these areas specifically. Had validation data been available in these areas, we believe that the application of the decision tree would have resulted in larger gains in classification accuracy.

The reclassification of 38% of HSI generated mud pixels to "unclassified" for DEM elevations below -1.2 m illustrates an obvious coastal classification issue; i.e. the overall extent of exposed intertidal mud habitat is dependent on low tide stage at the time of image (or data) capture. Indeed, the areas of mud reclassified in Figure 3.5 bordered water-masked channel areas. Obtaining LIDAR on a low spring tide, as in this study, allows prediction of these exposed mud areas at higher water stages.

Classification of salt marsh habitats using image fusion techniques have generally produced higher accuracy results. Using a LIDAR-derived DEM and multispectral imagery, Chust et al. (2008) classified a coastal wetland with 88% accuracy. Similarly, Collin et al. (2010), using dual-band LIDAR and multispectral imagery, attained MLC accuracy of 92%. Geerling et al. (2007) mapped floodplain vegetation with 81% accuracy when they used LIDAR-derived DEMs in combination with HSI. These studies have all focused on the fusion of visible imagery with DEM elevations prior to classification. Our approach is unique in that we fused the two data sources via a decision tree after the visible imagery was initially classified. To our knowledge, no prior studies have addressed or ameliorated the *Spartina* problem as effectively as our approach of data fusion through a decision tree. The different height classes of *S. alterniflora* vary in biomass, productivity, carbon storage and palatability to herbivores (Goranson et al., 2004; Morris and Haskin, 1990; Turner, 1976), making their distinction important at the ecosystem scale. Accurate habitat maps are especially important at the creek bank-marsh interface (where mud and tall *S. alterniflora* intersect), for estimates of overbank flooding and transport of materials such as carbon and minerals through small tidal creeks, as well as the exchange of carbon, minerals and groundwater across the interface (Bouma et al., 2005; Townend et al., 2010; Zedler, 2001). Additionally, tall *S. alterniflora* stands are vulnerable to creek bank erosion and wrack deposition, making high accuracy habitat delineations useful for identifying these disturbances.

4.3. Objective 3. DEM modification and accuracy assessment

The second data fusion with the hyperspectral classification and application of class-specific correction factors to the LIDAR-derived DEM greatly improved the accuracy of the DEM (Figure 3.7). The overall mean DEM error was reduced from 0.10 to -0.003 m and the RMSE from 0.15 to 0.10 m. Applying the cover class-specific correction factors brought all DEM elevations in line with their true RTK elevations (Table 3.6, Figure 3.6B). These findings are in agreement with the results of DEM modification at four test sites within the Duplin River marshes using the same derived correction factors (Hladik and Alber, 2012). The slight negative value for the overall error indicates that the correction factors produced a DEM surface that was slightly lower than RTK elevations, but is within instrument error. The reduced errors in the modified DEM are less than the elevation differences between vegetation classes, making the corrected DEM appropriate for use in salt marsh studies where small differences in elevation can have important ecological effects.

The DEM correction method used in this study combined a hyperspectral classification with the DEM to modify DEM elevations by informing the DEM of the data fusion-derived HSI classifications. Sadro et al. (2007) used a similar approach and reported reduced LIDAR-derived DEM errors for extracted elevation values following the application of species-specific corrections in combination with an AVIRIS classification of a California salt marsh composed mostly of high marsh plants. Following correction, the authors found no mean difference between survey and extracted LIDAR-derived DEM elevations, with an overall RMSE of 0.06 m. The Sadro et al. (2007) study did not modify the actual DEM surface, but rather modified extracted elevations according to species-specific offsets. In contrast, we applied correction factors to modify the DEM and then performed a rigorous accuracy assessment.

Another approach to correcting LIDAR without data fusion is the analysis of LIDAR LAS point clouds and generation of a new LIDAR-derived bare earth DEM surface. Wang et al. (2009) used statistical techniques to better differentiate ground and canopy returns in marsh vegetation, while other authors (Schmid et al., 2011; Toyra et al., 2003) have experimented with various DEM interpolation algorithms to produce the most representative ground surface. The errors in these efforts, however, were generally greater than, or comparable to, those reported here. The current study shows that image fusion is an accurate and viable alternative for DEM correction.

5. Conclusion

Accurate habitat and elevation maps of salt marsh habitats are important for many applications, but existing methodologies have significant errors. This study demonstrates the applicability of data fusion for both salt marsh habitat delineation and LIDAR-derived DEM correction. The hyperspectral classification, when combined with the LIDAR-derived DEM through a decision tree, produced a habitat map with a 90% overall accuracy. Prior studies have noted the difficulty in correctly classifying *Spartina* areas but have not provided a solution to reduce class confusion. This study was not only comparable to previous efforts in terms of accuracy (*S. alterniflora* accuracy of 94.5%), but also provided a method for minimizing the *Spartina* problem. Fusing the classification with the DEM to apply cover class-specific elevation correction factors resulted in large reductions in mean error for nine cover classes with an overall mean error of -0.003 m. The data fusion approach used here minimized problems with both hyperspectral and LIDAR approaches, and represents a significant advance over evaluating hyperspectral and LIDAR data independently.

6. Acknowledgments

We thank Kristen Anstead, Caitlyn Connor, Nick Scoville and Jacob Shalack for all of their assistance with the RTK survey. We thank George Alfayo, Hongyu Guo, Ken Helm, Geoff Hemenway, Trey Kenemer, Megan Machmuller, Paul Merani, Evan Milton, Daniel Saucedo, Jim Schalles, Maria Volkmer Steele, and Kazimierz Więski for field assistance in the 2006 and 2007 HSI marsh surveys; Rick Perk and Mark Steele for flight planning and AISA data acquisition and initial processing; John Carpenter with assistance in GIS procedures and data analysis; Jon Garbisch, Bill Miller, and Mary Price and other staff for logistical support at the University of Georgia Marine Institute; and Aimee Gaddis for logistical support, Fred Hay, Dorsett Hurley and other staff at the Sapelo Island National Estuarine Research Reserve. This research was supported by the Georgia Coastal Ecosystems LTER Project (NSF Award OCE-0620959), a National Estuarine Research Reserve System Graduate Research Fellowship (NOAA Award NA09NOS4200046), the Environmental Cooperative Science Center (NOAA Award NS17AE1624), and the NASA-Nebraska Space Grant (NASA Award NNG05GJ03H) for Creighton student research support.

7. References

Adam, P. (Ed.) (1990). *Saltmarsh Ecology*. New York: Cambridge University Press.

Adler-Golden, S.M., Matthew, M.W, Bernstein, L.S., Levine, R.Y., Berk, A., Richtsmeier, S.C, Acharya, P.K, Anderson, G.P, Felde, G., J. Gardner, Hoke, M., Jeong, L.S., Pukall, B., Ratkowski, A., & Burke, H.K. (1999). Atmospheric Correction for Short-wave Spectral Imagery Based on MODTRAN4. *SPIE Proc. Imaging Spectrometry*, 3753, 61-69.

Artigas, F.J., & Yang, J.S. (2005). Hyperspectral remote sensing of marsh species and plant vigour gradient in the New Jersey Meadowlands. *International Journal of Remote Sensing*, 26, 5209-5220.

ASPRS Lidar Committee (2004). ASPRS Lidar guidelines: Vertical accuracy reporting for Lidar data. Retrieved November 16, 2011, from http://www.asprs.org/a/society/committees/lidar/Downloads/Vertical_Accuracy_Reporting_for_Lidar_Data.pdf.

Belluco, E., Camuffo, M., Ferrari, S., Modenses, L., Silvestri, S., Marani, A., & Marani, M. (2006). Mapping salt-marsh vegetation by multispectral and hyperspectral remote sensing. *Remote Sensing Environment*, 105, 54-67.

Berk, A., Bernstein, L.S., Anderson, G.P., Acharya, P. K., Robertson, D. C., Chetwynd, J.H., & Adler-Golden, S.M (1998). MODTRAN Cloud and Multiple Scattering Upgrades with Application to AVIRIS. *Remote Sensing of Environ*ment, 65, 367-375.

Bouma, T.J., De Vries, M.B., Low, E., Kusters, L., Herman1, P.M.J., Tanczos, I.C., Temmerman, S., Hesselink, A., Meire, P., & van Regenmortel, S. (2005). Flow hydrodynamics on a mudflat and in salt marsh vegetation: identifying general relationships for habitat characterisations. *Hydrobiologia*, 540, 259–274.

Breiman, L., Friedman, J., Stone, C.J., & Olshen, R.A. (Ed.) (1984). *Classification and Regression Trees*. Boca Raton, FL: CRC Press LLC.

Brennan, R., & Webster, T.L. (2006). Object-oriented land cover classification of lidar-derived surfaces. *Canadian Journal of Remote Sensing*, 32, 162–172.

Campbell, J.B. (Ed.) (2007). *Introduction to Remote Sensing,4th Edition*. New York: The Guilford Press.

Chust, G., Galparsoro, I., Borja, A., Franco, J., & Uriarte, A. (2008). Coastal and estuarine habitat mapping, using LIDAR height and intensity and multi-spectral imagery, *Estuarine, Coastal and Shelf Science*, 78, 633-643.

Collin, A., Long, B., & Archambault, P. (2010). Salt-marsh characterization, zonation assessment and mapping through a dual-wavelength LiDAR. *Remote Sensing of Environment*, 114, 520-530.

Congalton, R.G. (1991). A Review of Assessing the Accuracy of Classifications of Remotely Sensed Data. *Remote Sensing of Environment*, 37, 35-46.

Danson, F. M., Steven, M. D., Malthus, T. J., & Clark, J. A. (1992). High-spectral resolution data for determining leaf water content. *International Journal of Remote Sensing*, 13, 461-470.

Foody, G.M. (2002). Status of land cover classification accuracy assessment. *Remote Sensing of Environment*, 80, 185-201.

Gallagher, J.L. (1975). Effects of an ammonium nitrate pulse on the growth and elemental composition of natural strands of *Spartina alterniflora* and *Juncus roemerianus*. *American Journal of Botany*, 62, 644–648.

Geerling, G.W., Labrador-Garcia, M., Clevers, J.G.P.W., Ragas, A.M.J., & Smits, A.J.M. (2007). Classification of floodplain vegetation by data-fusion of Spectral (CASI) and LiDAR data. *International Journal of Remote Sensing*, 28, 4263-4284.

Gesch, D.B. (2009). Analysis of Lidar elevation data for improved identification and delineation of lands vulnerable to sea-level rise. *Journal of Coastal Research,* 53, 49-58.

Gilmore, M. S., Wilson, E. H., Barrett, N., Civco, D. L., Prisloe, S., Hurd, J. D., & Chadwick, C. (2008). Integrating multi-temporal spectral and structural information to map wetland vegetation in a lower Connecticut River tidal marsh. *Remote Sensing of Environment*, 112, 4048-4060.

Goranson, C.E., Ho, C.K., & Pennings, S.C. (2004). Environmental gradients and herbivore feeding preferences in coastal salt marshes. Oecologia, 140, 591-600.

Hardisky, M.A., Gross, M.F., & Klemas, V. (1986). Remote sensing of coastal wetlands. *Bioscience*, 36, 453-460.

Hladik, C., & Alber, M. (2012). Accuracy assessment and correction of a LIDAR-derived salt marsh digital elevation model. *Remote Sensing of Environment*, 121, 224-235.

Hoffbeck, J.P. (1995). Classification of high dimensional multispectral data. PhD thesis, Purdue University, West Lafayette, Indiana.

Hughes, G.F. (1968). On the mean accuracy of statistical pattern recognizers. *IEEE Transactions on Information Theory*, 14, 55-63.

Hunter, E.L., & Power, C.H. (2002). An assessment of two classification methods for mapping Thames Estuary intertidal habitats using CASI data. *International Journal of Remote Sensing*, 23, 2989-3008.

Jollineau, M.Y., & Howarth, P.J. (2008). Mapping an inland wetland complex using hyperspectral imagery. *International Journal of Remote Sensing*, 29, 3609-3631.

Klemas, V. (2011). Remote sensing of wetlands: Case studies comparing practical techniques. *Journal of Coastal Research*, 27, 418-427.

Kruse, F.A., Lebkoff, A.B., Boardman, J.W., Heidebrecht, K.B., Shapiro, A.T., Barloon, P.J., & Goetz, A.F.H. (1993). The spectral image processing system (SIPS) -interactive visualization and analysis of imaging spectrometer data. *Remote Sensing of Environment*, 44, 145-163.

Leckie, D.G., Cloney, E., Jay, C., & Paradine, D. (2005). Automated mapping of stream features with high-resolution multispectral imagery: an example of the capabilities. *Photogrammetric Engineering and Remote Sensing*, 71, 145–155.

Lillesand, T.M., Kiefer, R.W., & Chipman, J.W. (Ed.) (2004). *Remote Sensing and Image Interpretation, 5th Ed*. New York: John Wiley and Sons Inc.

Lu, D., & Weng, Q. (2004). A survey of image classification methods and techniques for improving classification performance. *International Journal of Remote Sensing*, 28, 823-870.

Lucas, K.L., & Carter, G.A. (2008). The use of hyperspectral remote sensing to assess vascular plant species richness on Horn Island, Mississippi. *Remote Sensing of Environment*, 112, 3908-3915.

Marani, M., Silvestri, S., Belluco, E., Camuffo, M., DAlpaos, A., Defina, A., Lanzoni, S., Marani, A., Tortato, M., & Rinaldo, A. (2003). Patterns in tidal environments: salt-marsh channel networks and vegetation. In *Proceedings of the IEEE International Geoscience and Remote Sensing Symposium*, 21-25 July 2003, Toulouse, France.

Marani, M., Belluco, E., Ferrari, S., Silvestri, S., D'Alpaos, A., & Lanzoni, S. (2006). Analysis, synthesis and modeling of high-resolution observations of salt-marsh eco-geomorphological patterns in the Venice lagoon. *Estuarine, Coastal and Shelf Science*, 69, 414−426.

Maune, D.F.; Maitra, J.B., & McKay, E.J. (2007). Accuracy standards and guidelines. In: Maune, D. (Ed.), *Digital Elevation Model Technologies and Applications: The DEM Users Manual, 2nd Edition* (pp. 65-97). Bethesda, Maryland: American Society for Photogrammetry and Remote Sensing.

Mendelssohn, I.A., & Morris, J.T. (2000). Eco-physiological controls on the productivity of *Spartina Alterniflora* Loisel. In: Kreeger, D.A. (Ed.), *Concepts and Controversies in Tidal Marsh Ecology* (pp. 59-80). Dordrecht: Kluwer Academic.

Merani, P.B.T. (2007). Salt marsh species discrimination and mapping in the Chesapeake Bay using hyperspectral remote sensing. M.A. Thesis. University of Nebraska, Lincoln, NE.

Mitsch, W. J., & Gosselink, J. G.(Ed.) (2000). *Wetlands 3rd Edition*. New Jersey: John Wiley and Sons.

Montane, J.M., & Torres, R.T. (2006). Accuracy assessment of Lidar salt marsh topographic data using RTK GPS. *Photogrammetric Engineering and Remote Sensing*, 72, 961-967.

Morris, J.T., & Haskin, B. (1990). A 5-Yr Record of Aerial Primary Production and Stand Characteristics of Spartina-Alterniflora. *Ecology, 71*, 2209-2217.

Morris, J. T., Porter, D., Neet, M., Noble, P. A., Schmid, T, L., & Lapine, L. A. (2005). Integrating LIDAR elevation data, multi-spectral imagery and neural network modeling for marsh characterization. *International Journal of Remote Sensing*, 26, 5221−5234.

Moselund J.E., Arge, L., Bocher, P.K., Nygaard, B., & Svenning, J. (2011). Geographically comprehensive assessment of salt-meadow vegetation-elevation relations using LiDAR. *Wetlands*, 31, 471-482.

Optech (2011). Gemini summary specification sheet. Retrieved August 11, 2011, from http://www.optech.ca/pdf/ALTM_Gemini_SpecSheet_110309_Web.pdf.

Pahl, M., & Mather, P.M. (2003). An assessment of the effectiveness of decision tree methods for land cover classification, *Remote Sensing of Environment*, 86, 554-565.

Pezeshki, S. R. (2001). Wetland plant responses to flooding. *Environmental and Experimental Botany*, 46, 299-312.

Pohl, C., & Van Genderen, J.L. (1998). Multisensor image fusion in remote sensing: concepts, methods and applications. *International Journal of Remote Sensing*, 19, 823–854.

Raber, G.T., Jensen, J.R., Hodgson, M.E., Tullis, J.A., Davis, B.A., & Berglund, J. (2007). Impact of Lidar nominal post-spacing on DEM accuracy and flood zone delineation. *Photogrammetric Engineering and Remote Sensing*, 73, 793-804.

Reimold, R. J., Gallagher, J. L., & Thompson, D. E. (1973). Remote sensing of tidal marsh. *Photogrammetric Engineering*, 39, 477-488.

Richards, J.A., & Jia, X. (2006). *Remote Sensing Digital Image Analysis*. Berlin: Springer-Verlag.

Rosso, P. H., Ustin, S. L., & Hastings, A. (2006). Use of lidar to study changes associated with Spartina invasion in San Francisco Bay marshes. *Remote Sensing of Environment*, 100, 295−306.

Rosenfield, G. H., & Fitzpatrick-Lins, K. (1986). A coefficient of agreement as measure of thematic classification accuracy. *Photogrammetric Engineering and Remote Sensing*, 52, 223−227.

Rouse, J. W., Haas, R. H., Schell, J. A., & Deering, D. W. (1974). Monitoring vegetation systems in the Great Plains with ERTS. In *Proceedings of the Third Earth Resources Technology Satellite-1 Symposium*, 301−317.

Sadro, S., Gastil-Buhl, M., & Melack, J. (2007). Characterizing patterns of plant distribution in a southern California salt marsh using remotely sensed topographic and hyperspectral data and local tidal fluctuations. *Remote Sensing of Environment*, 110, 226-239.

Sanders, B.F. (2007). Evaluation of on-line DEMs for flood inundation modeling. *Advances in Water Resources*, 30, 1831-1843.

Schmid, K.A., Hadley, B.C., & Wijekoon, N. (2011). Vertical accuracy and use of topographic LIDAR data in coastal marshes. *Journal of Coastal Research*, 27, 116-132.

Schmidt, K. S., & Skidmore, K.A. (2003). Spectral discrimination of vegetation types in a coastal wetland. *Remote Sensing of Environment*, 85, 92–108.

Sellars, J.D., & Jolls, C.L. (2007). Habitat modeling for *Amaranthus pumilus*: an application of light detection and ranging (LIDAR) data. *Journal of Coastal Resources*, 23, 1193-1202.

Silvestri, S., Marani, M., & Marani, A. (2003). Hyperspectral remote sensing of salt marsh vegetation and morphology. *Physics and Chemistry of the Earth*, 28**,** 15–25.

Specim Imaging LTD (2011). AISA EAGLE hyperspectral sensor. Retrieved December 7, 2011, from http://www.specim.fi/media/aisa-datasheets/aisaeagle_datasheet_ver2-2011.pdf.

Thomson, A.G., Fuller, R.M., Yates, M.G., Brown, S.L., Cox, R., & Wadsworth, R.A. (2003). The use of airborne remote sensing for extensive mapping of intertidal sediments and saltmarshes in eastern England. *International Journal of Remote Sensing*, 24, 2717–2737.

Thomson, A.G., Huiskes, A., Cox, R., Wadsworth, R.A., & Boorman, L.A. (2004). Short-term vegetation succession and erosion identified by airborne remote sensing of Westerschelde salt marshes, The Netherlands. *International Journal of Remote Sensing*, 25, 4151-4176.

Toyra, J., Pietroniro, A., Hopkinson, C., & Kalbfleisch, W. (2003). Assessment of airborne scanning laser altimetry, lidar, in a deltaic wetland environment. *Canadian Journal of Remote Sensing*, 29, 718-728.

Townend, I., Fletcher, C., Knappen, M., & Rossington, K. (2010). A review of salt marsh dynamics. *Water and Environment Journal*, 1-12.

Trimble (2009). Trimble R6 GPS receiver datasheet. Retrieved August 11, 2011, from http://trl.trimble.com/docushare/dsweb/Get/Document-333155/022543-259D_Trimble_R6_DS_1109_LR.pdf.

Turner, R.E. (1976). Geographic variations in salt marsh macrophyte productions: A review. *Contributions to Marine Sciences*, 20, 47-68.

Wang, C., Menenti, M., Stoll, M.P., Belluco, E., & Marani, M. (2007). Mapping mixed vegetation communities in salt marshes using airborne spectral data. *Remote Sensing of Environment*, 107, 559–570.

Wang, C., Menenti, M., Stoll, M., Feola, A., Belluco, E., & Marani, M. (2009). Separation of ground and low vegetation signatures in LIDAR measurements of salt-marsh environments. *IEEE Transactions on Geoscience and Remote Sensing*, 47, 2014-2023.

Webster, T.L., Forbes, D.L., MacKinnon, E., & Roberts, D. (2006). Flood-risk mapping for storm-surge events and sea-level rise using lidar for southeast New Brunswick. *Canadian Journal of Remote Sensing*, 32, 194-211.

Wiegert, R.G., & Freeman, B.J. (1990). *Tidal Salt Marshes of the Southeast Atlantic Coast: a Community Profile*. Washington, DC: U.S. Department of the Interior, Fish and Wildlife Service.

Yang, J., & Artigas, F. (2010). Mapping Salt Marsh Vegetation by Integrating Hyperspectral and LiDAR Remote Sensing. In Wang, Y. (Ed.), *Remote Sensing of Coastal Environments* (pp.173-187). Boca Raton, FL: CRC Press.

Zedler, J.B., Callaway, J. C., Desmond, J. S., Vivian-Smith, G., Williams, G. D., & Sullivan, G. (1999). Californian salt-marsh vegetation: An improved model of spatial pattern. *Ecosystems*, 2, 19‒35.

Zedler, J. B. (Ed.) (2001). *Handbook for Restoring Tidal Wetlands*. Boca Raton, Florida: CRC Press.

Table 3.1. LIDAR and hyperspectral sensor system specifications used to acquire the remote sensing data for this study.

	LIDAR	Hyperspectral
Sensor	Optech ALTM Gemini	AISA Eagle
Flight Date	March 2009	June 2006
Altitude (m)	800	1650
Swath Width (m)	370	1000
Overlap (%)	50	50
Number of Spectral Bands	1	63
Wavelengths (nm)	1047	400-980
Bandwidth (nm)	–	9
FOV (degrees)	–	68
Laser PRF (kHz)	125	–
Scan Freq (Hz)	40	–
Scan Angle (degrees)	16	–
Scan Cutoff (degrees)	3	–
Footprint (cm)	60	–
Pulse Length (ns)	7	–
Pixel Resolution (m)	1	1

Table 3.2. Cover class-specific correction factors used to modify the LIDAR-derived DEM when fused with the hyperspectral classification. The sample size (N), standard deviation (SD, 1 sigma) and standard error (SE, 1 sigma) for the derivation of the correction factors are also shown. Please refer to section 2.9 for details regarding correction factors. All units (except N) are in meters (m).

Cover Class	Correction Factor (m)	N	SD (m)	SE (m)
Tall *S. alterniflora*	0.25	152	0.17	0.01
Medium *S. alterniflora*	0.11	267	0.07	0.00
Short *S. alterniflora*	0.05	214	0.05	0.00
Intertidal Mud	0.04	53	0.06	0.01
S. virginica	0.04	227	0.05	0.00
B. maritima	0.04	160	0.04	0.00
Salt Pan	0.03	62	0.04	0.01
J. roemerianus	0.17	117	0.09	0.01
B. frutescens	0.12	78	0.07	0.01

Table 3.3. Maximum likelihood classification (MLC) and spectral angle mapper (SAM) classification confusion matrices after application of the decision tree for the nine marsh cover classes. Columns represent the reference data (what the pixel actually was based on validation data) and rows represent the image data (what the pixel was classified as). Shaded cells are those where the classification was accurate. Percentages are rounded to the nearest decimal place and may not sum to 100% for each cover class.

Cover Class	Tall *S. alterniflora*	Medium *S. alterniflora*	Short *S. alterniflora*	Intertidal Mud	*S. virginica*	*B. maritima*	Salt Pan	*J. roe-merianus*	*B. fru-tescens*
MLC									
Unclassified	0	0	0	0	0	0	0	0	0
Tall *S. alterniflora*	94.50	2.71	0	1.76	0	0	0	2.10	0
Medium *S. alterniflora*	5.16	88.2	12.12	0.29	6.71	0	0	2.34	2.04
Short *S. alterniflora*	0	6.43	86.32	11.14	1.47	0	0	0	0
Intertidal Mud	0	0.15	0.68	86.80	0	0	0	0	0
S. virginica	0	1.07	0.88	0	79.87	2.83	1.19	0	0
B. maritima	0	0	0	0	7.36	91.30	0	1.05	2.35
Salt Pan	0	0	0	0	4.58	0	98.81	0	0
J. roemerianus	0	1.43	0	0	0	0	0	94.51	0
B. frutescens	0.34	0	0	0	0	5.87	0	0	95.61
Total	100	100	100	100	100	100	100	100	100

Table 3.3 (continued).

Cover Class	Tall *S. alterniflora*	Medium *S. alterniflora*	Short *S. alterniflora*	Intertidal Mud	*S. virginica*	*B. maritima*	Salt Pan	*J. roe-merianus*	*B. fru-tescens*
SAM									
Unclassified	1.95	0.40	0	5.64	0	0	0	1.05	0
Tall *S. alterniflora*	57.85	0.82	0	1.78	1.96	0	0	0	7.52
Medium *S. alterniflora*	1.48	42.73	6.70	0	15.88	0	4.76	1.05	1.72
Short *S. alterniflora*	0	25.14	62.51	2.67	6.71	0	26.98	0	0
Intertidal Mud	0.20	0	15.32	88.72	0	0	0	0	0
S. virginica	4.90	17.74	1.50	0	63.01	2.63	0	1.78	0
B. maritima	2.68	0	0	0	0	72.06	0	0	6.74
Salt Pan	0	0	13	1.19	0	0	68.25	0	0
J. roemerianus	4.09	9.23	0.70	0	12.44	0	0	88.21	2.82
B. frutescens	26.85	3.93	0	0	0	25.30	0	7.92	81.19
Total	100	100	100	100	100	100	100	100	100

Table 3.4. Maximum likelihood classification (MLC) and spectral angle mapper (SAM) classification errors of commission, errors of omission, producer's accuracies and user's accuracies for each cover class following application of the decision tree for the nine cover classes. Percentages are rounded to the nearest decimal place and may not sum to 100% for each cover class.

Cover Class	Errors of Commission	Errors of Omission	Producer's Accuracy	User's Accuracy
MLC				
Tall *S. alterniflora*	7.90	5.50	94.50	92.10
Medium *S. alterniflora*	12.41	11.80	88.20	87.59
Short *S. alterniflora*	12.70	13.68	86.32	87.30
Intertidal Mud	6.03	13.20	86.80	93.97
S. virginica	13.01	20.13	79.87	86.99
B. maritima	13.93	8.70	91.30	86.07
Salt Pan	5.32	1.19	98.81	94.68
J. roemerianus	3.86	5.49	94.51	96.14
B. frutescens	5.28	4.39	95.61	94.72
SAM				
Tall *S. alterniflora*	9.74	42.15	57.85	90.26
Medium *S. alterniflora*	17.24	57.27	42.73	82.76
Short *S. alterniflora*	46.42	37.49	62.51	53.58
Intertidal Mud	49.15	11.28	88.72	50.85
S. virginica	65.10	36.99	63.01	34.90
B. maritima	18.91	27.94	72.06	81.09
Salt Pan	42.28	31.75	68.25	57.72
J. roemerianus	30.13	11.79	88.21	69.87
B. frutescens	59.21	18.81	81.19	40.79

Table 3.5. Cover class areas based on the initial MLC classification and following the application of the decision tree for three areas in the upper Duplin River (corresponding to locations 1, 2 and 3 in Figures 3.4 and 3.5) and for the entire study domain. The 'MLC' column contains the area assigned for each class expressed as a proportion of the total number of pixels in each location prior to application of the decision tree. The 'Decision Tree' column contains the proportion of the area for each class following the application of the decision tree. 'Change in Proportion Per Class' represents the change in cover class area, calculated on a per class basis, whereas 'Change is Total Proportion' is calculated based on the total number of pixels in the area following the application of the decision tree ('Decision Tree' minus 'MLC' column values). The values in parentheses for the *Whole Duplin* are the proportion of the areas when Unclassified pixels are excluded.

Cover Class	MLC	Decision Tree	Change in Proportion Per Class	Change in Total Proportion
<u>*Location 1*</u>				
Tall *S. alterniflora* (ST)	0.15	0.22	0.51	0.08
Medium *S. alterniflora* (SM)	0.60	0.48	-0.20	-0.12
Short *S. alterniflora* (SS)	0.01	0.00	-0.32	0.00
Intertidal Mud (MUD)	0.17	0.17	0.02	0.00
Unclassified	0.07	0.12	0.63	0.05
<u>*Location 2*</u>				
Tall *S. alterniflora* (ST)	0.03	0.14	3.19	0.11
Medium *S. alterniflora* (SM)	0.58	0.39	-0.33	-0.19
Short *S. alterniflora* (SS)	0.00	0.00	-0.70	0.00
Intertidal Mud (MUD)	0.31	0.35	0.13	0.04
Unclassified	0.08	0.12	0.63	0.05

Table 3.5 (continued).

Cover Class	MLC	Decision Tree	Change in Proportion Per Class	Change in Total Proportion
Location 3				
Tall *S. alterniflora* (ST)	0.08	0.18	1.64	0.13
Medium *S. alterniflora* (SM)	0.49	0.32	-0.31	-0.22
Short *S. alterniflora* (SS)	0.00	0.00	-0.36	0.00
Intertidal Mud (MUD)	0.28	0.24	0.29	0.06
Unclassified	0.15	0.25	1.88	0.02
Whole Classification				
Tall *S. alterniflora* (ST)	0.09 (0.13)	0.11 (0.17)	0.02	0.24
Medium *S. alterniflora* (SM)	0.33 (0.50)	0.30 (0.47)	-0.03	-0.10
Short *S. alterniflora* (SS)	0.08 (0.12)	0.08 (0.12)	0.00	-0.03
Intertidal Mud (MUD)	0.07 (0.11)	0.06 (0.09)	-0.02	-0.23
S. virginica (SV)	0.03 (0.05)	0.03 (0.05)	0.00	0.00
B. maritima (BM)	0.002 (0.01)	0.002 (0.01)	0.00	0.00
Salt Pan (SALT)	0.003 (0.02)	0.003 (0.01)	0.00	-0.17
J. roemerianus (JR)	0.03 (0.05)	0.03 (0.05)	0.00	0.00
B. frutescens (BF)	0.003 (0.01)	0.003 (0.01)	0.00	0.00
Shell	0.00	0.0005 (0.003)	0.00	1.00
Unclassified	0.34	0.37	0.03	0.01

Table 3.6. Summary of LIDAR-derived DEM accuracies. Accuracies for each cover class are presented for both the unmodified and modified DEM relative to the RTK ground survey elevation. The table lists mean error (Mean Error), number of observations (N), standard deviation (SD), standard error (SE), root mean square error (RMSE), fundamental vertical accuracy (FVA) and 95th percentile error (95th Percentile). *p*-values are from a paired t-test between the RTK elevations and the predicted DEM elevations for each cover class. All error units are in meters.

Cover Class	Mean Error (m)	N	SD (m)	SE (m)	RMSE (m)	FVA (m)	95th Percentile (m)	*p*-value
<u>Unmodified DEM</u>								
Tall *S. alterniflora* (ST)	0.28	51	0.20	0.03	0.34	0.67	0.56	< 0.001
Medium *S. alterniflora* (SM)	0.11	89	0.07	0.01	0.13	0.26	0.22	< 0.001
Short *S. alterniflora* (SS)	0.05	71	0.05	0.01	0.07	0.14	0.13	0.006
Intertidal Mud (MUD)	0.06	17	0.06	0.01	0.08	0.16	0.14	0.431
S. virginica (SV)	0.04	73	0.04	0.00	0.06	0.11	0.10	0.003
B. maritima (BM)	0.05	53	0.04	0.01	0.06	0.11	0.11	0.003
Salt Pan (SALT)	0.03	21	0.04	0.01	0.05	0.09	0.08	0.250
J. roemerianus (JR)	0.16	37	0.09	0.01	0.18	0.35	0.27	< 0.001
B. frutescens (BF)	0.11	21	0.08	0.02	0.13	0.26	0.22	0.003
Overall	0.10	450	0.12	0.01	0.15	0.30	0.34	< 0.001

Table 3.6 (continued).

Cover Class	Mean Error (m)	N	SD (m)	SE (m)	RMSE (m)	FVA (m)	95th Percentile (m)	*p*-value
<u>Modified DEM</u>								
Tall *S. alterniflora* (ST)	0.08	51	0.20	0.03	0.22	0.42	0.41	0.129
Medium *S. alterniflora* (SM)	-0.01	89	0.08	0.01	0.08	0.16	0.12	0.506
Short *S. alterniflora* (SS)	-0.03	71	0.06	0.01	0.07	0.14	0.06	0.081
Intertidal Mud (MUD)	-0.05	17	0.10	0.02	0.11	0.22	0.08	0.495
S. virginica (SV)	-0.01	73	0.05	0.01	0.05	0.09	0.06	0.522
B. maritima (BM)	0.00	53	0.04	0.01	0.04	0.08	0.07	0.911
Salt Pan (SALT)	-0.01	21	0.04	0.01	0.04	0.08	0.05	0.535
J. roemerianus (JR)	0.00	37	0.08	0.01	0.08	0.16	0.12	0.914
B. frutescens (BF)	0.00	21	0.08	0.02	0.08	0.15	0.08	0.985
Overall	0.00	450	0.10	0.00	0.10	0.19	0.17	0.870

Table 3.S1. Jeffries-Matusita and Transformed Divergence Region of Interest (ROI) separability measures calculated for each cover class pairing in this study. Larger values (greater than 1.9, on a scale of 0 to 2) indicate good separability, whereas values less than 1 indicate poor spectral separability. Training data pairs had values greater than 1.9 for both measures except the short *S. alterniflora* and medium *S. alterniflora* pair, which had a value of 1.62 for the Jeffries-Matusita distance measure. Short and medium *S. alterniflora* were kept as two distinct classes in this analysis as it is recommended that only pairs with values less than one be combined.

Cover Class	Tall *S. alterniflora*	Medium *S. alterniflora*	Short *S. alterniflora*	Intertidal Mud	*S. virginica*	*B. maritima*	Salt Pan	*J. roe-merianus*
Jeffries-Matusita								
Tall *S. alterniflora*								
Medium *S. alterniflora*	1.9053							
Short *S. alterniflora*	1.9921	**1.6174**						
Intertidal Mud	1.9997	1.9864	1.9642					
S. virginica	1.9941	1.9423	1.9423	1.9983				
B. maritima	1.9984	1.9990	1.9999	2.0000	1.9429			
Salt Pan	2.0000	2.0000	2.0000	1.9999	2.0000	2.0000		
J. roemerianus	1.9821	1.9541	1.9715	1.9994	1.9962	1.9992	2.0000	
B. frutescens	1.9594	1.9866	1.9996	2.0000	1.9962	1.9622	2.0000	1.9818

Table 3.S1 (continued).

Cover Class	Tall *S. alterniflora*	Medium *S. alterniflora*	Short *S. alterniflora*	Intertidal Mud	*S. virginica*	*B. maritima*	Salt Pan	*J. roe-merianus*
Transformed Divergence								
Tall *S. alterniflora*								
Medium *S. alterniflora*	2.0000							
Short *S. alterniflora*	2.0000	1.9209						
Intertidal Mud	2.0000	2.0000	1.9999					
S. virginica	2.0000	1.9982	2.0000	2.0000				
B. maritima	2.0000	2.0000	2.0000	2.0000	2.0000			
Salt Pan	2.0000	2.0000	2.0000	2.0000	2.0000	2.0000		
J. roemerianus	2.0000	1.9985	2.0000	2.0000	2.0000	2.0000	2.0000	
B. frutescens	2.0000	2.0000	1.9989	2.0000	1.9874	2.0000	1.9999	2.0000

Table 3.S2. Maximum likelihood (MLC) and spectral angle mapper (SAM) classification error matrices for initial HSI classifications in this study prior to the decision tree. Columns represent reference data (what the pixel actually is based on validation data) and rows represent image data (what the pixel was classified as). Percentages are rounded to the nearest decimal place and may not sum to 100% for each cover class.

Cover Class	Tall *S. alterniflora*	Medium *S. alterniflora*	Short *S. alterniflora*	Intertidal Mud	*S. virginica*	*B. maritima*	Salt Pan	*J. roe-merianus*	*B. fru-tescens*
MLC									
Unclassified	0	0	0	0	0	0	0	0	0
Tall *S. alterniflora*	93.30	2.93	0	1.76	0.16	0	0	2.26	0
Medium *S. alterniflora*	5.76	86.77	13.24	0.00	6.06	0	0	2.02	2.04
Short *S. alterniflora*	0	7.99	85.44	10.56	0.98	0	0	0	0
Intertidal Mud	0.2	0	0.54	86.80	0	0	0	0	0
S. virginica	0	1.19	0.68	0	82.49	3.64	2.38	0	0
B. maritima	0	0	0	0	5.73	89.27	0	0.97	2.66
Salt Pan	0	0	0	1	4.58	0	97.62	0	0
J. roemerianus	0	1.12	0.1	0	0	0	0	94.35	0
B. frutescens	0.74	0	0	0	0	7.09	0	0	95.30
Total	100	100	100	100	100	100	100	100	100

Table 3.S2 (continued).

Cover Class	Tall *S. alterniflora*	Medium *S. alterniflora*	Short *S. alterniflora*	Intertidal Mud	*S. virginica*	*B. maritima*	Salt Pan	*J. roe-merianus*	*B. fru-tescens*
SAM									
Unclassified	1.65	0.51	0	6.45	0	0	0	0.87	0
Tall *S. alterniflora*	57.13	0.87	0	2.35	2.22	0	0	0	9.92
Medium *S. alterniflora*	1.52	39.38	6.30	0	17.25	0	5.22	1.27	0.00
Short *S. alterniflora*	0	28.77	55.24	1.17	6.80	0	26.51	0	0
Intertidal Mud	0.00	0	14.81	87.39	0	0	0	0	0
S. virginica	4.62	17.88	1.38	0	63.45	2.83	0	1.67	0
B. maritima	3.43	0	0	0	0	70.65	0	0	7.97
Salt Pan	0	0	22	2.64	0	0	68.27	0	0
J. roemerianus	4.03	8.56	0.64	0	10.28	0	0	87.60	3.58
B. frutescens	27.08	4.01	0	0	0	26.52	0	8.43	78.54
Total	100	100	100	100	100	100	100	100	100

Table 3.S3. Maximum likelihood (MLC) and spectral angle mapper (SAM) errors of commission, errors of omission, producer's accuracies and user's accuracies for each cover class for the initial HSI classification prior to the decision tree.

Cover Class	Errors of Commission	Errors of Omission	Producer's Accuracy	User's Accuracy
MLC				
Tall *S. alterniflora*	8.60	6.70	93.30	91.40
Medium *S. alterniflora*	13.20	13.23	86.77	86.80
Short *S. alterniflora*	14.76	14.56	85.44	85.24
Intertidal Mud	4.52	13.20	86.80	95.48
S. virginica	14.14	17.51	82.49	85.86
B. maritima	12.67	10.73	89.27	87.33
Salt Pan	5.93	2.38	97.62	94.07
J. roemerianus	3.23	5.65	94.35	96.77
B. frutescens	7.60	4.70	95.30	92.40
SAM				
Tall *S. alterniflora*	11.64	42.87	57.13	88.36
Medium *S. alterniflora*	18.78	60.62	39.38	81.22
Short *S. alterniflora*	50.38	44.76	55.24	49.62
Intertidal Mud	50.25	12.61	87.39	49.75
S. virginica	64.42	36.55	63.45	35.58
B. maritima	22.44	29.35	70.65	77.56
Salt Pan	56.96	31.73	68.27	43.04
J. roemerianus	28.77	12.40	87.60	71.23
B. frutescens	61.76	21.46	78.54	38.24

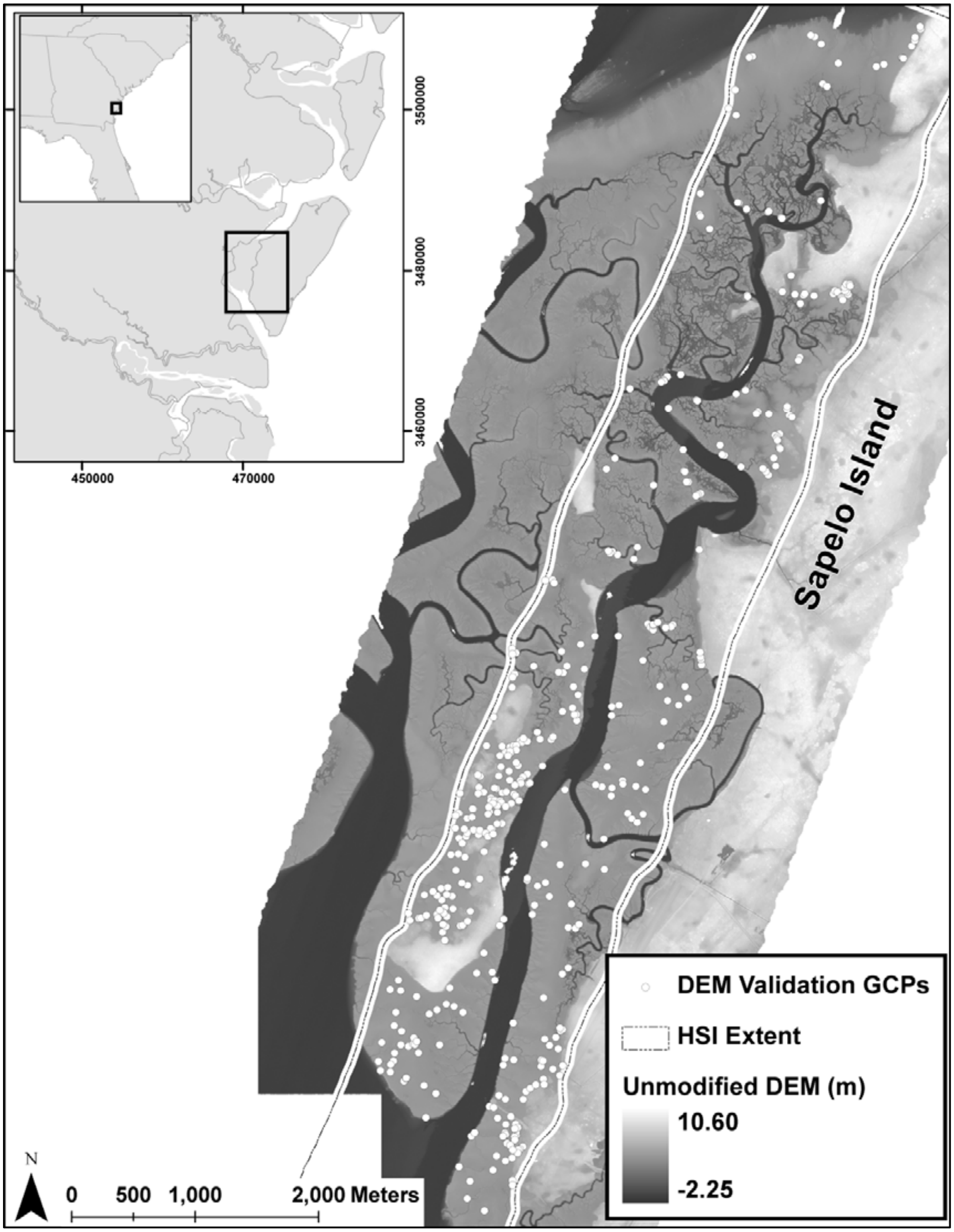

Figure 3.1. The unmodified LIDAR-derived bare earth DEM showing the location of the study area surrounding the Duplin River adjacent to Sapelo Island, GA and the extent of the HSI imagery evaluated for this study (white outline). White dots indicate RTK ground control point (GCP) sampling locations used to validate DEM elevation accuracy.

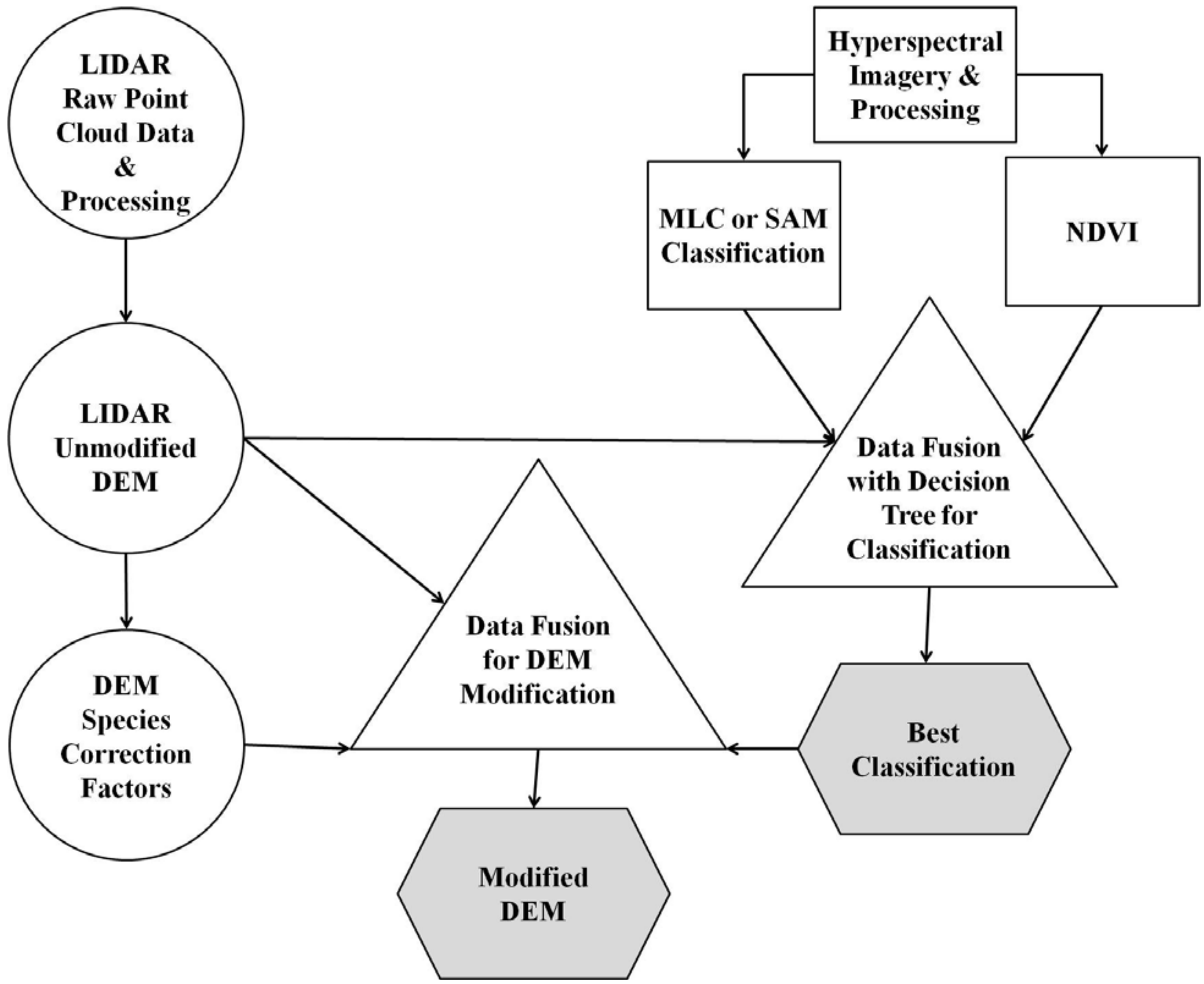

Figure 3.2. Hyperspectral classification and LIDAR-derived DEM correction work flow. Circles represent LIDAR data processing steps; rectangles represent HSI processing; triangles represent data fusion; gray hexagons represent the products of data fusion.

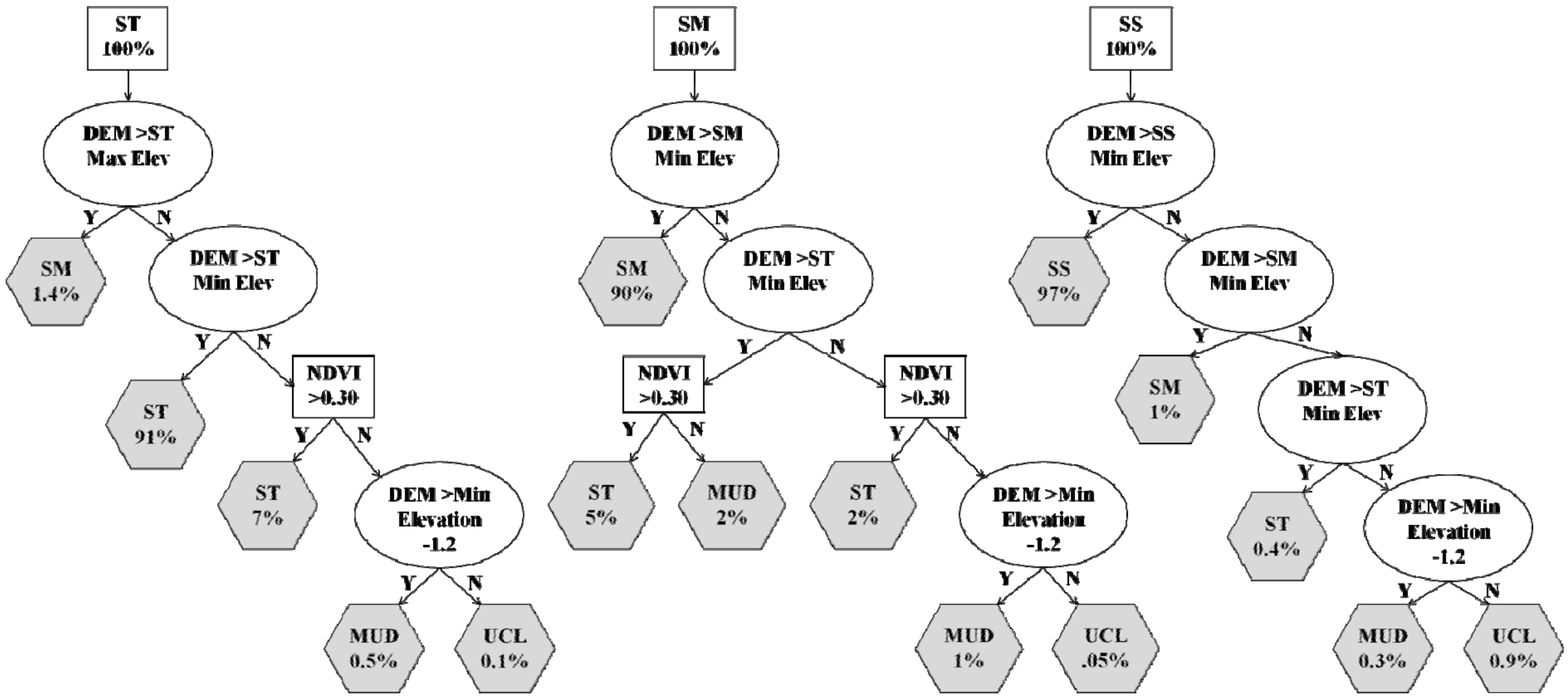

Figure 3.3. Decision tree classification workflows for evaluating pixels classified as tall, medium and short *S. alterniflora* (ST, SM, SS), fusing HSI and LIDAR-derived DEM data sources. Circles represent LIDAR-derived DEM data; rectangles represent HSI data (MLC or SAM initial classification and NDVI); gray hexagons represent the cover class products of data fusion following the application of the decision tree. Percentages represent the percent of pixels reassigned to each of the respective classes based on the decision tree rules. Percentages are rounded and do not sum to 100% for each tree.

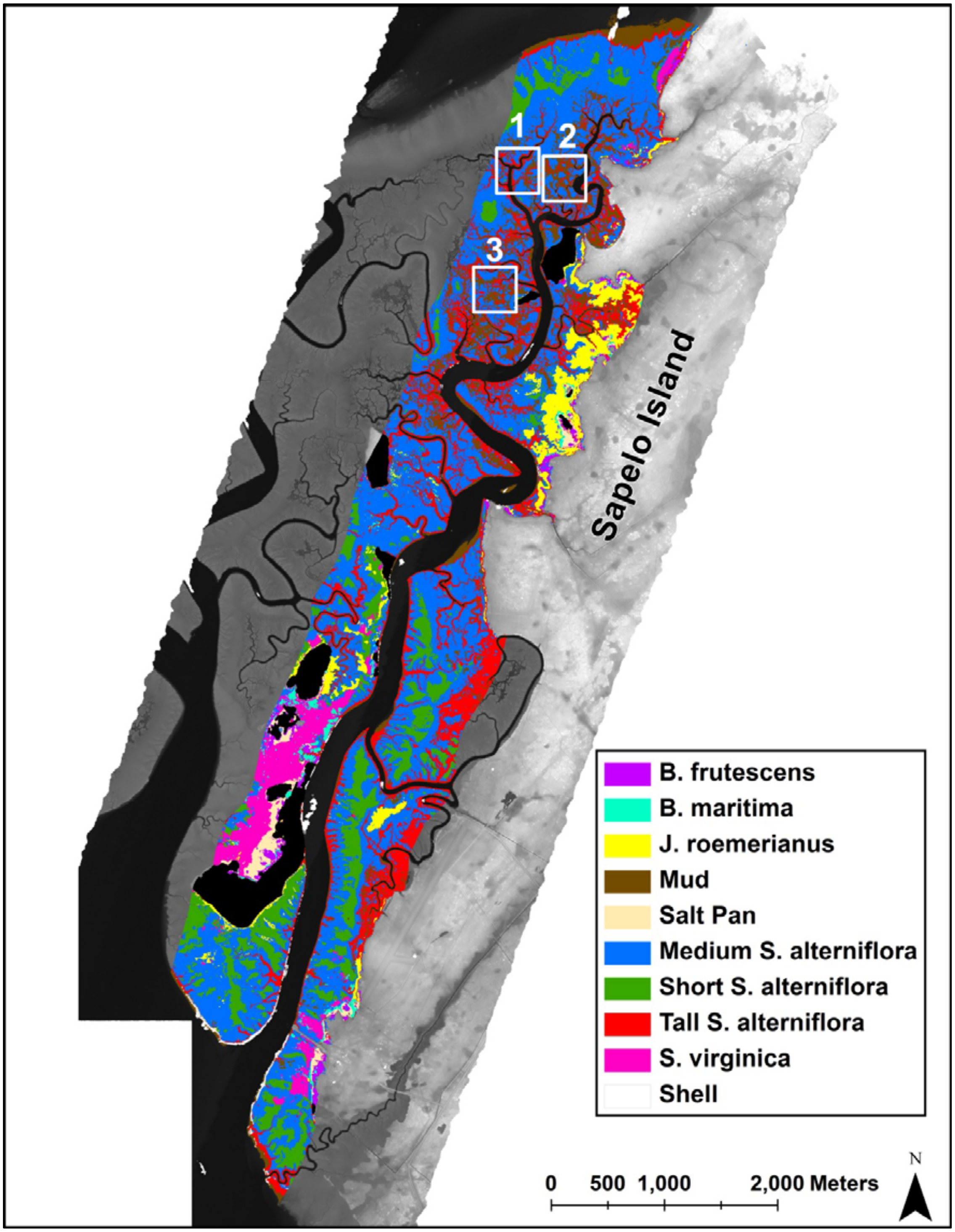

Figure 3.4. The final MLC hyperspectral classification product (after application of decision tree). Areas 1, 2 and 3 represent locations of examples shown in Figure 3.5.

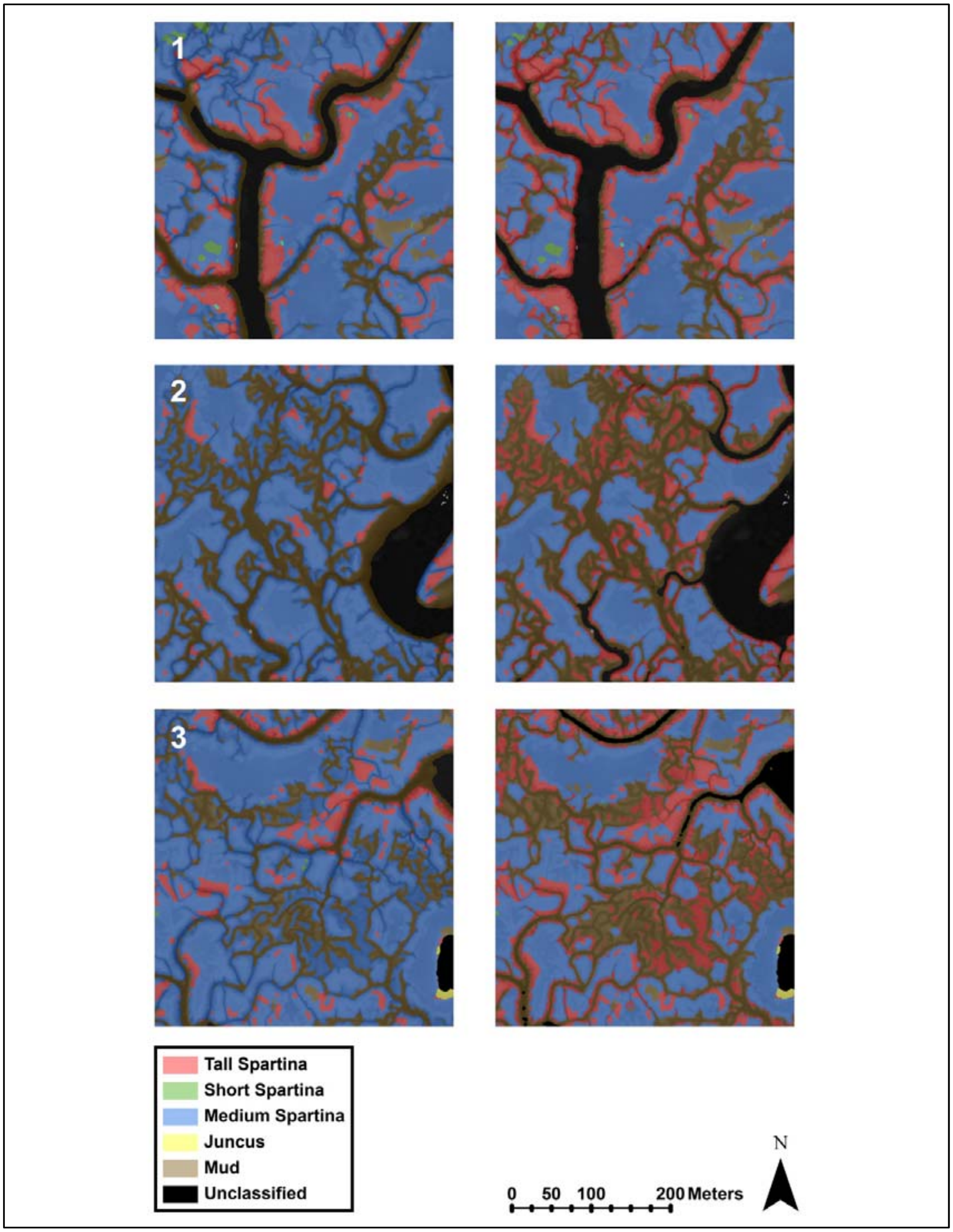

Figure 3.5. Before (left) and after (right) application of the decision tree on the MLC classification for example locations 1, 2 and 3 shown in Figure 3.4. Note the reassignment of medium *S. alterniflora* pixels (blue) to tall *S. alterniflora* (red) and mud (brown). Black areas are unclassified and are either upland areas or water pixels that gave unreliable LIDAR water returns. Each location is 0.15 km^2 and was selected to demonstrate the effect of the decision tree on class distributions.

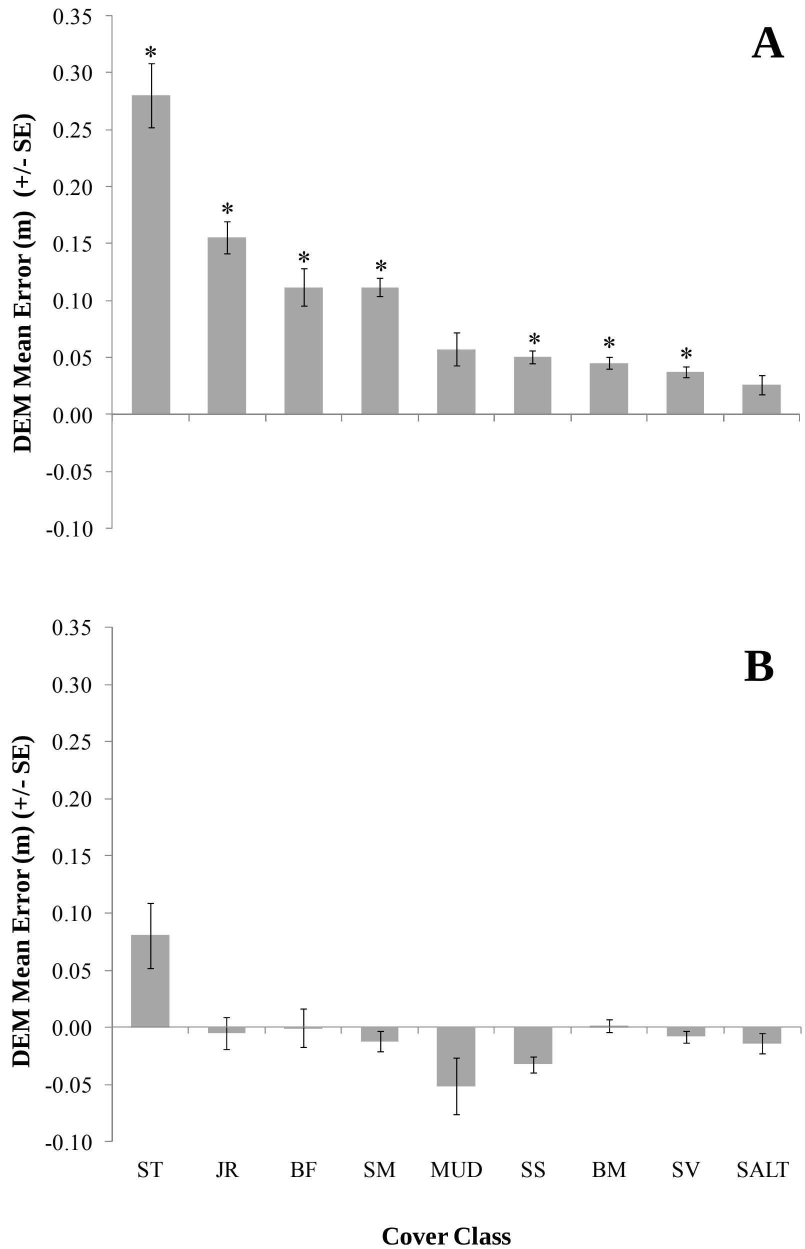

Figure 3.6. LIDAR-derived DEM mean elevation errors from the RTK validation data set (N = 450) for each cover class before (A) and after (B) correction. Bars represent mean errors in meters (m) +/- standard error. Asterisks (*) above bars indicate significant *p*-values ($p < 0.05$) from a paired t-test between the RTK elevations and the predicted DEM elevations for each cover class (see Table 3.6). Cover class abbreviations are as follows: ST: tall *S. alterniflora*; BF: *B. frutescens*; JR: *J. roemerianus*; SM: medium *S. alterniflora*; SV: *S. virginica*; BM: *B. maritima*; SS: short *S. alterniflora*; and SALT: salt pan.

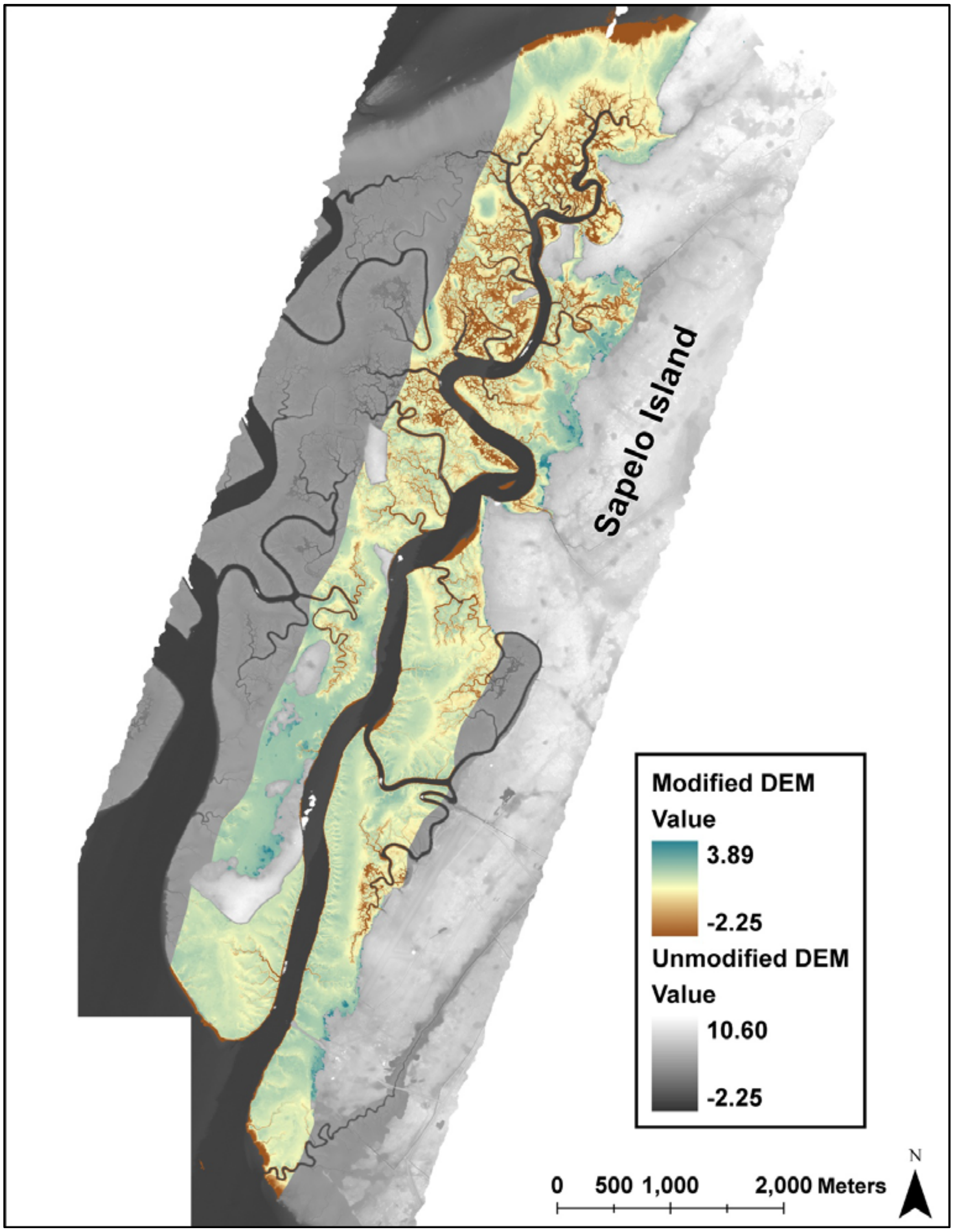

Figure 3.7. The modified bare earth LIDAR-derived DEM product (warm color ramp) produced through data fusion with the final MLC classification and correction factors. Cool colors indicate higher elevations and warmer colors represent lower elevations. Note the low elevations in the upper Duplin River in brown where the decision tree had the greatest effect on reducing the *Spartina* problem. The modified DEM is overlaid on the unmodified bare earth LIDAR-derived DEM (grayscale color ramp), with higher elevations in white and lower elevations in black. Elevations were all positioned in the NAD 83 reference frame and projected into UTM coordinate zone 17 N. Elevations are NAVD 88 orthometric heights (in meters) computed using the National Geodetic Survey GEOID 03.

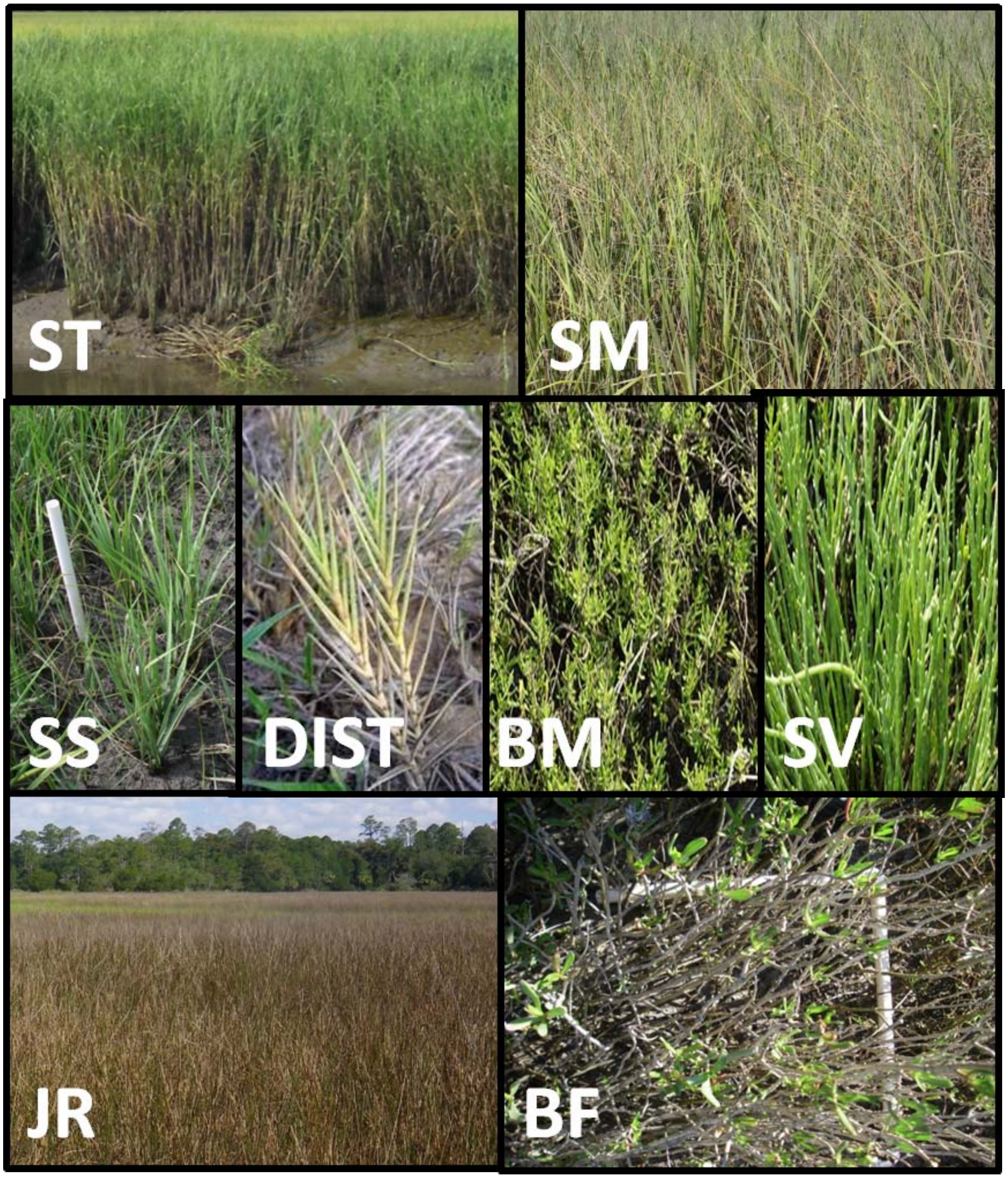

Figure 3.S1. Vegetated cover classes examined in this study. ST: *Spartina alterniflora* tall height, SM: *Spartina alterniflora* medium height; JR: *Juncus roemerianus*; SV: *Salicornia virginica*; SS: *Spartina alterniflora* short height; BM: *Batis maritima*; and BF: *Borrichia frutescens*. The two non-vegetated cover classes (intertidal mud (MUD) and salt pan (SALT)) are not depicted. Photo credits: Steve Pennings (DIST) and Christine Hladik (all others).

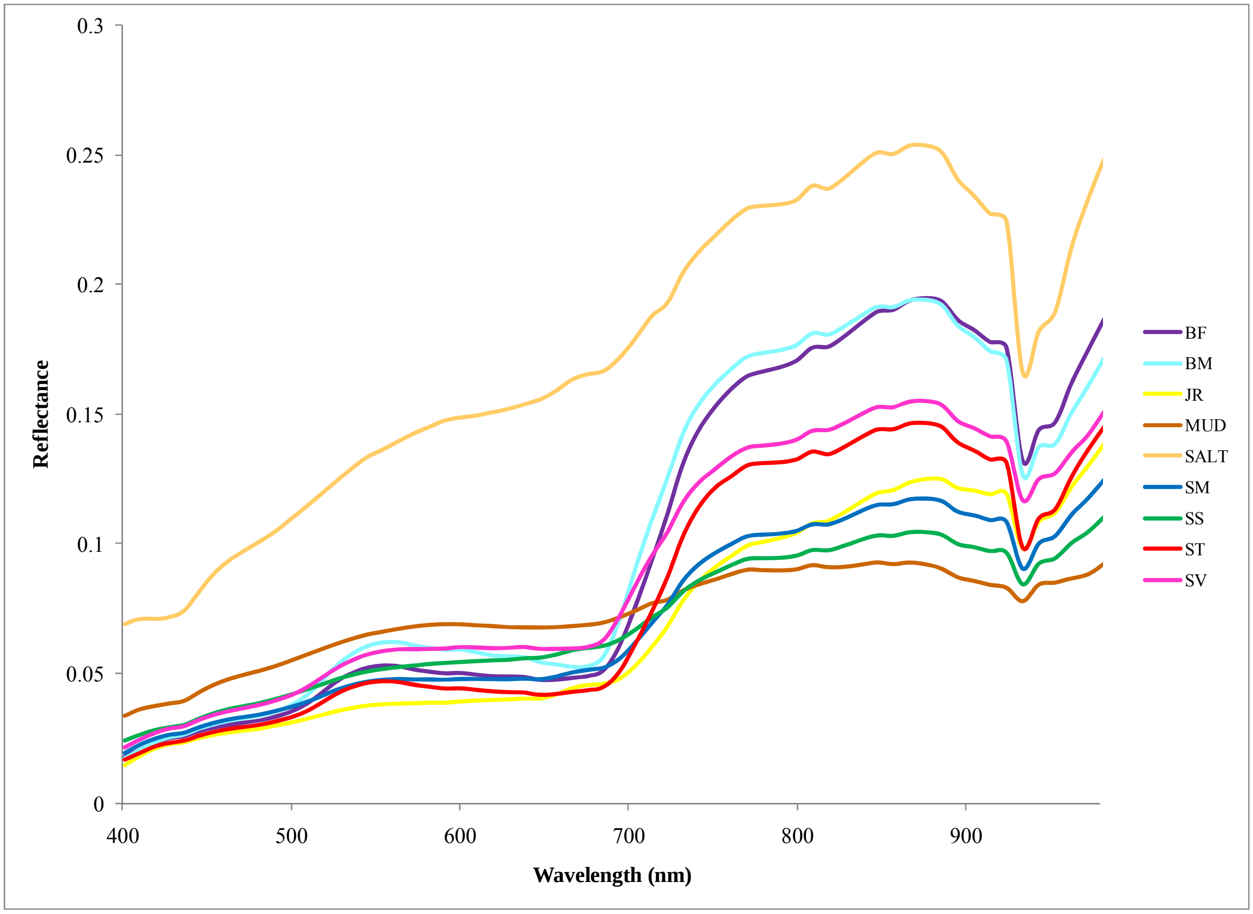

Figure 3.S2. Mean reflectance spectra for the training ROIs of the various habitat classes used in the MLC and SAM hyperspectral classifications. The magnitude of reflectance varied, with salt pan (SALT) having the greatest overall reflectance and *B. maritima* (BM) having the highest vegetation reflectance. In the visible range, *J. roemerianus* (JR) had the lowest reflectance. The reflectance characteristics for vegetated cover classes are broad pigment absorption in the blue wavelengths (400-500 nm); a sharp chlorophyll pigment absorption feature in the NIR near 675 nm; a red edge feature with sharply increasing reflectance between 680-770 nm; high reflectance in the NIR; and a water absorption band near 940 nm. Although similar in shape and magnitude, all cover classes were spectrally separable (Table 3.S1). For the non-vegetated classes, mud and salt pan (MUD, SALT), the general spectral shape showed steadily increasing reflectance throughout the visible with no identifiable absorbance features with the exception of the water absorption bands.

CHAPTER 4

CLASSIFICATION OF SALT MARSH VEGETATION USING EDAPHIC AND REMOTE SENSING-DERIVED VARIABLES[3]

[3] Hladik, C. and Alber, M. To be submitted to *Ecological Applications.*

Abstract

Salt marshes are well known for their striking macrophyte zonation patterns. Although many variables affect species distribution, soil salinity and waterlogging have been shown to be two of the most important edaphic parameters. These variables are largely determined by the frequency and duration of tidal flooding, which is dependent on topographical variations. Light detection and ranging (LIDAR) can be used to generate digital elevation models (DEMs) from which elevation and landscape metrics can be derived with GIS, as an alternative to the collection of edaphic data in the field. The primary objective of this study was to classify four marsh vegetation classes (tall *Spartina alterniflora*, medium *S. alterniflora*/short *S. alterniflora*, marsh meadow and *Borrichia frutescens*/*J.roemerianus*) based on edaphic and remote sensing-derived variables in order to determine which combination of variables best describe plant distributions in a Southeastern salt marsh. Although multivariate statistical techniques such as linear discriminant analysis (LDA) are commonly used to classify and predict plant distributions based on edaphic and/or remote sensing-derived metrics, nonparametric classification and regression trees (CART) is being used increasingly as an alternative as it may better capture nonlinear and collinear relationships in environmental data sets. Our second objective was to compare the performance of LDA and CART for the classification of marsh vegetation. Models based on the edaphic variables soil organic matter content, water content, salinity and redox, attained accuracies of 0.63 and 0.72, with LDA and CART respectively. When the remote sensing variables DEM elevation, slope, distance to mean high water line and distance to upland area were used, classification accuracies improved to 0.78 for LDA and 0.79 for CART. The greatest

accuracies (0.82 for LDA and 0.83 for CART) were attained by combining soil organic matter content with the four remote sensing metrics in the combination models. Our results suggest that remote sensing-derived metrics can capture edaphic gradients effectively, which makes them especially suited to landscape level analyses of salt marsh plant habitats. Although the two classification techniques had similar overall accuracies, we recommend a workflow wherein CART is used for variable reduction and selection prior to training and subsequent prediction of new observations by LDA.

1. Introduction

Salt marsh macrophytes exhibit characteristic patterns of vertical zonation (Chapman, 1974; Sanchez et al., 1996; Silvestri et al., 2005). Zonation is usually described in terms of elevation relative to the tidal frame, and can be used to separate the marsh into low, mid and high marsh zones based on flooding frequency. In salt marshes along the coast of the Southeastern United States *Spartina alterniflora* is typically the dominant plant in the low marsh, with taller plants found closest to the water. *S. alterniflora* is also dominant in the mid-marsh zone, but can be replaced by marsh meadow or salt meadow species, *Salicornia virginica*, *Batis maritima* and *Distichlis spicata*, at higher elevations within this zone. In high marsh areas along the upland fringe, where the marsh is inundated only at the highest tides, *Juncus roemerianus* and *Borrichia frutescens* become the dominant species (Weigert and Freeman, 1990).

The relative importance of the processes that control plant zonation and the ability to predict salt marsh patterns have been the subject of intense study, especially in the context of sea level rise and climate change. Although biological interactions such as competition and facilitation can influence where particular plants are found (Pennings and Callaway, 1992; Pennings et al., 2005; Vince and Snow, 1984), salt marsh plant zonation has been largely attributed to two environmental gradients: soil salinity and flooding (Adam, 1990; Pennings and Bertness, 2001; Pennings et al., 2005). Elevated soil salinities affect regulation of internal solutes, metabolic functions and nutrient uptake by plants (Morris, 1984; Pennings and Bertness, 2001). Flooding or waterlogging results in anaerobic conditions and subsequent changes in soil chemistry, specifically lower soil redox potential and higher sulfide concentration (Adam, 1990; Delaune et al., 1987;

Pezeshki, 2001). Salt marsh plants have varying physiological tolerances for both salinity and flooding, with *S. alterniflora* generally better adapted to high salinities and prolonged inundation than most other plants, with the exception of high salt tolerant succulents such as *S. virginica* (Mendelssohn and Morris, 2000; Pennings et al., 2005).

Since patterns of tidal inundation are the result of location in the marsh and topographical variations, elevation and distance metrics have both been used as proxies for inundation frequency and duration (Adams, 1963; Deleeuw et al., 1991; Earle and Kershaw, 1989). Elevation is often correlated with soil salinity and flooding (Adam, 1990; Adams, 1963; Sanderson et al., 2001), as well as other edaphic parameters, including oxygen availability (Chapman, 1974; Patterson and Mendelssohn, 1991), soil redox potential (Delaune et al., 1983; Pezeshki, 2001), nutrient availability (Gallagher, 1975), organic matter content (Morris and Haskin, 1990) and sulfide concentration (Mendelssohn and Morris, 2000). The distance to mean high water (MHW) and other tidal elevations indicate position within the marsh and the direction of tidal flooding, and are similarly related to flooding and salinity gradients. Elevation and distance to MHW have been shown to be related to plant distribution (Earle and Kershaw, 1989; Silvestri et al., 2005; Zedler et al., 1999), productivity (Mendelssohn and Morris, 2000; Morris et al., 2002) and sedimentation rates (Marion et al., 2009; van Wijnen and Bakker, 2001) in salt marshes. Other landscape metrics, such as slope and distance to upland area (Andrew and Ustin, 2009; Griffin et al., 2011; Sellars and Jolls, 2007), have also been included in some analyses. Although simple correlations of elevation and/or distance metrics alone have been unable to fully explain zonation (Bockelmann et al., 2002; Silvestri et al., 2005; Zedler et al., 1999), many investigators have successfully used elevation in combination with edaphic variables to explain plant zonation (Byrd and Kelly, 2006; Lang et al., 2010; Suchrow and Jensen, 2010; Woerner and Hackney, 1997). However, no prior studies have examined the effectiveness of landscape variables such as elevation and distance metrics for predicting plant zonation in comparison to edaphic variables from the same study site.

A major advantage of using information on elevation and tidal inundation to predict plant distributions is that data can be collected synoptically at the landscape level via remote sensing. GIS and Light detection and ranging (LIDAR) can be used to generate digital elevation models (DEMs) from which elevation and landscape metrics can be derived. In one of the most successful applications of landscape metrics, Sanderson et al. (2001) quantified the influence of tidal channels (using a cumulative inverse squared distance function) by combining distance to channel and channel size to predict the probability of salt marsh species presence with 90% accuracy. However, it is not clear that this approach would work in other systems because the proportion of marsh cover correctly predicted was highly skewed by very high or low species coverage.

Regardless of which variables are included, analyses of plant distributions generally use multivariate statistical approaches such as canonical correspondence analysis (CCA). CCA has been extensively used to explain species composition by constructing linear combinations of multiple environmental variables that best separate vegetation along environmental gradients (Ter Braak, 1987). In Northwestern Atlantic and Mediterranean Sea salt marshes, CCA has been used to explain 23 to 95% of the variance in species composition based on salinity and soil moisture (Batriu et al., 2011; Cacador et al., 2007; Rogel et al., 2000; Rogel et al., 2001). In North Sea marshes, CCA axes related to salinity, soil moisture and elevation accounted for 94% of the plant community variance (Engels and Jensen, 2009; Suchrow and Jensen, 2010). Although CCA can be used to better understand species relationships along ecological gradients, the technique cannot classify vegetation type or predict group membership of new observations.

Two approaches commonly used to classify and predict plant distributions are discriminant analysis and logistic regression. Linear and quadratic discriminant analysis (LDA and QDA, respectively) use *a priori* knowledge of existing class membership to separate groups based on linear or quadratic combinations of predictor variables. Even though observations do not necessarily have a linear response along ecological gradients (Austin, 2007; Suchrow and Jensen, 2010), LDA has successfully explained and predicted vegetation zonation in Southwestern Atlantic marshes (Isacch et al., 2006; Sanchez et al., 1998) and Southeastern U.S. salt marshes (Woerner and Hackney, 1997), with classification accuracies ranging from 57-70%. When data do not meet LDA assumptions (namely multivariate normality and homogeneity of variances), binary logistic regressions have been used to determine species presence or absence as a function of multiple variables. Logistic regression models the probability of an outcome as a linear function of the predictor variables, and is similar to multiple linear regression but with a categorical, rather than continuous, dependent variable. Logistic regression has been used to predict salt marsh species presence/absence using elevation, edaphic data and landscape metrics with limited success (Moffett et al., 2010; Sellars and Jolls, 2007; Zedler et al., 1999).

Classification and regression trees (CART) is a nonparametric approach increasingly used as an alternative to discriminant analyses for the description and prediction of plant patterns using environmental data. Tree based classification methods are valuable data exploration tools that provide straightforward visualization of the data structure through binary classification (categorical) or regression (continuous) trees. CART has numerous advantages: data do not need to be normally distributed or transformed, homogeneity of covariances is not assumed, missing data and combinations of categorical and continuous variables are permitted, hierarchical and non-linear relationships are captured, as are interactions between explanatory variables, and the method is robust to outliers (Breiman et al., 1984; De'ath and Fabricius, 2000). In salt marshes, CART has been applied with accuracies that ranged from 54% to 90%. In California marshes, CART has been used for the differentiation of vegetation in relation to changes in upland sedimentation (Byrd and Kelly, 2006) and for modeling invasive species habitat near the marsh-upland border (Andrew and Ustin, 2009). CART has also been used to separate salt marsh vegetation in Australia using landscape position (Dale et al., 2007) and in the Lagoon of Venice using edaphic variables (Lang et al., 2010).

CART can be used as a tool to reduce the number of variables used to train a parametric classifier such as LDA (Breiman et al., 1984; De'ath, 2007; Maindonald and Braun, 2007); however, we were unable find any examples of this suggested workflow. Additionally, there are few comparative studies in which the two classification methods are applied to the same data set. Although the utility of CART has been compared to linear models in other ecosystems (De'ath and Fabricius, 2000; Guisan and Zimmermann, 2000; Pino-Mejias et al., 2010; Vayssieres et al., 2000), no assessment has been carried out for the classification of salt marsh vegetation using CART and LDA with the same data set.

The objectives of this study were: 1) To describe salt marsh plant distributions in terms of both field-collected edaphic variables and remote-sensing derived landscape metrics; 2) to compare classifications based on edaphic and remote sensing-derived variables, to determine which variable sets produce the most accurate classifications and to address the question of whether remote sensing data can be effective predictors of plant distribution; and 3) to compare discriminant analysis and CART to determine which classification technique best predicts salt marsh plant distributions.

2. Methods

2.2. Study Site

This study was located in the salt marshes in and around Sapelo and Blackbeard Islands, Georgia, USA (UTM Zone 17 N, 471480 E 3473972 N, Figure 4.1). The study area included 23 km^2 of salt marshes. Tides are semi-diurnal with a mean tide range of 2.5 m at this location. *S. alterniflora* is the dominant macrophyte in these marshes, covering over 80% of the total area. *S. alterniflora* can grow up to 2 m tall and is the primary plant found along the regularly flooded creek banks in the low marsh. Medium height *S. alterniflora* (approximately 0.5-1.0 m) dominates the mid-marsh and shorter plants are found in the irregularly flooded high marsh. The high marsh contains a mixed marsh meadow community (*S. virginica*, *B. maritima*, *D. spicata* and short *S. alterniflora*). At the highest elevations, *J. roemerianus* and *B. frutescens* become the dominant species.

Data from both the Sapelo and Blackbeard Island marshes were combined in this portion of our study for multiple reasons. First, CART cannot accurately reveal the data structure of smaller data sets (De'ath, 2007; Moore et al., 1991). The combined data set, although still small, is of similar size to other studies that have successfully used CART (De'ath and Fabricius, 2000; Suchrow et al., 2012). Secondly, and related to sample size, the Blackbeard data were necessary to increase the sample size of plant classes with lower relative frequencies of occurrence (namely, *D. spicata*, *B. maritima*, *B. frutescens* and *J. roemerianus*). To be sure that site did not have an impact on our results, it was included in preliminary CART analyses. The resultant trees did not retain site, producing identical classifications to those without site as an input variable.

2.3. Field Variables

Plant characteristics and edaphic variables were measured at 369 locations throughout the Duplin River (N = 217) and neighboring Blackbeard Island (N = 152) salt marshes in February 2010 for eight vegetation cover classes: *S. alterniflora* (short, medium and tall height classes), *J. roemerianus*, *B. maritima*, *D. spicata*, *S. virginica* and *B. frutescens*. For this study, *S. alterniflora* that was taller than 1 m was considered “tall”; *S. alterniflora* that ranged from 0.50 m to 1.0 m tall was considered “medium” and plants < 0.5 m were considered “short” (Reimold et al., 1973). The sampling locations were randomly selected using the ArcGIS 9.3 software program and a hyperspectral vegetation classification of the salt marshes. The number of RTK points sampled per cover class ranged from 10 (*D. spicata*) to 88 (medium *S. alterniflora*) (Table 4.S1).

At each sampling location, we measured the following plant parameters in 0.25 x 0.25 m quadrats: plant species presence, percent cover of each species, stem counts and height. Oxidation-reduction potential of the soil was measured by inserting a portable redox potential probe (Pt electrode, Ag-AgCl reference solution) into the soil to a depth of ~7 cm. We collected two 5-cm deep soil cores from each quadrat to measure soil porewater salinity, soil water content and soil organic matter content (SOM). The cores were taken back to the lab and processed following Pennings and Richards (1998). Samples were immediately weighed and then dried at 50° C for four days and reweighed to calculate water content. Dried soils were rehydrated with a known volume of deionized water, the salinity of the supernatant was measured and the porewater water salinity was determined by back-calculation. Cores for SOM content were dried at 50 degrees C for five days, weighed, placed in an ashing oven for 12 hours at 500 degrees C and then reweighed to determine the mass of organic matter lost on ignition.

2.4. Remote sensing data

2.4.1. LIDAR-derived DEM

The National Center for Airborne Laser Mapping (NCALM) acquired 35 km^2 of LIDAR data for Duplin River and Blackbeard Creek marshes on March 9 and 10, 2009 (Figure 4.1). Data were acquired when plant growth and biomass were seasonally low and during a spring low tide (-0.33 m) to maximize laser penetration of the vegetation canopy and minimize the amount of standing water on the marsh surface. Data were collected with an Optech GEMINI Airborne Laser Terrain Mapper (ALTM) mounted in a twin-engine Cessna Skymaster flown at an altitude of 800 m above ground level. The survey was conducted with a laser pulse rate frequency of 125 kHz, up to 4 returns and a point density of 9 hits m^{-2}. Reported vertical and horizontal accuracies (root mean squared error) for the sensor are 0.05-0.10 m and 0.10-0.20 m, respectively. LIDAR processing routines are described in (Hladik and Alber, 2012).

A bare earth LIDAR-derived DEM was produced in SURFER Version 8 (Golden Software, http://www.goldensoftware.com) at 1.0 x 1.0 m resolution using a kriging algorithm that calculated the mean elevation value of all laser hits within each grid cell with a maximum variance of 0.15 m. Elevations were all positioned in the NAD 83 reference frame and projected into UTM coordinate zone 17 N. DEM elevations are NAVD 88 orthometric heights (in meters) computed using the National Geodetic Survey GEOID 03.

2.4.2. Remote sensing variables

The LIDAR-derived DEM was used to generate the following metrics: DEM elevation in relation to mean high water (DEM-MHW), slope, distance to mean low water (MLW) contour, distance to mean sea level (MSL) contour, distance to MHW contour and distance to upland areas. In ArcGIS, DEM elevation and slope were extracted for the field survey sampling coordinates using the Spatial Analyst toolbox. ArcGIS was also used to contour the DEM at specified tidal datum heights (MLW, MSL and MHW). The contour values were determined based on data from the NOAA tide gauge station at St. Simon's Island (station ID 8677344). The same tide station was used to convert the DEM elevations from the NAVD 88 vertical datum to heights above or below MHW. Upland areas, which included back barrier islands, Sapelo Island and Blackbeard Island were digitized in ArcGIS to delineate upland boundaries. All distance metrics were calculated using the open source program R package Analysis of Moving Boundaries Using R (ambur) (Jackson, 2011), which uses a nearest distance algorithm to cast transects from each sampling location to each contoured tidal datum or the nearest upland area.

Elevation in relation to MHW is indicative of tidal flooding frequency and duration as well as salinity, and represents an important gradient in salt marshes that influences species zonation pattern (Morris et al., 2002; Silvestri et al., 2005) and sedimentation rates (Marion et al., 2009; van Wijnen and Bakker, 2001). Distance to MLW contour approximates the boundaries of the Duplin River and larger creeks and, as such, also represents the marsh edge. Creeks are sources of sediment and nutrients, and they also aerate and flush soils leading to increased plant productivity (Mendelssohn and Morris, 2000; Zedler et al., 1999). MSL contour represents the average tidal height and is again a proxy for flooding and salinity. MHW contour is the boundary demarcating the marsh platform and has a strong relationship with flooding, salinity and sedimentation (Krone, 1985). Distance to the nearest upland represents gradients of groundwater (fresh water), sediment and nutrients, as well as elevation.

2.5. Classification

Classification models (CART and discriminant analysis) were both implemented using three groupings of the predictor variables to predict salt marsh vegetation cover class. The ‘edaphic’ grouping included SOM content, soil salinity, soil water content and redox potential. The ‘remote sensing’ variables consisted of DEM-MHW, slope, distance to MLW contour, MSL contour, MHW contour and distance to the nearest upland area. The final group, ‘combined variables,’ combined the edaphic and remote sensing variables to determine which combination of all possible predictors best discriminated amongst dominant salt marsh vegetation classes.

2.5.1. Class selection

We tested for differences between cover classes using one-way ANOVAs of each edaphic and remote sensing-derived predictor variable followed by Tukey's honest significance test. Classes that were not significantly different for the majority of the predictor variables were combined prior to classification. Statistical results for all analyses in this study were considered significant when p-value < 0.05. All statistical analyses were done using the open source program R version 2.14.1 (http://cran.r-project.org/). The mean values for all edaphic and remote sensing-derived landscape metrics for all eight vegetation classes are summarized in Table 4.S1 along with the results of the Tukey's tests. Based on those analyses, short and medium *S. alterniflora* were combined into a single class, *B. maritima*, *D. spicata* and *S. virginica* were also merged into one vegetation class identified as marsh meadow, as were *J. roemerianus* and *B. frutescens*. This resulted in four vegetation classes that were classified using both CART and discriminant analysis: tall *S. alterniflora* (ST), short and medium *S. alterniflora* (SS-SM), marsh meadow (MM), and *B. frutescens* and *J. roemerianus* (BF-JR).

2.5.2. Classification and regression trees (CART)

We used the R package rpart (Therneau and Atkinson, 2012) to implement classification trees using the dominant plant classes as the categorical grouping and the edaphic and remote sensing metrics as predictor variables. Rpart splits a data set into homogeneous subsets through the binary recursive partitioning of the data (Breiman et al., 1984). At each split, rpart performs stepwise variable selection to reduce the dimensionality of the data, ranking predictor variables based on a goodness-of-split criterion (the Gini diversity index) that rates the degree of homogeneity attained to find the best split in the data (Therneau and Atkinson, 2012; Venables and Ripley, 2002). Predictor variables that contribute little to the model have a low rank and are not used. The best split maximizes group homogeneity (and between group heterogeneity) while at the same time improving classification accuracy (De'ath and Fabricius, 2000). Splitting continues until all samples are classified or until additional splits no longer increase group homogeneity. The first split of the data is termed the root node, whereas terminal nodes represent the final classification result.

The general practice in producing a classification tree is to grow an overly large tree and then cut or prune it back using cross-validation estimates of error (Breiman et al., 1984; De'ath and Fabricius, 2000). Cross-validation, as carried out in rpart, uses 10-fold cross-validation to compute errors by spitting the data randomly into ten subsets, repeatedly using nine of these subsets to build (train) a tree and using the remaining group to validate the tree (Breiman et al., 1984). This is repeated until all subsets have been used (averaging error estimates for all subsets) for all possible tree sizes and has been found to be a robust estimate of error (Breiman et al., 1984; Ripley, 1996). The tree size with the minimum cross-validation error is selected and used for description and prediction. A drawback to recursive partitioning is that single trees can be unstable since they do not fit a smooth function to the data, making the tree especially sensitive to small changes in the predictor variables (Breiman et al., 1984).

Random forest is an alternative CART method to rpart that can produce more stable and accurate classifications and is robust against over-fitting (Breiman, 2001). Random forest was implemented using the R package randomForest (Liaw and Wiener, 2002). It was used here to ensure that rpart was producing a stable tree and that the important predictor variables were retained. In random forest, bootstrapping is used to construct 500 independent trees and the predictions are combined based on a majority vote (Breiman, 2001; Cutler et al., 2007). As opposed to rpart where all variables are tried at each split, random forest only uses a small subset of randomly selected variables at each split (Liaw and Wiener, 2002). Each tree is fully grown and the error is computed. Random forest provides a measure of variable importance by estimating how much prediction error decreases when each variable is removed from the tree (Breiman, 2001; Liaw and Wiener, 2002). Variable importance is calculated based on the contribution of all variables and, therefore, a variable does not have to be a primary splitter to have a high importance rank. Unlike rpart, random forest is an ensemble classifier and does not produce a single binary tree. The structure of individual trees can be examined but an average tree does not exist in random forest. The structure of selected random forest trees were compared to the final pruned tree generated using rpart as well as the cross-validation accuracy. Additionally, confusion matrices were used to examine individual class errors for both rpart and random forest.

2.5.3. Discriminant Analysis

Discriminant analysis, like CART, uses a Bayesian framework, generating posterior probabilities for each group based on the combination of all variables (Hastie et al., 2009; Venables and Ripley, 2002). A sample is assigned to the class with the largest posterior probability and discriminant functions are functions of the posterior probabilities. The discriminant functions can then be used to predict the class membership of new observations. LDA and QDA are parametric classifiers which assume that the data are multivariate normal and that the predictor variables are independent and not highly correlated. LDA assumes that groups have homogenous covariances, whereas QDA allows for unequal variance-covariance matrices by calculating the covariance matrix of each group based on quadratic functions. To meet these assumptions, the data were transformed to increase the normality and homogeneity of variance. Salinity and slope were logarithmically transformed and all distance metrics were square root transformed. LDA and QDA were carried out using the R package MASS (Venables and Ripley, 2002).

Variable selection is important for LDA and QDA, as high-order interactions and collinearity among explanatory variables can obscure the data structure. To minimize this, the variables identified as important using CART (rpart and random forest) were selected for input in LDA and QDA. Thus, not all edaphic and remote sensing variables were included in discriminant analyses. Predictor variable importance within each analysis was determined based on the scaled discriminant coefficients: the larger the standardized coefficient, the greater the contribution of the respective variable to the discrimination between groups. To determine if the vegetation groups had significantly different means for each discriminant function, ANOVAs followed by Tukey's honest significance tests were carried out.

Correlations between predictor variables and the discriminant functions indicate which predictor is most related to the discriminant function and were assessed using Spearman's rank correlation coefficient, rho. Similarly, class posterior probabilities were correlated with each predictor variable to determine the strength of association between the variables and each vegetation class based on Spearman's rank correlation coefficient, rho. As with rpart, accuracy was assessed through 10-fold cross-validation. Confusion matrices were used to examine individual class errors and performance.

2.5.4. Classification method comparison

Rpart, random forest, LDA and QDA were evaluated for the various predictor variable groupings (edaphic, remote sensing, combined variables) based on overall cross-validation accuracy and individual class errors from confusion matrices. Predictor variable importance was also compared for all statistical techniques. Note that rpart variable importance is based on random forest rank, as it was better able to quantify variable rank (Liaw and Wiener, 2002). For brevity, and as random forest and QDA performed similarly to rpart and LDA, respectively, only rpart and LDA are presented here. Results for random forest and QDA can be found in Tables 4.S2, 4.S3 and 4.S4.

3. Results

3.1. Survey data

The mean values for all edaphic and remote sensing-derived landscape metrics for the four vegetation classes evaluated here are summarized in Table 4.1. Our results for edaphic parameters are in the range of previously reported values for Georgia marshes (Pennings et al., 2005; Pennings et al., 2003; Weigert and Freeman, 1990). In general, the soils of the ST and SS-SM classes were characterized by higher water content and SOM content than those of BF-JR and MM. SS-SM soils were characterized by low redox potential (-51.6 mV) and MM soils by high salinity (53.6 PSU) compared to all other classes, as has been observed previously for both habitats (Weigert and Freeman, 1990).

The landscape metrics corresponded to the position of the various classes across the marsh landscape and are in agreement with previously reported spatial relationships (Adams, 1963; Hinde, 1954; Mckee and Patrick, 1988; Weigert and Freeman, 1990). The four classes spanned the marsh elevation gradient from ST (-0.13 m below MHW) to BF-JR (0.41 above MHW) and were each significantly different from each other based on Tukey's tests (Table 4.1), as previously reported by Hladik and Alber (2012). The SS-SM and ST classes were situated at low elevations in close proximity to MLW, MSL and MHW contours and far from upland areas, whereas MM and BF-JR were in close proximity to upland areas and were further from the MLW, MSL and MHW contours (Table 4.1). Note that class ST had the shortest mean distance to MHW line resulting from its proximity to creek bank levees, which are at an elevation equal to MHW. Thus, when the MHW elevation was contoured based on DEM values, both the upper extent of flooding nearest to upland areas and the creek bank levee that forms in close proximity to ST habitat were contoured. As such, ST distances to the MHW contour were less than those for the other plant classes (Table 4.1). The majority of the marsh surface was characterized by shallow slopes, although the ST habitat was associated with the most severe slopes (6.7 degrees) for these data.

3.2. Edaphic model

Rpart discriminated between the four salt marsh vegetation groups using all four edaphic predictor variables: SOM content, soil salinity, soil water content and redox potential (Figure 4.2A). The primary node split in the tree was based on the proportion of SOM content (Figure 4.2A) and can be interpreted as follows: if SOM content is less than 0.125 observations are then assessed as to whether or not their salinity is less than 29.5

PSU, whereas if SOM content is greater than 0.125, observations are evaluated based on redox potential. In this case, SOM content separated the low marsh (ST and SS-SM) from the high marsh (MM and BF-JR) plant classes. Breiman et al. (1984) stated that classification trees are optimized to choose the variable that splits the data into groups with maximum within group homogeneity. Variable masking can be detected by looking at surrogate or alternative splits and their association with the optimal split and by identifying splits with index values (indicating classification improvement) close to the optimal split. We examined the alternative splits for SOM content and found that water content was the variable that produced the next best split, with an index value close to that for SOM content (index value of 47 versus 53 for SOM content, data not shown). Thus, an alternative tree path could have had water content as the root node but with slightly less homogenous groupings.

Following the root node split, data were then assessed based on salinity and redox potential, with water content and SOM content constituting the final splits with eight terminal nodes. Random forest (not shown) also ranked SOM content as the variable with the greatest importance followed by water content, salinity and redox potential. The overall cross-validation accuracy was 0.72 for the pruned tree (Figure 4.2A, Table 4.2). Class errors ranged from 0.16 for SS-SM to 0.59 for ST (Table 4.2). The confusion matrix shows that 0.55 of ST observations were misclassified as SS-SM (Table 4.3). The next highest error was for BF-JR, with 0.21 misclassified as MM and 0.10 as ST (Tables 4.2 and 4.3).

When the four edaphic variables were evaluated with discriminant analysis, LDA scaled coefficients were in agreement with CART in the rank order of predictor variable importance (Table 4.4). The first linear discriminant function explained 80% of the between group variance, with an additional 15% explained by the second linear discriminant function (Table 4.4). The third discriminant function only explained an additional 5 to 9% of the variance for all models (edaphic, remote sensing and combined variables) and is not discussed further. A bi-plot of the individual scores for the first two discriminant functions in the edaphic variable analysis shows the separation of the vegetation classes (Figure 4.3A). The first discriminant function differentiated between all classes pairs (p-value < 0.001) except for of SS-SM and ST (p-value = 0.07, data not shown). Group means for the second discriminant function were significantly different (p-value < 0.001) between all groups except for BF-JR and ST (p-value = 0.08). The first discriminant function was positively correlated with water content and SOM content (Spearman's rho of 0.93 and 0.88, respectively) whereas the second function was negatively correlated with salinity (Spearman's rho of -0.81, Table 4.4). These variables were also important in predicting individual classes. All classes had their strongest correlations (either negative or positive) with SOM content and water content, with the exception of MM, which had a strong correlation with salinity, i.e. observations with a high probability of being classified as MM had high salinities (Table 4.5).

The overall cross-validation accuracy of the LDA classification was 0.63, which is lower than that obtained with rpart (Table 4.2). Model errors were again largest for ST and MM, with 0.69 of ST observations being misclassified as SS-SM and 0.41 of MM observations misclassified as either SS-SM (0.25) or BF-JR (0.16) (Tables 4.2 and 4.6).

3.3. Remote sensing model

The rpart classifications based on the remote sensing-derived predictor variables better discriminated between the salt marsh plants than the rpart classification with edaphic variables, with an overall cross-validation accuracy of 0.79 for the pruned trees (Table 4.2, Figure 4.2B). Of the remote sensing variables considered (DEM-MHW, slope, and distances to MLW contour, MSL contour, MHW contour and upland area), rpart retained only DEM-MHW, slope and distances to MHW contour and uplands, in order of decreasing importance, for classification. Distance to MHW contour formed the initial split in the data (Figure 4.2B). Secondary splits assessed observations based on DEM-MHW slope. Distance to upland area formed the tertiary split on both branches of the tree. The remote sensing tree contained six terminal nodes. Of particular note, there was only one pathway to ST class membership: distance to MHW contour less than 25.85 m and a slope greater than 4.4 degrees. Class error values ranged widely, from 0.37 (BF-JR) to 0.15 (SS-SM) (Table 4.2). Errors for BF-JR (0.37) were slightly greater than those based on edaphic variables (0.33) and resulted largely from misclassifications with MM (0.14) and SS-SM (0.17) (Table 4.3). ST class error was substantially reduced from 0.59 in the tree with only edaphic variables to 0.27 in this model, with the primary misclassification as SS-SM (0.25). Class accuracies for MM and SS-SM were also improved when only remote sensing-derived were used for class separation.

When the four remote sensing variables retained by rpart were evaluated with discriminant analysis, LDA scaled discriminate function coefficients showed that DEM-MHW and slope had the greatest contribution to class separation, in agreement with rpart (Table 4.4). The first discriminant function accounted for 71% of the between class variance and the second discriminant function explained an additional 20% of variance. The plot of the first two linear discriminant functions shows the relative positions of the vegetation classes (Figure 4.3B). The first discriminant function discriminated between all vegetation pairs (*p*-value < 0.001). All class pairings were also separable for the second linear function except SS-SM and MM and BF-JR and ST (*p*-value = 1 for both). The first discriminant function was correlated with DEM-MHW, distance to MHW and distance to upland area (-0.86, - 0.73 and 0.71, respectively), whereas slope loaded heavily on the second discriminant function (0.90, Table 4.4). Correlations between posterior probabilities and explanatory variables point to the importance of specific predictor variables in the model (Table 4.5). BF-JR and ST were correlated with DEM-MHW but in opposing directions. MM had a strong positive correlation with distance to MHW contour, whereas ST was negatively correlated with distance to MHW contour (Table 4.5). In general, MM and SS-SM had correlations of moderate strength with the majority of variables.

Using the remote sensing-derived variables, LDA separated plant classes with an overall cross-validation accuracy of 0.78, which is equivalent to the rpart accuracy for these variables, and is again higher than that obtained in the edaphic model (Table 4.2). In the LDA analysis of the remote sensing variables, BF-JR observations were misclassified as MM and SM (0.21 and 0.13, respectively), whereas 0.18 of MM observations were misclassified as SM and 0.25 of ST observations as SS-SM (Table 4.6). LDA's greatest error reduction in comparison to rpart was for ST, where the proportion of observations misclassified decreased from 0.69 to 0.25 (Table 4.2).

3.4. Combined variables model

Marsh vegetation was most accurately classified by both rpart and LDA when the edaphic and remote sensing-derived variables were combined. The pruned rpart tree had an overall cross-validated accuracy of 0.83 (Table 4.2). Only five splitting variables were retained in the combined tree. In order of decreasing importance these were: slope, DEM-MHW, distance to MHW contour, SOM content and distance to upland (Figure 4.2C). SOM content formed the root node, splitting the data into low (ST and SS-SM) and high (MM and BF-JR) marsh branches. Secondary splits assessed observations based on DEM-MHW and slope (Figure 4.2C). Data were then assessed based on the distance to MHW contour and distance to upland areas, with seven terminal nodes. As in the remote sensing model, there is only one path to ST class membership in this tree, through assessments of SOM content and slope. Class errors were reduced or remained the same for ST, SS-SM and BF-JR when compared to the edaphic and remote sensing models, whereas that for MM was increased over the remote sensing model. Of note, SS-SM had a class error of only 0.07, whereas ST had the greatest error (0.27), due to persistent misclassification as SS-SM (0.25) (Tables 4.2 and 4.3).

When the variables retained by rpart were evaluated with LDA, SOM content was weighted the most heavily, followed by DEM-MHW. Slope, distance to MHW contour and distance to uplands all had lower scaled coefficients (Table 4.4). The first discriminant function explained 74% of the total variance and the second explained an additional 18% (Table 4.4). The bi-plot of the first two linear discriminant functions shows the separation of vegetation classes (Figure 4.3B). Tukey's pairwise comparisons between groups were consistent with the remote sensing model: The first discriminant function again discriminated between all vegetation pairs (*p*-value < 0.001), whereas class pairings were separable for the second linear function except SS-SM and MM (*p*-value = 1). The first discriminant function was correlated with DEM-MHW, SOM content and distance to uplands and MHW contour (0.82, - 0.75, - 0.70 and 0.67 respectively), whereas slope loaded heavily on the second discriminant function (0.91, Table 4.4). The positions of all classes along the first discriminant in the bi-plot are reversed in comparison to the remote sensing model as a result of the addition of SOM content; scores along the second discriminant remain unchanged (Figure 4.3C).

Predictor variable correlations with LDA class posterior probabilities were again similar to the remote sensing model and reinforced the bi-plot results (Table 4.5, Figure 4.3C). BF-JR and ST were correlated with DEM-MHW but in opposite directions (-0.82 and 0.82, respectively). BF-JR observations were negatively correlated with SOM content (-0.75), whereas SS-SM were positively correlated with SOM content (0.77). MM had a strong positive correlation with distance to MHW contour (0.66), whereas ST correlated with distance to MHW contour (-0.68) (Table 4.5). In general, MM and SS-SM had correlations of moderate strength with the majority of variables. Note that although slope was the most important predictor variable in rpart, its strongest LDA correlation was with MM (-0.59) (Table 4.5).

When all variables were combined, LDA had an overall cross-validation accuracy of 0.82, nearly the same as obtained using rpart, and LDA classification followed the same trends as rpart (Table 4.2). Class errors were reduced or remained the same for all classes when compared to the LDA edaphic and remote sensing models (Table 4.2). BF-JR and ST had the largest class errors (0.30 and 0.25, respectively), whereas SS-SM and

MM had class errors of 0.12 and 0.17, representing the lowest class errors for LDA in this study (Table 4.2). The majority of misclassifications were the result of BF-JR observations being misclassified as MM (0.24) and ST misclassified as SS-SM (0.25) (Table 4.6).

4. Discussion

These results gave us the opportunity to compare the use of remote sensing-derived versus edaphic variables for the classification of salt marsh vegetation, as well as the performance of rpart versus LDA. Both, rpart and LDA effectively classified salt marsh vegetation classes in this study. Depending on which variables were used, rpart overall cross-validation accuracies ranged from 0.72 to 0.83 (Table 4.2). LDA had a similar range, with accuracies ranging from 0.63 to 0.82. Although, greatest accuracies were attained by combining SOM content with the remote sensing metrics in the combination model, remote sensing alone performed nearly as well (Table 4.2). As detailed below, these are some of the best classifications of salt marsh vegetation to date.

4.1. Rpart versus LDA classifiers

Rpart performed slightly better than LDA, with the exception of the edaphic model where differences were greater (Table 4.2). Both techniques were in general agreement on which predictor variables best discriminated between salt marsh classes, and classified vegetation types similarly (Tables 4.2, 4.3 and 4.6). In general, classification errors were the result of confusion between BF-JR and MM classes and between SS-SM and ST classes (Tables 4.3 and 4.6). As these two groups represent low and high marsh communities, they share similar edaphic conditions and distance metrics, making their separation difficult. Interestingly, rpart performed substantially better than

LDA when only edaphic variables were used for prediction. This may be because classification trees such as rpart are more suitable for environmental data sets where variables are often collinear and not independent (Table 4.S5) and thus fail to meet the assumptions of LDA. Of particular note, SOM content and water content were highly correlated (Spearman's rho = 0.80, Table 4.S5) and were strong drivers of the edaphic models generated by both rpart and LDA.

No prior studies have compared the performance of parametric classifiers such as LDA to classification trees but previous work indicates that CART tends to perform slightly better than LDA. Previous studies reported overall accuracies ranging from 57-68% using LDA (Fischer et al., 2000; Sanchez et al., 1998), and 50-90% when CART was used to classify observations (Andrew and Ustin, 2009; Byrd and Kelly, 2006; Dale et al., 2007; Lang et al., 2010). However, it is impossible to truly compare across models when different data sets were used.

In cases where both LDA and CART give similar results, the literature suggests that LDA should be favored as parametric methods have more power for describing algebraic relationships (Feldesman, 2002; Maindonald and Braun, 2007). Another approach for determining which analysis is appropriate is to run CART on a data set that combines the linear discriminant functions with the original predictor variables (Maindonald and Braun, 2007; Steinberg and Colla, 1997). If the linear discriminant functions are the primary splitting variables with high importance in the combined data set, LDA is more appropriate for the data; if the discriminant functions are not retained, CART may capture the data structure better and should be used. We did this for the edaphic, remote sensing and combined models and found that in each case the first two

LDA discriminant functions were the primary splitting variables in the rpart analysis, with the first function being the most important variable in each model. This suggests that, despite the fact that our data did not meet all of its assumptions, LDA is a robust and appropriate classifier for these data. Although LDA may be the classifier of choice, the classification trees were still valuable for selecting the subset of predictor variables that best separated the various groupings for LDA, and also for describing the structure of the data. Without variable reduction using rpart, LDA accuracies ranged from 0.63 to 0.75 (data not shown), due to the additional multivariate noise. Importantly, the robustness of LDA cannot be assessed without comparing it against the nonparametric alternative, rpart (Feldesman, 2002).

Based on the results of this study, we recommend a workflow in which classification trees are used for description and variable selection with subsequent classification and prediction of new classes using LDA. CART is useful for selecting data and the resultant classification trees are more readily interpreted than discriminant functions. However, the binary nature of rpart might make them less useful for making predictions due to limitations in tree structure, which classifies observations at each node based on values for one parameter. In the trees produced with both the remote sensing and the combined variables, for example, ST class membership is evaluated based primarily on slope (Figures 4.2B and 4.2C). This is not unreasonable as ST is typically found on creek banks with more severe slopes compared to the marsh platform. However, it prevents ST observations without a steep slope from being correctly identified as ST. This limitation might be problematic if one were interested in predicting ST distribution due to a change in sea level, for example, unless slopes were also allowed to change. In comparison, LDA separates groups using a linear combination of all variables rather than one variable at a time. Because of this, slope is not the only variable defining the ST class, and observations with shallower slopes would have a higher probability of being classified as ST in the LDA model.

4.2. Edaphic versus remote sensing predictor variables

4.2.1. Edaphic model

We found that rpart and LDA classified salt marsh vegetation with accuracies of 0.72 and 0.63, respectively, when using the edaphic variables SOM content, water content, salinity and redox potential (Table 4.2). Previous studies have found that salinity and soil moisture (flooding) are the most important predictor variables for explaining variance in plant zonation using CCA (Batriu et al., 2011; Cacador et al., 2007; Rogel et al., 2000; Rogel et al., 2001), LDA (Sanchez et al., 1998; Woerner and Hackney, 1997) and CART (Byrd and Kelly, 2006). Although most of these studies considered elevation in addition to edaphic variables, the highest accuracy for a study that considered edaphic variables alone was Sanchez et al. (1998), which used LDA to classify Spanish salt marshes based on salinity, water content and redox potential with an accuracy of 57%.

Our results suggest that SOM content is an important edaphic parameter for the prediction of salt marsh vegetation, with water content being a suitable alternate. SOM content formed the root node in the rpart model, which means it was the variable that best split the data into two homogenous groups (Figure 4.2A), and it also had the largest LDA scaled coefficient (Table 4.4). However, SOM was highly correlated with water content, which is more commonly measured. SOM is related to water content as prolonged flooding results in lower soil redox potential and anaerobic conditions, which lead to the incomplete degradation of SOM (Brinson et al., 1981). Additionally, soils typical of ST and SS-SM (high SOM) are composed of fine textured silts and clays that hold water well due to reduced interstitial space (Frey & Howard, 1969). The SOM content may have produced a better split in the data than water content because it does not vary with respect to changes in tidal inundation. In contrast, water content is highly dependent on tide stage and the time since the soil was last flooded and hence has a larger coefficient of variation (61% for water content compared to 6% for SOM content, data not shown), which would have added noise to the model. However, water content may be a more appropriate predictor since SOM is related to both grain size and organic detritus from vegetation, making it highly site-specific. Moreover, SOM content may be a result of water content rather than a true predictor of plant type. It would be interesting to further explore the utilization of SOM content as a potential substitute for water content in predictions of salt marsh plant distribution.

In the LDA results the first linear discriminant was correlated strongly with both SOM content and water content. BF-JR and SS-SM classes had the strongest correlations, with lower SOM content and water content for BF-JR and higher proportions for SS-SM (Table 4.1 and 4.5). These results are in agreement with previous characterizations of the respective habitats of BF-JR and SS-SM based on SOM content and water content (Bradley and Morris, 1990; Weigert and Freeman, 1990). ST followed the same trend as SS-SM although with weaker correlation coefficients (Table 4.5). MM was best correlated with the second linear discriminant function, with observations having a high probability of MM class membership when soil salinities are high (Table 4.5). This was again in agreement with the literature, as MM is generally found in close proximity to hypersaline salt pans and is known to have high salt tolerance (Pennings and Bertness, 2001).

4.2.2. Remote sensing-derived model

The models composed of only the remote-sensing derived variables were better able to describe and predict salt marsh plant patterns than the edaphic variables alone, with rpart and LDA accuracies of 0.79 and 0.78, respectively. Previous studies have used landscape metrics to explain variance in forbe panne species abundance (Griffin et al., 2011), predict dune vegetation based on DEM elevation and slope (Sellars and Jolls, 2007) and predict invasive plant habitat near the marsh-upland border using distance metrics (Andrew and Ustin, 2009). These previous studies, which attained accuracies ranging from 46-90%, did not focus on salt marshes or encompass landscape-scale zonation. In a Georgia salt marsh, in close proximity to our study site, Fischer et al. (2000) used LDA to predict the location of disturbed patches based on tidal creek morphology with an accuracy of 70%. Although they were able to link tidal creek characteristics to the location of disturbed patches, their goal was not to describe or predict marsh-wide plant distributions as in the present study.

Our rpart model identified DEM-MHW and slope as the two variables that made the largest contribution in classifying the vegetation types, followed by distance to MHW contour and distance to upland area (Table 4.2). Distance to MHW contour was the root node for the rpart classification tree with DEM-MHW a competing surrogate split (Figure 4.2B). Both of these variables are related to gradients in flooding and salinity, which affect species establishment and zonation patterns (Adam, 1990; Ranwell, 1972; Suchrow and Jensen, 2010) as well as sedimentation rates (Marion et al., 2009; van Wijnen and Bakker, 2001).

In the LDA model, the first linear discriminant function was negatively correlated with DEM-MHW and distance to MHW contour. Vegetation classes were separated along an elevation gradient from BF-JR in the high marsh (negative scores for the first function) to ST in the low marsh (positive function scores), with significantly different means for all classes (Figure 4.3B, Tables 4.4 and 4.5). Observations had a high probability of ST membership when the site was at a low elevation and a short distance from the MHW contour. Although it may be expected that ST would have greater distances to MHW based on its low position in the tidal prism, creek bank levees are positioned at the elevation of MHW as a result of marsh geomorphology and hydrology in Southeastern US marshes (Stumpf, 1983; Weigert and Freeman, 1990). BF-JR was characterized by sites with high elevations and in close proximity to an upland area (Table 4.1). MM had the strongest relationship with distance to MHW contour (0.70, Table 4.5), which is related to the extent of tidal flooding and high soil salinities (Pennings and Bertness, 2001). The second linear discriminant function was related to slope, with BF-JR and ST having high scores (steep slopes) and SS-SM and MM having low scores (shallow slopes). These results are all consistent with salt marsh morphology across the elevation gradient from low to high marsh.

Although the relative strengths of correlations in the two variable sets differed across classes the remote sensing-derived metrics were more effective predictors of vegetation type compared to edaphic variables no matter which classifier was used (Tables 4.2, 4.3 and 4.6). ST had much stronger correlations with the remote sensing predictor variables and lower class errors whereas SS-SM and MM had weaker correlations when compared to the edaphic model, but still had lower class errors (Tables 4.2 and 4.5). BF-JR was strongly correlated to both the edaphic and remote sensing variables, having similar class errors for all models.

No previous studies have explicitly compared the predictive value of edaphic versus landscape metrics for classifying salt marsh vegetation type as investigators tend to combine both categories of variables when they are all available. Based on our results, the success of the remote sensing only model reported here may be because the variables we used were suitable proxies for the edaphic variables and underlying processes, many of which are related to elevation and flooding patterns (Adams, 1963; Chapman, 1974; Morris and Haskin, 1990; Sanchez et al., 1998; Silvestri et al., 2005). For example, the two most important variables in the edaphic model, SOM content and water content, both vary with distance from shore due to gradients in elevation and flooding. These relationships may explain the effectiveness of the remote sensing-derived variables, which not only integrate known edaphic gradients but may also account for additional, unmeasured edaphic parameters insofar as they correlate with elevation and other distance metrics. An additional reason for the superior performance of the remote sensing over edaphic variables is the fact that redox potential, salinity and water content can all vary substantially temporally with tidal inundation (LaRiviere et al., 2004; Silvestri et al., 2005; Woerner and Hackney, 1997), whereas elevation and the position of creeks and uplands areas change on the order of decades to centuries (Adam, 1990; Frey and Basan, 1985). This makes the remote sensing metrics more temporally stable compared to edaphic variables.

4.2.3. Combination of all variables

When all predictor variables were combined to predict salt marsh vegetation class, accuracies were improved slightly over the remote sensing model, from 0.79 to 0.83 with rpart and from 0.78 to 0.82 for LDA (Table 4.2). The combined model was dominated by the remote sensing variables (DEM-MHW, slope, distance to MHW contour and uplands), with SOM content being the only edaphic variable retained. The rpart tree structure was similar to that produced with the remote sensing variables alone, with the addition of SOM content as the root node (Figure 4.2C). The LDA bi-plot of the combined model (Figure 4.3C) also represents similar gradients as those produced by in the LDA remote sensing model. Correlations with posterior probabilities were similar to the remote sensing model but with strong correlations with SOM content for BF-JR and SS-SM, which was similar to the edaphic model (see section 4.2.1, Table 4.5). Given that the accuracies of our remote sensing models were comparable to the combined models, our results suggest that measuring edaphic variables, with the possible exception of SOM content, are not necessary for plant classification.

Other studies using edaphic and landscape variables in combination to separate salt marsh vegetation have attained predictive accuracies that ranged from 50-79%, with only some overlap with the variables that emerged as important in our study. Using CART, (Byrd and Kelly, 2006) found that salinity and elevation were the most important variables for predicting salt and brackish marsh vegetation response to edaphic and topographic changes resulting from upland sedimentation in California, with accuracies that ranged from 55-68%. Australian salt marshes were classified using both edaphic and landscape metrics, again with CART, with 50% accuracy (Dale et al., 2007). In this case, distance to the nearest creek was the most important determinant of vegetation type. Moffett et al. (2010) used logistic regression to model zonation in a California salt marsh with elevation, salinity, and landscape metrics and found that, while *S. alterniflora* could be classified with 79% accuracy, other species did not have significant relationships with these variables. They concluded that each zone is characterized by different combinations of variables. In contrast, we attained vegetation class accuracies that ranged from 0.70 to 0.93 in the combined models, and found that the same variables could be used across all classes. Moreover, the variables that were most important in our models were slope, DEM-MHW, distance to MHW contour, SOM content and distance to upland area.

4.3. Model Applications

The high classification accuracies attained in this study demonstrate the effectiveness of our overall approach and workflow. The use of rpart for description and variable selection prior to classification by either rpart or LDA has been recommended, but to our knowledge has not been previously reported. We suggest that this is an efficient method for variable selection that could be broadly applied in vegetation analyses.

The models developed here successfully predicted plant distributions based on edaphic and remote sensing-derived landscape metrics that were related to gradients in elevation and flooding. These models should be applicable to other Southeastern US marshes, although they would need to be validated. However, we would caution against applying these models directly to other geographic regions. Our edaphic models may be restricted owing to the differences in the relative importance of edaphic variables in different geographic areas: Pennings et al. (2005) found that salinity is more important in Southeastern US marshes whereas flooding largely accounts for Northeastern marsh patterns. Our remote sensing model was developed for areas where levees form near creek banks, which are geomorphological features not found in all areas. This will influence the distance between ST and MHW contour. Finally, in salt marsh plant communities structured by competitive interactions, our model would be limited or would need to be modified to include competition (Pennings and Callaway, 1992; Pennings et al., 2005; Vince and Snow, 1984).

A potentially important application of these models would be to predict changes in future plant distributions due to sea level rise. The remote sensing model, in particular, could be nested into models that predict how landscape metrics may change in the future. Note, however, that this will require accurate predictions of how elevation will change with increased flooding, which will in turn affect remote sensing-derived variables, including DEM-MHW and distance to MHW contour. Such a model will need to account for sedimentation, biological feedbacks and change in slope with sea level rise (Fagherazzi et al., 2012; Morris et al., 2002). In particular, the rpart tree structure (Figures 4.2B and 4.2C) would be of limited use without the proper modeling of slope, as in its current configuration no observation with a shallow slope would be classified as ST. In contrast to rpart, LDA predicts class membership on the combined linear coefficients for each variable and may be better suited for sea level rise modeling.

5. Summary

This study presented the opportunity to assess the effectiveness of remote sensing-derived landscape metrics versus edaphic variables for the discrimination of vegetation classes. Moreover, we were able to examine the value of nonparametric classification trees in comparison to traditional LDA for salt marsh vegetation classification. Rpart and LDA achieved comparable accuracies, thus the LDA model is recommended for the prediction of new observations. However, we recommend a workflow that uses rpart for variable reduction and selection prior to training by LDA. We found that the remote sensing-derived variables were more effective predictors of salt marsh plant distribution compared to edaphic variables, regardless of which classification technique was used. Although the addition of SOM content to the remote sensing variables generated the most accurate classifications, it resulted in only small improvements over the remote sensing models, suggesting that the remote sensing variables alone are adequate for classifying marsh vegetation. These results highlight the value of the remote sensing approach and show great promise for landscape level analyses of salt marsh plant habitats.

6. Acknowledgements

We thank Kristen Anstead, Nick Scoville and Jacob Shalack for all of their assistance with this project. The Sapelo Island National Estuarine Research Reserve and the University of Georgia Marine Institute also provided logistical support and laboratory space. This research was supported by the Georgia Coastal Ecosystems LTER Project (NSF Award OCE-0620959) and a National Estuarine Research Reserve System Graduate Research Fellowship (NOAA Award NA09NOS4200046).

7. References

Adam, P. (1990). *Saltmarsh ecology*. Cambridge, UK: Cambridge University Press.

Adams, D.A. (1963). Factors Influencing Vascular Plant Zonation in North-Carolina Salt Marshes. *Ecology, 44*, 445-456.

Andrew, M.E., & Ustin, S.L. (2009). Habitat suitability modelling of an invasive plant with advanced remote sensing data. *Diversity and Distributions, 15*, 627-640.

Austin, M. (2007). Species distribution models and ecological theory: A critical assessment and some possible new approaches. *Ecological Modelling, 200*, 1-19.

Batriu, E., Pino, J., Rovira, P., & Ninot, J.M. (2011). Environmental control of plant species abundance in a microtidal Mediterranean saltmarsh. *Applied Vegetation Science, 14*, 358-366.

Bockelmann, A.C., Bakker, J.P., Neuhaus, R., & Lage, J. (2002). The relation between vegetation zonation, elevation and inundation frequency in a Wadden Sea salt marsh. *Aquatic Botany, 73*, 211-221.

Bradley, P.M., & Morris, J.T. (1990). Influence of oxygen and sulfide concentration on nitrogen uptake kinetics on *Spartina alterniflora*. *Ecology, 71*, 282-287.

Breiman, L. (2001). Random forests. *Machine Learning, 45*, 5-32.

Breiman, L., Feidman, J., Olshen, R., & Stone, C. (1984). *Classification and Regression Trees*. Belmont, CA: Wadsworth, Inc.

Brinson, M.M., Lugo, A.E., & Brown, S. (1981). Primary Productivity, Decomposition and Consumer Activity in Fresh-Water Wetlands. *Annual Review of Ecology and Systematics, 12*, 123-161.

Byrd, K.B., & Kelly, M. (2006). Salt marsh vegetation response to edaphic and topographic changes from upland sedimentation in a pacific estuary. *Wetlands, 26*, 813-829.

Cacador, I., Tiberio, S., & Cabral, H.N. (2007). Species zonation in Corroios salt marsh in the Tagus esturary (Portugal) and its dynamics in the past fifty years. *Hydrobiologia, 587*, 205-211.

Chapman, V.J. (1974). *Salt marshes and salt deserts of the world*. Lehre, Germany: J. Cramer.

Cutler, D.R., Edwards, T.C., Beard, K.H., Cutler, A., & Hess, K.T. (2007). Random forests for classification in ecology. *Ecology, 88*, 2783-2792.

Dale, M.B., Dale, P.E.R., & Tan, P. (2007). Supervised clustering using decision trees and decision graphs: An ecological comparison. *Ecological Modelling, 204*, 70-78.

De'ath, G. (2007). Boosted trees for ecological modeling and prediction. *Ecology, 88*, 243-251.

De'ath, G., & Fabricius, K.E. (2000). Classification and regression trees: A powerful yet simple technique for ecological data analysis. *Ecology, 81*, 3178-3192.

Delaune, R.D., Pezeshki, S.R., & Patrick, W.H. (1987). Response of Coastal Plants to Increase in Submergence and Salinity. *Journal of Coastal Research, 3,* 535-546.

Delaune, R.D., Smith, C.J., & Patrick, W.H. (1983). Relationship of Marsh Elevation, Redox Potential, and Sulfide to Spartina-Alterniflora Productivity. *Soil Science Society of America Journal, 47*, 930-935.

Deleeuw, J., Vandendool, A., Demunck, W., Nieuwenhuize, J., & Beeftink, W.G. (1991). Factors Influencing the Soil-Salinity Regime Along an Intertidal Gradient. *Estuarine Coastal and Shelf Science, 32*, 87-97.

Earle, J.C., & Kershaw, K.A. (1989). Vegetation patterns in James Bay (Canada) coastal marshes: III. Salinity and elevation as factors influencing plant zonations. *Canadian journal of Botany, 67*, 2967-2974.

Engels, J.G., & Jensen, K. (2009). Patterns of wetland plant diversity along estuarine stress gradients of the Elbe (Germany) and Connecticut (USA) Rivers. *Plant Ecology & Diversity, 2*, 301-311.

Fagherazzi, S., Kirwan, M.L., Mudd, S.M., Guntenspergen, G.R., Temmerman, S., D'Alpaos, A., van de Koppel, J., Rybczyk, J.M., Reyes, E., Craft, C., & Clough, J. (2012). Numerical Models of Salt Marsh Evolution: Ecological, Geomorphic, and Climatic Factors. *Reviews of Geophysics, 50*, 1-28.

Feldesman, M.R. (2002). Classification trees as an alternative to linear discriminant analysis. *American Journal of Physical Anthropology, 119,* 257-275.

Fischer, J.M., Klug, J.L., Reed-Andersen, T., & Chalmers, A.G. (2000). Spatial pattern of localized disturbance along a southeastern salt marsh tidal creek. *Estuaries, 23,* 565-571.

Frey, R.W., & Basan, P.B. (1985). Coastal salt marshes. In R.A. Davis, Jr. (Ed.), *Coastal Sedimentary Environments* (pp. 225-301). New York: Springer.

Frey, R. W., & Howard, J.D. (1969). A profile of biogenic sedimentary structures in a Holocene barrier island-salt marsh complex, Georgia. *Transactions-Gulf Coast Association of Geological Societies*, 19:427-444.

Gallagher, J.L. (1975). Effects of an ammonium nitrate pulse on the growth and elemental composition of natural strands of *Spartina alterniflora* and *Juncus roemerianus*. *American Journal of Botany, 62*, 644-648.

Griffin, P.J., Theodose, T., & Dionne, M. (2011). Landscape Patterns of Forb Pannes Across a Northern New England Salt Marsh. *Wetlands, 31*, 25-33.

Guisan, A., & Zimmermann, N.E. (2000). Predictive habitat distribution models in ecology. *Ecological Modelling, 135*, 147-186.

Hastie, T., Tibshirani, R., Friedman, J.H., & SpringerLink (Online service) (2009). The elements of statistical learning data mining, inference, and prediction. In, *Springer series in statistics* (p. 745). New York: Springer.

Hinde, H.P. (1954). The Vertical Distribution of Salt Marsh Phanerogams in Relation to Tide Levels. *Ecological Monographs, 24*, 209-225.

Hladik, C., & Alber, M. (2012). Accuracy assessment and correction of a LIDAR-derived salt marsh digital elevation model. *Remote Sensing of Environment, 121*, 224-235.

Isacch, J.P., Costa, C.S.B., Rodriguez-Gallego, L., Conde, D., Escapa, M., Gagliardini, D.A., & Iribarne, O.O. (2006). Distribution of saltmarsh plant communities associated with environmental factors along a latitudinal gradient on the south-west Atlantic coast. *Journal of Biogeography, 33*, 888-900.

Jackson, C.J. (2011). ambur: Analyzing Moving Boundaries Using R. In

Krone, R.B. (1985). Simulation of marsh growth under rising sea levels. In W.R. Waldrop (Ed.), *Hydraulics and hydrology in the small computer age* (pp. 106–115). Reston, Virginia: Hydraulics Division, ASCE.

Lang, F., von der Lippe, M., Schimpel, S., Scozzafava-Jaeger, T., & Straub, W. (2010). Topsoil morphology indicates bio-effective redox conditions in Venice salt marshes. *Estuarine Coastal and Shelf Science, 87*, 11-20.

LaRiviere, D., Autenrieth, R.L., & Bonner, J.S. (2004). Redox dynamics of a tidally-influenced wetland on the San Jacinto River. *Estuaries, 27*, 253-264.

Liaw, A., & Wiener, M. (2002). Classification and Regression by randomForest. *R News, 2*, 18-22.

Maindonald, J.H., & Braun, J. (2007). *Data analysis and graphics using R : an example-based approach*. Cambridge ; New York: Cambridge University Press.

Marion, C., Anthony, E.J., & Trentesaux, A. (2009). Short-term (< = 2 yrs) estuarine mudflat and saltmarsh sedimentation: High-resolution data from ultrasonic altimetery, rod surface-elevation table, and filter traps. *Estuarine Coastal and Shelf Science, 83*, 475-484.

Mckee, K.L., & Patrick, W.H. (1988). The Relationship of Smooth Cordgrass (Spartina-Alterniflora) to Tidal Datums - a Review. *Estuaries, 11*, 143-151.

Mendelssohn, I.A., & Morris, J.T. (2000). Eco-physiological controls on the productivity of Spartina Alterniflora Loisel In D.A. Kreeger (Ed.), *Concepts and Controversies in Tidal Marsh Ecology* (pp. 59-80). Dordrecht Kluwer Academic.

Moffett, K.B., Robinson, D.A., & Gorelick, S.M. (2010). Relationship of Salt Marsh Vegetation Zonation to Spatial Patterns in Soil Moisture, Salinity, and Topography. *Ecosystems, 13*, 1287-1302.

Moore, D.M., Lees, B.G., & Davey, S.M. (1991). A New Method for Predicting Vegetation Distributions Using Decision Tree Analysis in a Geographic Information-System. *Environmental Management, 15*, 59-71.

Morris, J.T. (1984). Effects of Oxygen and Salinity on Ammonium Uptake by Spartina-Alterniflora Loisel and Spartina-Patens (Aiton) Muhl. *Journal of Experimental Marine Biology and Ecology, 78*, 87-98.

Morris, J.T., & Haskin, B. (1990). A 5-Yr Record of Aerial Primary Production and Stand Characteristics of Spartina-Alterniflora. *Ecology, 71*, 2209-2217.

Morris, J.T., Sundareshwar, P.V., Nietch, C.T., Kjerfve, B., & Cahoon, D.R. (2002). Responses of coastal wetlands to rising sea level. *Ecology, 83*, 2869-2877.

Patterson, C.S., & Mendelssohn, I.A. (1991). A Comparison of Physicochemical Variables across Plant Zones in a Mangal Salt-Marsh Community in Louisiana. *Wetlands, 11*, 139-161.

Pennings, S.C., & Bertness, M.D. (2001). Salt marsh communities. In M.D. Bertness, S.D. Gaines & M.E. Hay (Eds.), *Marine Community ecology* (p. 550). Sunderland, MA: Sinauer Associates, Inc.

Pennings, S.C., & Callaway, R.M. (1992). Salt-Marsh Plant Zonation - the Relative Importance of Competition and Physical Factors. *Ecology, 73*, 681-690.

Pennings, S.C., Grant, M.B., & Bertness, M.D. (2005). Plant zonation in low-latitude salt marshes: disentangling the roles of flooding, salinity and competition. *Journal of Ecology, 93*, 159-167.

Pennings, S.C., & Richards, C.L. (1998). Effects of wrack burial in salt-stressed habitats: Batis maritima in a southwest Atlantic salt marsh. *Ecography, 21*, 630-638.

Pennings, S.C., Selig, E.R., Houser, L.T., & Bertness, M.D. (2003). Geographic variation in positive and negative interactions among salt marsh plants. *Ecology, 84*, 1527-1538.

Pezeshki, S.R. (2001). Wetland plant responses to soil flooding. *Environmental and Experimental Botany, 46*, 299-312.

Pino-Mejias, R., Cubiles-de-la-Vega, M.D., Anaya-Romero, M., Pascual-Acosta, A., Jordan-Lopez, A., & Bellinfante-Crocci, N. (2010). Predicting the potential habitat of oaks with data mining models and the R system. *Environmental Modelling & Software, 25,* 826-836.

Ranwell, D.S. (1972). *Ecology of salt marshes and sand dunes*. London,: Chapman and Hall.

Reimold, R.J., Gallaghe.Jl, & Thompson, D.E. (1973). Remote Sensing of Tidal Marsh. *Photogrammetric Engineering and Remote Sensing, 39*, 477-488.

Ripley, B.D. (1996). *Pattern recognition and neural networks.* Cambridge, UK: Cambridge University Press.

Rogel, J.A., Ariza, F.A., & Silla, R.O. (2000). Soil salinity and moisture gradients and plant zonation in Mediterranean salt marshes of southeast Spain. *Wetlands, 20,* 357-372.

Rogel, J.A., Silla, R.O., & Ariza, F.A. (2001). Edaphic characterization and soil ionic composition influencing plant zonation in a semiarid Mediterranean salt marsh. *Geoderma, 99*, 81-98.

Sanchez, J.M., Izco, J., & Medrano, M. (1996). Relationships between vegetation zonation and altitude in a salt-marsh system in northwest Spain. *Journal of Vegetation Science, 7*, 695-702.

Sanchez, J.M., Otero, X.L., & Izco, J. (1998). Relationships between vegetation and environmental characteristics in a saltmarsh system on the coast of Northwest Spain. *Plant Ecology, 136*, 1-8.

Sanderson, E.W., Foin, T.C., & Ustin, S.L. (2001). A simple empirical model of salt marsh plant spatial distributions with respect to a tidal channel network. *Ecological Modelling, 139*, 293-307.

Sellars, J.D., & Jolls, C.L. (2007). Habitat modeling for Amaranthus pumilus: An application of light detection and ranging (LIDAR) data. *Journal of Coastal Research, 23,* 1193-1202.

Silvestri, S., Defina, A., & Marani, M. (2005). Tidal regime, salinity and salt marsh plant zonation. *Estuarine Coastal and Shelf Science, 62*, 119-130.

Steinberg, D., & Colla, P. (1997). *CART: tree-structured non-parametric data analysis*. San Diego: Salford Systems.

Stumpf, R.P. (1983). The Process of Sedimentation on the Surface of a Salt-Marsh. *Estuarine Coastal and Shelf Science, 17*, 495-508.

Suchrow, S., & Jensen, K. (2010). Plant Species Responses to an Elevational Gradient in German North Sea Salt Marshes. *Wetlands, 30*, 735-746.

Suchrow, S., Pohlmann, N., Stock, M., & Jensen, K. (2012). Long-term surface elevation changes in German North Sea salt marshes. *Estuarine, Coastal and Shelf Science, 98*, 71-83.

Ter Braak, C.J.F. (1987). The analysis of vegetation-environment relationships by canonical correspondence analysis. *Vegetatio, 69*, 69-77.

Therneau, M.T., & Atkinson, B. (2012). rpart: Recursive Partitioning. In

van Wijnen, H.J., & Bakker, J.P. (2001). Long-term surface elevation change in salt marshes: a prediction of marsh response to future sea-level rise.

Estuarine,Coastal and Shelf Science, 52, 381-390.

Vayssieres, M.P., Plant, R.E., & Allen-Diaz, B.H. (2000). Classification trees: An alternative non-parametric approach for predicting species distributions. *Journal of Vegetation Science, 11*, 679-694.

Venables, W.N., & Ripley, B.D. (2002). *Modern Applied Statistics with S*. New York: Springer.

Vince, S.W., & Snow, A.A. (1984). Plant Zonation in an Alaskan Salt-Marsh .1. Distribution, Abundance and Environmental-Factors. *Journal of Ecology, 72*, 651-667.

Weigert, R.G., & Freeman, B.J. (1990). Tidal Salt Marshes of the Southeast Atlantic Coast: a Community Profile In. Washington, DC: U.S. Department of the Interior, Fish and Wildlife Service.

Woerner, L.S., & Hackney, C.T. (1997). Distribution of Juncus roemerianus in North Carolina tidal marshes: The importance of physical and biotic variables. *Wetlands, 17*, 284-291.

Zedler, J.B., Callaway, J.C., Desmond, J.S., Vivian-Smith, G., Williams, G.D., Sullivan, G., Brewster, A.E., & Bradshaw, B.K. (1999). Californian salt-marsh vegetation: An improved model of spatial pattern. *Ecosystems, 2*, 19-35.

Table 4.1. Summary of mean values (± standard deviation) of predictor variables (water content, salinity, soil organic matter (SOM) content, redox, DEM elevation in relation to MHW (DEM-MHW), slope, distance to MHW contour and distance to uplands) for the four classes used in the current study. Superscripts indicate significant (p-value < 0.05) groupings based on Tukey's pairwise comparisons. All variables (edaphic and remote sensing) have the same sample size (N).

	Water Content (proportion)	Salinity (PSU)	SOM (proportion)	Redox (mV)	N
Edaphic variables					
Tall *S. alterniflora* (ST)	0.49 ± 0.05 ^{a}	33.9 ± 9.4 ^{a}	0.15 ± 0.02 ^{a}	74.2 ± 69.2 ^{a}	51
Short/Medium *S. alterniflora* (SS SM)	0.49 ± 0.08 ^{a}	39.3 ± 12.0 ^{a}	0.17 ± 0.05 ^{a}	-51.6 ± 152.0 ^{b}	166
Marsh Meadow (MM)	0.32 ± 0.12 ^{b}	53.6 ± 21.0 ^{b}	0.09 ± 0.05 ^{b}	47.3 ± 103.7 ^{c}	89
B. frutescens/*J. roemerianus* (BF JR)	0.23 ± 0.13 ^{c}	39.4 ± 18.4 ^{a}	0.05 ± 0.04 ^{c}	122.8 ± 53.8 ^{ac}	63

	DEM-MHW (m)	Slope (degrees)	MLW (m)	MSL (m)	MHW (m)	Uplands (m)
Remote sensing variables						
Tall *S. alterniflora* (ST)	-0.13 ± 0.19 ^{a}	6.7 ± 5.4 ^{a}	60 ± 120 ^{a}	5 ± 24 ^{a}	2 ± 2 ^{a}	297 ± 184 ^{a}
Short/Medium *S. alterniflora* (SS SM)	0.08 ± 0.14 ^{b}	1.6 ± 1.0 ^{b}	157 ± 136 ^{a}	98 ± 95 ^{b}	16 ± 20 ^{b}	289 ± 205 ^{a}
Marsh Meadow (MM)	0.2 ± 0.09 ^{c}	1.1 ± 0.6 ^{c}	264 ± 132 ^{b}	192 ± 105 ^{c}	58 ± 32 ^{c}	80 ± 70 ^{b}
B. frutescens/*J. roemerianus* (BF JR)	0.41 ± 0.19 ^{d}	3.3 ± 2.4 ^{d}	259 ± 140 ^{b}	157 ± 108 ^{c}	50 ± 47 ^{c}	71 ± 98 ^{b}

Table 4.2. Summary of rpart and LDA errors and overall cross-validation accuracy for all three models: edaphic, remote sensing and combined variables. Rpart values are for the pruned tree. In order of decreasing importance, the variables used in the edaphic model were soil organic matter (SOM) content, water content, salinity and redox. The variables used in the remote sensing model were DEM elevation in relation to MHW (DEM-MHW), slope, distance to MHW contour and distance to uplands. The variables used in the combined model were slope, DEM-MHW, distance to MHW contour, SOM and distance to upland area.

Species Class	Model Error	
	Rpart	LDA
Edaphic Model		
B. frutescens/*J. roemerianus*	0.33	0.37
Marsh Meadow	0.25	0.43
Short/Medium *S. alterniflora*	0.16	0.22
Tall *S. alterniflora*	0.59	0.69
Overall Accuracy	0.72	0.63
Remote Sensing Model		
B. frutescens/*J. roemerianus*	0.37	0.33
Marsh Meadow	0.19	0.21
Short/Medium *S. alterniflora*	0.15	0.18
Tall *S. alterniflora*	0.27	0.25
Overall Accuracy	0.79	0.78
Combined Model		
B. frutescens/*J. roemerianus*	0.22	0.30
Marsh Meadow	0.25	0.17
Short/Medium *S. alterniflora*	0.07	0.12
Tall *S. alterniflora*	0.27	0.25
Overall Accuracy	0.83	0.82

Table 4.3. Rpart confusion matrices for the edaphic, remote sensing and combined variables models based on pruned trees. Rows represent the reference data (what the observation actually was based on validation data) and rows represent the classified data (what the observation was classified as). Shaded cells are those where the classification was accurate and show the proportion of correctly classified observations for each class.

	B. frutescens/J. roemerianus (BF JR)	Marsh Meadow (MM)	Short/Medium *S. alterniflora* (SS SM)	Tall *S. alterniflora* (ST)	Total
Edaphic Model					
B. frutescens/J. roemerianus (BF JR)	**0.67**	0.21	0.03	0.10	1
Marsh Meadow (MM)	0.05	**0.75**	0.21	0.00	1
Short/Medium *S. alterniflora* (SS SM)	0.01	0.11	**0.84**	0.05	1
Tall *S. alterniflora* (ST)	0.02	0.02	0.55	**0.41**	1
Remote Sensing Model					
B. frutescens/J. roemerianus (BF JR)	**0.63**	0.14	0.17	0.05	1
Marsh Meadow (MM)	0.08	**0.81**	0.11	0.00	1
Short/Medium *S. alterniflora* (SS SM)	0.05	0.09	**0.85**	0.01	1
Tall *S. alterniflora* (ST)	0.02	0.00	0.25	**0.73**	1
Combined Model					
B. frutescens/J. roemerianus (BF JR)	**0.78**	0.11	0.08	0.03	1
Marsh Meadow (MM)	0.11	**0.75**	0.14	0.00	1
Short/Medium *S. alterniflora* (SS SM)	0.04	0.02	**0.93**	0.01	1
Tall *S. alterniflora* (ST)	0.02	0.00	0.25	**0.73**	1

Table 4.4. Linear discriminant function scalings and proportion of variance explained for linear discriminant one (LD 1), two (LD 2) and three (LD 3). Values in parentheses are Spearman's correlation coefficients, rho, for correlations between each linear discriminant function corresponding and predictor variables (water content, salinity, soil organic matter (SOM) content, redox, DEM elevation in relation to MHW (DEM-MHW), slope, distance to MHW contour and distance to uplands).

	LD 1	LD 2	LD 3
Edaphic Model			
Variance Explained	0.80	0.15	0.05
Water Content	7.02 (0.93)	2.03 (0.24)	8.73 (-0.01)
Salinity	0.9 (-0.17)	-2.47 (-0.81)	2.09 (0.49)
Redox	-0.001 (-0.6)	0.005 (0.37)	0.007 (0.51)
SOM	9.13 (0.88)	-0.54 (0.14)	-10.23 (-0.17)
Remote Sensing Model			
Variance Explained	0.71	0.20	0.09
DEM-MHW	-4.82 (-0.86)	1.47 (0.12)	-4.83 (-0.28)
Slope	0.29 (0.37)	1.25 (0.9)	0.21 (-0.06)
MHW	0.09 (-0.73)	-0.06 (-0.2)	-0.06 (0.56)
Uplands	-0.13 (0.71)	-0.03 (-0.17)	0.31 (-0.4)
Combined Model			
Variance Explained	0.74	0.18	0.07
SOM	-11.58 (-0.75)	-6.77 (-0.34)	-5.19 (-0.23)
DEM-MHW	4.03 (0.82)	-0.32 (-0.05)	-5.6 (-0.37)
Slope	-0.23 (-0.29)	1.2 (0.91)	-0.04 (-0.18)
MHW	0.11 (0.67)	-0.04 (-0.25)	0.27 (0.49)
Uplands	-0.08 (-0.7)	-0.03 (-0.08)	-0.03 (-0.28)

Table 4.5. Spearman's Correlation Coefficients, rho, for correlations between LDA class posterior probabilities and corresponding predictor variables (water content, salinity, soil organic matter (SOM) content, redox, DEM elevation in relation to MHW (DEM-MHW), slope, distance to MHW contour and distance to uplands) for the edaphic, remote sensing and combined variables models.

	WaterContent	Salinity	Redox	SOM	DEM-MHW	Slope	MHW	Uplands
Edaphic Model								
B. frutescens/*J. roemerianus*	-0.86	-0.02	0.58	-0.81	--	--	--	--
Marsh Meadow	-0.69	0.70	0.29	-0.63	--	--	--	--
Short/Medium *S. alterniflora*	0.84	-0.16	-0.72	0.86	--	--	--	--
Tall *S. alterniflora*	0.62	-0.38	0.11	0.49	--	--	--	--
Remote Sensing Model								
B. frutescens/*J. roemerianus*	--	--	--	--	0.85	0.00	0.47	-0.66
Marsh Meadow	--	--	--	--	0.46	-0.65	0.70	-0.59
Short/Medium *S. alterniflora*	--	--	--	--	-0.37	-0.20	-0.54	0.61
Tall *S. alterniflora*	--	--	--	--	-0.81	0.56	-0.69	0.54
Combined Model								
B. frutescens/J. roemerianus	--	--	--	-0.75	0.82	-0.04	0.49	-0.65
Marsh Meadow	--	--	--	-0.50	0.47	-0.59	0.66	-0.58
Short/Medium S. alterniflora	--	--	--	0.77	-0.39	-0.19	-0.49	0.58
Tall S. alterniflora	--	--	--	0.56	-0.82	0.53	-0.68	0.55

Table 4.6. LDA confusion matrices for the edaphic, remote sensing and combined models. Rows represent the reference data (what the observation actually was based on validation data) and rows represent the classified data (what the observation was classified as). Shaded cells are those where the classification was accurate and show the proportion of correctly classified observations for each class.

	B. frutescens/J. roemerianus (BF JR)	Marsh Meadow (MM)	Short/Medium *S. alterniflora* (SS SM)	Tall *S. alterniflora* (ST)	Total
Edaphic Model					
B. frutescens/J. roemerianus (BF JR)	**0.63**	0.22	0.05	0.10	1
Marsh Meadow (MM)	0.16	**0.57**	0.25	0.02	1
Short/Medium *S. alterniflora* (SS SM)	0.01	0.10	**0.78**	0.10	1
Tall *S. alterniflora* (ST)	0.00	0.00	0.69	**0.31**	1
Remote Sensing Model					
B. frutescens/J. roemerianus (BF JR)	**0.67**	0.21	0.13	0.00	1
Marsh Meadow (MM)	0.03	**0.79**	0.18	0.00	1
Short/Medium *S. alterniflora* (SS SM)	0.01	0.12	**0.82**	0.05	1
Tall *S. alterniflora* (ST)	0.00	0.00	0.25	**0.75**	1
Combined Model					
B. frutescens/J. roemerianus (BF JR)	**0.70**	0.24	0.06	0.00	1
Marsh Meadow (MM)	0.04	**0.83**	0.13	0.00	1
Short/Medium *S. alterniflora* (SS SM)	0.00	0.07	**0.88**	0.05	1
Tall *S. alterniflora* (ST)	0.00	0.00	0.25	**0.75**	1

Table 4.S1. Summary of mean values (± standard deviation) of predictor variables (water content, salinity, soil organic matter (SOM) content, redox, DEM elevation in relation to MHW (DEM-MHW), slope, distance to MHW contour and distance to uplands) for all eight vegetation classes. Superscripts indicate significant (p-value < 0.05) groupings based on Tukey's pairwise comparisons. All variables (edaphic and remote sensing) have the same sample size (N).

	Water Content	Salinity	SOM	Redox	N
Edaphic variables					
Tall *S. alterniflora*	0.48 ± 0.05^{a}	34 ± 9.4^{abd}	0.15 ± 0.02^{a}	85.2 ± 69.2^{ad}	51
Medium *S. alterniflora*	0.49 ± 0.08^{a}	35.6 ± 12.4^{abcd}	0.15 ± 0.04^{a}	54.4 ± 127.8^{bd}	88
Short *S. alterniflora*	0.5 ± 0.1^{a}	39.7 ± 10.9^{bcd}	0.16 ± 0.06^{a}	-139 ± 140.3^{c}	78
D. spicata	0.38 ± 0.11^{bc}	46.1 ± 16.1^{abcde}	0.08 ± 0.06^{bc}	40.35 ± 125.9^{abd}	10
S. virginica	0.29 ± 0.12^{bcd}	46.5 ± 22.2^{de}	0.09 ± 0.05^{b}	63.1 ± 87.1^{d}	62
B. maritima	0.24 ± 0.08^{cde}	63.7 ± 23.2^{de}	0.07 ± 0.03^{bc}	133.1 ± 49.1^{ad}	17
J. roemerianus	0.25 ± 0.16^{bcd}	29.7 ± 14.8^{abcd}	0.05 ± 0.04^{bc}	93.1 ± 51.9^{ad}	37
B. frutescens	0.17 ± 0.05^{ed}	40.5 ± 21.9^{abcd}	0.03 ± 0.04^{bc}	151.9 ± 43.9^{a}	26

	DEM-MHW	Slope	MLW	MSL	MHW	Uplands
Remote sensing variables						
Tall *S. alterniflora*	-0.11 ± 0.19^{a}	6.7 ± 5.4^{a}	60 ± 120^{a}	5 ± 24^{a}	2 ± 2^{a}	297 ± 184^{a}
Medium *S. alterniflora*	0.09 ± 0.15^{b}	1.9 ± 1.2^{b}	47 ± 128^{a}	21 ± 88^{b}	5 ± 7^{a}	260 ± 204^{a}
Short *S. alterniflora*	0.07 ± 0.12^{b}	1.1 ± 0.6^{bc}	260 ± 130^{b}	142 ± 93^{cd}	19 ± 25^{b}	153 ± 206^{a}
D. spicata	0.21 ± 0.08^{c}	0.9 ± 0.4^{c}	279 ± 160^{b}	210 ± 101^{cd}	65 ± 21^{c}	30 ± 52^{b}
S. virginica	0.21 ± 0.08^{c}	1 ± 0.6^{c}	290 ± 125^{b}	221 ± 105^{de}	75 ± 34^{c}	63 ± 62^{b}
B. maritima	0.26 ± 0.07^{c}	1 ± 0.6^{c}	207 ± 108^{b}	99 ± 90^{cde}	53 ± 22^{c}	43 ± 107^{b}
J. roemerianus	0.32 ± 0.21^{cd}	2.2 ± 2.2^{d}	282 ± 135^{b}	152 ± 92^{cde}	33 ± 38^{bc}	26 ± 34^{b}
B. frutescens	0.51 ± 0.14^{d}	4.1 ± 2.7^{d}	180 ± 132^{b}	115 ± 129^{cde}	36 ± 58^{c}	72 ± 133^{b}

Table 4.S2. Summary of rpart, random forest (RF), LDA and QDA errors and overall cross-validation accuracy for all three models: edaphic, remote sensing and combined. Rpart values are for the pruned tree. In order of decreasing importance, the variables used in the edaphic model were soil organic matter (SOM) content, water content, salinity and redox. The variables used in the remote sensing model were DEM-MHW, slope, distance to MHW contour and distance to uplands. The variables used in the combined model were slope, DEM-MHW, distance to MHW contour, SOM and distance to upland area.

Species Class	Model Error			
	Rpart	RF	LDA	QDA
Edaphic Model				
B. frutescens/*J. roemerianus*	0.33	0.24	0.37	0.30
Marsh Meadow	0.25	0.34	0.43	0.40
Short/Medium *S. alterniflora*	0.16	0.24	0.22	0.36
Tall *S. alterniflora*	0.59	0.53	0.69	0.31
Overall Accuracy	0.72	0.69	0.63	0.64
Remote Sensing Model				
B. frutescens/*J. roemerianus*	0.37	0.19	0.33	0.25
Marsh Meadow	0.19	0.22	0.21	0.20
Short/Medium *S. alterniflora*	0.15	0.17	0.18	0.20
Tall *S. alterniflora*	0.27	0.31	0.25	0.22
Overall Accuracy	0.79	0.79	0.78	0.79
Combined Model				
B. frutescens/*J. roemerianus*	0.22	0.25	0.30	0.27
Marsh Meadow	0.25	0.19	0.17	0.20
Short/Medium *S. alterniflora*	0.07	0.12	0.12	0.16
Tall *S. alterniflora*	0.27	0.29	0.25	0.16
Overall Accuracy	0.83	0.81	0.82	0.82

Table 4.S3. Random forest confusion matrices and class errors for the edaphic, remote sensing and combined models. Rows represent the reference data (what the observation actually was based on validation data) and rows represent the classified data (what the observation was classified as). Shaded cells are those where the classification was accurate and show the proportion of correctly classified observations for each class.

	B. frutescens/J. roemerianus (BF JR)	Marsh Meadow (MM)	Short/Medium *S. alterniflora* (SS SM)	Tall *S. alterniflora* (ST)	Total	Class Error
Edaphic Model						
B. frutescens/J. roemerianus (BF JR)	**0.76**	0.17	0.03	0.03	1	0.24
Marsh Meadow (MM)	0.12	**0.66**	0.23	0.00	1	0.34
Short/Medium *S. alterniflora* (SS SM)	0.01	0.13	**0.76**	0.10	1	0.24
Tall *S. alterniflora* (ST)	0.04	0.02	0.47	**0.47**	1	0.53
Remote Sensing Model						
B. frutescens/J. roemerianus (BF JR)	**0.81**	0.08	0.11	0.00	1	0.19
Marsh Meadow (MM)	0.06	**0.78**	0.16	0.00	1	0.22
Short/Medium *S. alterniflora* (SS SM)	0.05	0.08	**0.83**	0.04	1	0.17
Tall *S. alterniflora* (ST)	0.00	0.00	0.31	**0.69**	1	0.31
Combined Model						
B. frutescens/J. roemerianus (BF JR)	**0.75**	0.14	0.10	0.02	1	0.25
Marsh Meadow (MM)	0.07	**0.81**	0.12	0.00	1	0.19
Short/Medium *S. alterniflora* (SS SM)	0.02	0.06	**0.88**	0.05	1	0.12
Tall *S. alterniflora* (ST)	0.00	0.00	0.29	**0.71**	1	0.29

Table 4.S4. QDA confusion matrices and class errors for the edaphic, remote sensing and combined models. Rows represent the reference data (what the observation actually was based on validation data) and rows represent the classified data (what the observation was classified as). Shaded cells are those where the classification was accurate and show the proportion of correctly classified observations for each class.

	B. frutescens/J. roemerianus (BF JR)	Marsh Meadow (MM)	Short/Medium *S. alterniflora* (SS SM)	Tall *S. alterniflora* (ST)	Total	Class Error
Edaphic Model						
B. frutescens/J. roemerianus (BF JR)	**0.70**	0.24	0.03	0.03	1	0.30
Marsh Meadow (MM)	0.13	**0.60**	0.23	0.05	1	0.40
Short/Medium *S. alterniflora* (SS SM)	0.01	0.11	**0.64**	0.24	1	0.36
Tall *S. alterniflora* (ST)	0.00	0.00	0.31	**0.69**	1	0.31
Remote Sensing Model						
B. frutescens/J. roemerianus (BF JR)	**0.75**	0.13	0.13	0.00	1	0.25
Marsh Meadow (MM)	0.03	**0.80**	0.17	0.00	1	0.20
Short/Medium *S. alterniflora* (SS SM)	0.01	0.12	**0.80**	0.07	1	0.20
Tall *S. alterniflora* (ST)	0.00	0.00	0.22	**0.78**	1	0.22
Combined Model						
B. frutescens/J. roemerianus (BF JR)	**0.73**	0.19	0.08	0.00	1	0.27
Marsh Meadow (MM)	0.06	**0.80**	0.14	0.00	1	0.20
Short/Medium *S. alterniflora* (SS SM)	0.01	0.08	**0.84**	0.07	1	0.16
Tall *S. alterniflora* (ST)	0.00	0.00	0.16	**0.84**	1	0.16

Table 4.S5. Spearman's correlation coeffient, rho, for correlations between all predictor variable pairings. Variables included were water content, salinity, soil organic matter (SOM) content, redox potential, DEM elevation in relation to MHW (DEM-MHW), slope, distance to MHW, MLW and MSL contours and distance to uplands.

	Elevation	Water Content	Salinity	SOM	Redox	DEM-MHW	Slope	MHW	MLW	MSL	Uplands
Elevation	1	-0.61	0.23	-0.42	0.22	0.90	-0.35	0.56	0.29	0.42	-0.35
Water Content	-0.61	1	-0.44	0.80	-0.49	-0.60	0.03	-0.47	-0.19	-0.22	0.42
Salinity	0.23	-0.44	1	-0.27	0.15	0.12	-0.15	0.14	-0.05	-0.01	-0.13
OM	-0.42	0.80	-0.27	1	-0.42	-0.43	0.00	-0.38	-0.19	-0.18	0.39
Redox	0.22	-0.49	0.15	-0.42	1	0.31	0.26	0.12	-0.16	-0.15	-0.16
DEM-MHW	0.90	-0.60	0.12	-0.43	0.31	1	-0.21	0.49	0.18	0.30	-0.30
Slope	-0.35	0.03	-0.15	0.00	0.26	-0.21	1	-0.15	-0.25	-0.31	0.13
MHW	0.56	-0.47	0.14	-0.38	0.12	0.49	-0.15	1	0.47	0.63	-0.36
MLW	0.29	-0.19	-0.05	-0.19	-0.16	0.18	-0.25	0.47	1	0.84	-0.45
MSL	0.42	-0.22	-0.01	-0.18	-0.15	0.30	-0.31	0.63	0.84	1	-0.39
Uplands	-0.35	0.42	-0.13	0.39	-0.16	-0.30	0.13	-0.36	-0.45	-0.39	1

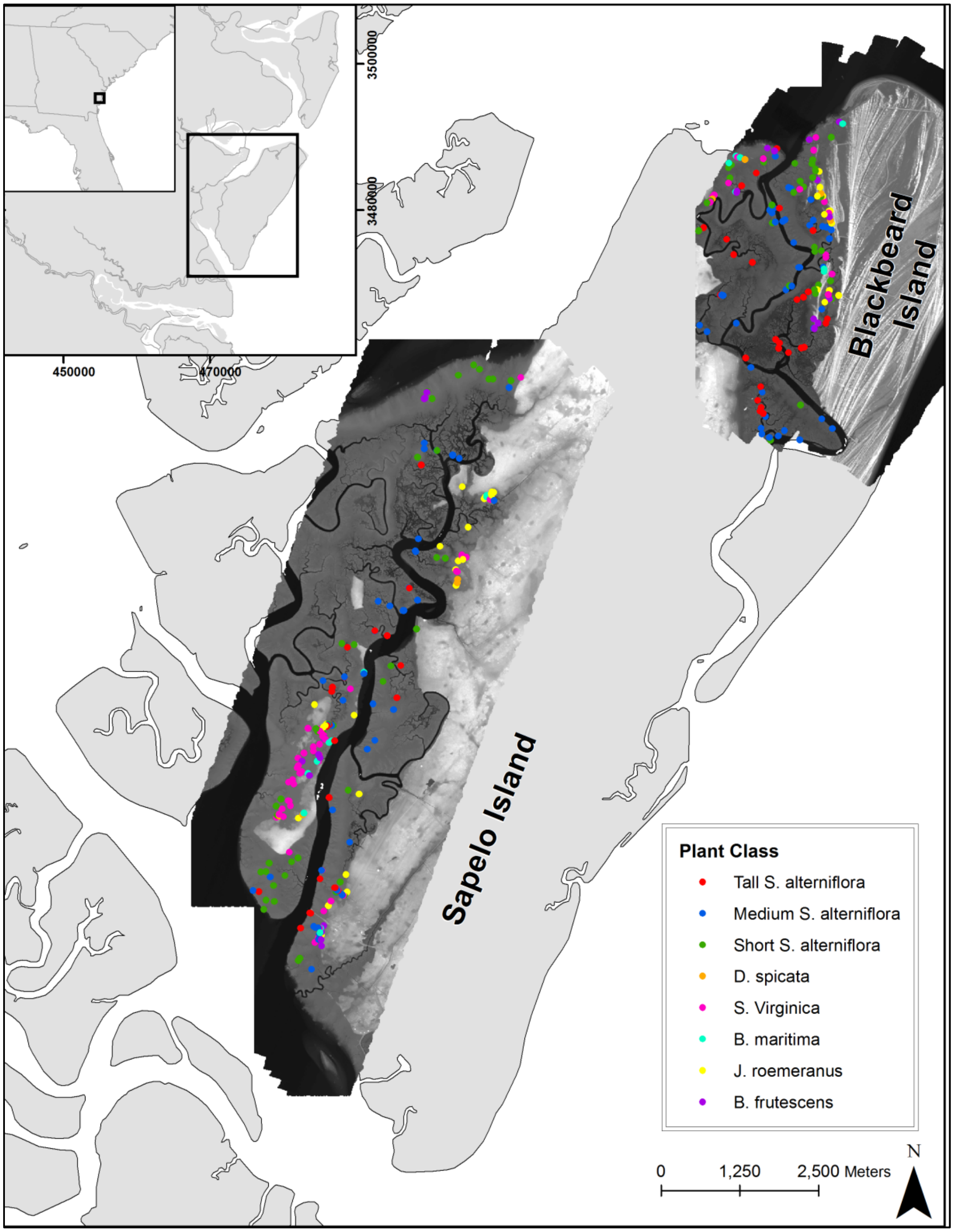

Figure 4.1. The LIDAR-derived bare earth DEM showing the location of the study area near Sapelo and Blackbeard Islands, GA. Dots indicate field sampling locations colored by dominant species.

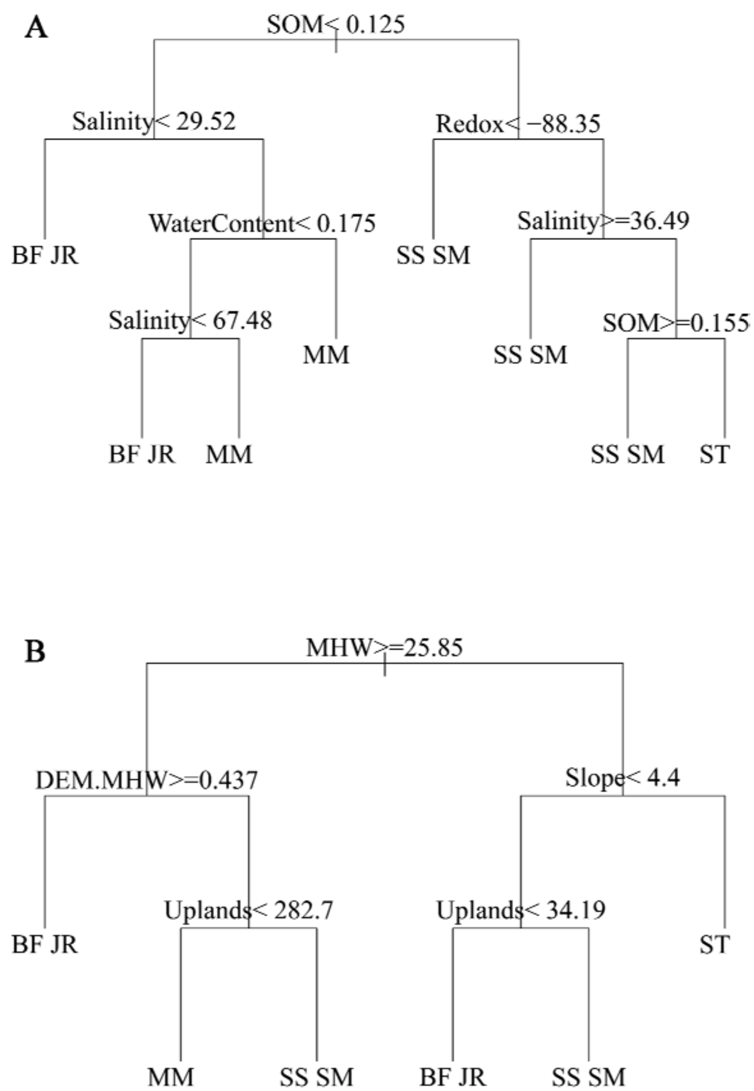

Figure 4.2. Rpart classification trees using the: (A) edaphic predictor variables (soil organic matter (SOM), water content, salinity and redox); (B) remote sensing-derived predictor variables (DEM elevation in relation to MHW (DEM-MHW), slope and distances to mean high water (MHW) and uplands); and (C) combination of all predictor variables. ST: tall *S. alterniflora*; SS-SM: short and medium *S. alterniflora*; MM: marsh meadow; and BF-JR: *B. frutescens* and *J. roemerianus*.

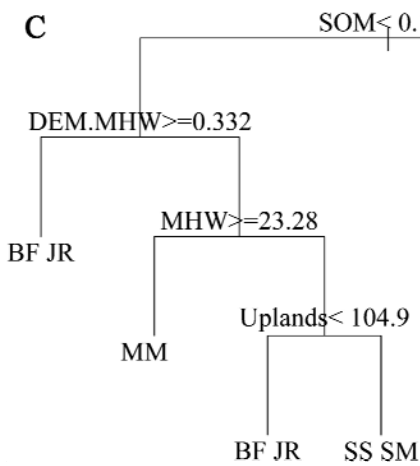

Figure 4.2 (continued).

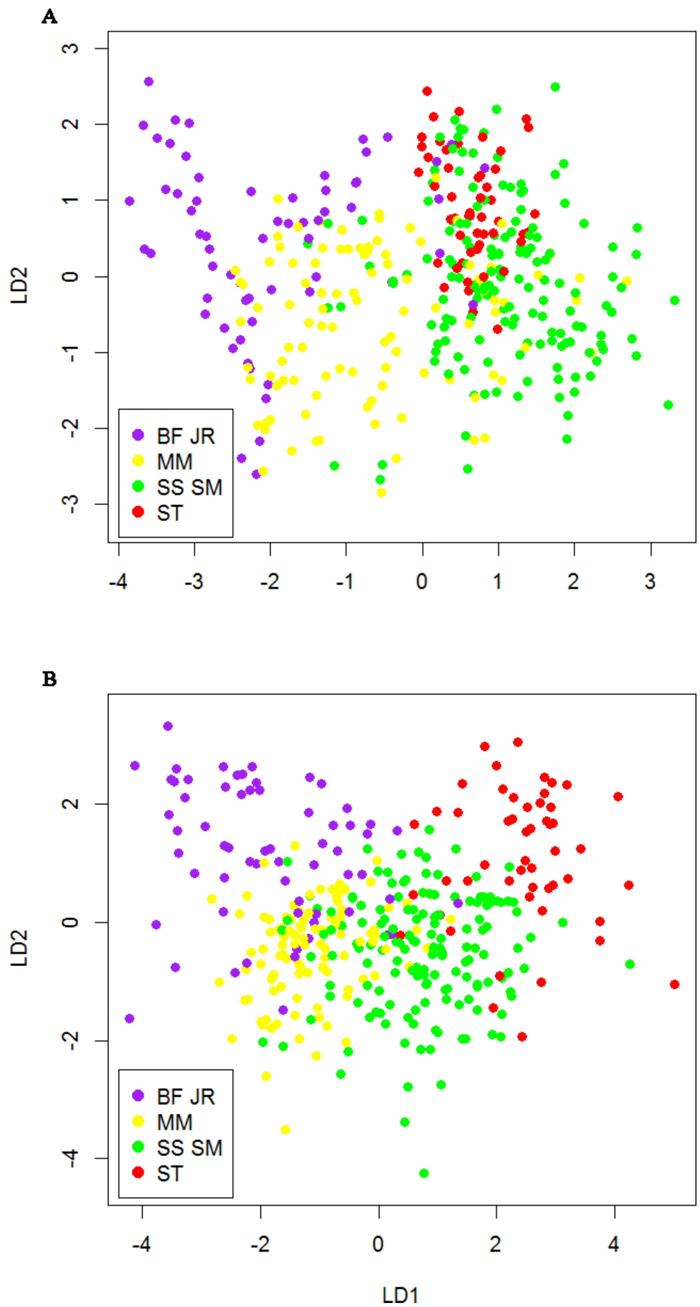

Figure 4.3. Biplots of linear discriminant function one (LD1) and two (LD2) for (A) edaphic predictor variables (soil organic matter (SOM), water content, salinity and redox); (B) remote sensing-derived predictor variables (DEM elevation in relation to MHW (DEM-MHW), slope and distances to mean high water (MHW) contour and uplands); and (C) combination of all predictor variables. Colors indicate LDA class assignments. ST: tall *S. alterniflora*; SS-SM: short and medium *S. alterniflora*; MM: marsh meadow; and BF-JR: *B. frutescens* and *J. roemerianus*.

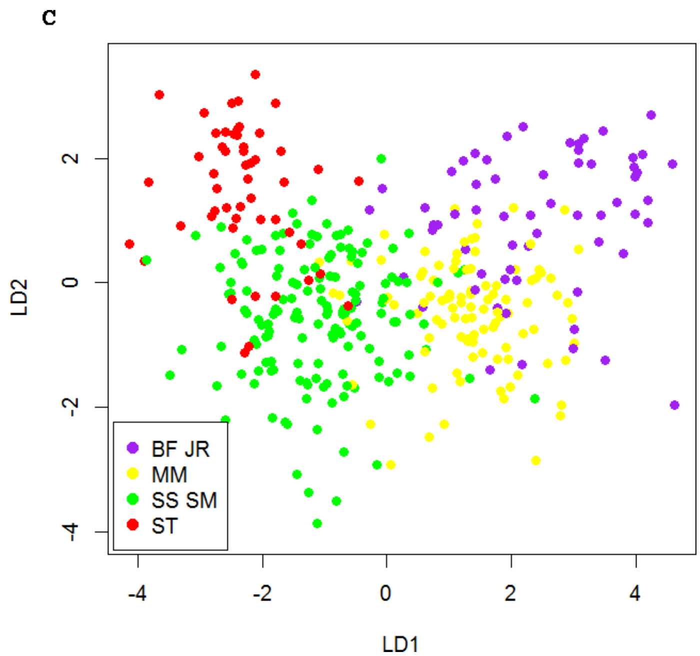

Figure 4.3 (continued).

Chapter 5

CONCLUSIONS

Accurate habitat and elevation mapping in salt marshes is important for management and conservation goals. Marshes are susceptible to habitat loss due to changes in sea level and coastal flooding, and there is growing interest in obtaining accurate elevation maps for these areas in order to understand how small topographic differences affect water flow, sediment distribution, and the extent and frequency of tidal inundation. Differences in elevation also affect plant distributions, as salt marsh macrophytes exhibit characteristic patterns of vertical zonation, with gradients in elevation influencing edaphic parameters. There is therefore a need for accurate habitat and elevation mapping in salt marshes to identify sensitive areas and predict how marshes will respond to perturbations such as sea level rise or changes in sediment delivery.

In this dissertation I evaluated the use of remote sensing data to map plant distributions and elevation in a Southeastern salt marsh by 1) assessing the accuracy of a digital elevation model (DEM) derived from Light Detection and Ranging (LIDAR) data for different vegetation classes; 2) fusing hyperspectral imagery (HSI) and a LIDAR-derived DEM to modify both habitat classification and elevation information; and 3) comparing the use of edaphic and remote sensing-derived variables for the prediction of salt marsh plants using linear discriminant analysis (LDA) and classification and regression trees (CART).

In Chapter 2, I found that high pulse rate frequency (PRF) LIDAR did not produce accurate DEMs of salt marsh habitats and is of limited utility without correction. DEM mean vertical errors for ten different cover classes ranged from 0.03 to 0.25 m in comparison to real time kinematic (RTK) GPS ground truth data. The magnitude of DEM error was greatest for taller vegetation; however, plant height could not fully explain errors and suggests that the relationship between DEM error and other vegetation characteristics, such as stem density, leaf orientation and biomass should be investigated. I used species-specific correction factors to modify the LIDAR-derived DEM in four areas of the study domain where vegetation boundaries were mapped directly in the field. Application of the derived correction factors greatly improved the accuracy of the LIDAR-derived DEM within these areas, reducing the overall mean DEM error from 0.10 ± 0.12 (SD) to -0.01 ± 0.09 m (SD), and the root mean squared error (RMSE) from 0.16 m to 0.10 m. In the corrected DEM, the ground elevations of all vegetation classes were no longer significantly different than the true RTK ground elevations.

My results suggest that these types of corrections are robust and can greatly improve the accuracy of DEMs obtained using high PRF LIDAR in salt marshes. However, more attention should be given to other LIDAR sensor parameters such as narrowing field of view and pulse width to better detect closely space returns, decreasing footprint size, or improving filtering routines to minimize misclassification of low vegetation as ground. It may also be possible to improve DEMs by using a different technique for the interpolation of LIDAR point clouds. In this study geostatistical kriging was used to generate a gridded DEM, but, it is possible that other interpolation techniques, such as the minimum bin method (deterministic), may produce a more accurate surface representation and this approach could be explored.

In order to apply the correction factors, it is necessary to have information on the distribution of cover classes in a LIDAR-derived DEM. HSI has been shown to be suitable for the separation of marsh vegetation species by spectral signatures, and can be used to determine cover classes; however, there is persistent confusion between the different height classes of *Spartina alterniflora* and mud due to mixed pixels. In Chapter 3, I compared maximum likelihood (MLC) and spectral angle mapper (SAM) classification methods for HSI, and presented a method to overcome the respective limitations of LIDAR and HSI through data fusion. MLC more accurately classified each of the nine cover classes in the HSI as compared to SAM, producing a habitat map of the Duplin River salt marshes with an overall accuracy of 90%, as compared to 61% when the SAM classifier was used. When the initial HSI classification was fused with the LIDAR data through a decision tree, I could apply class-specific elevation correction factors. This resulted in a large reduction in overall mean DEM error from 0.10 ± 0.12 (SD) to -0.003 ± 0.10 m (SD), and, in RMSE, from 0.15 to 0.10 m. The decision tree also resulted in slight improvements in plant classifications, with 1% and 2% increases in overall accuracy for MLC and SAM, respectively. These results suggest that the data fusion approach minimizes problems with both hyperspectral and LIDAR, and represents a significant advancement over evaluating hyperspectral and LIDAR data independently.

Future efforts should focus on acquiring ground survey data to better quantify the effect of data fusion on improving the classification of *S. alterniflora*. Although the decision tree did not greatly improve overall classification accuracies, it did produce small gains in separating the three height classes of *S. alterniflora* and mud. The majority of changes were seen in the upper part of the study area where tall and medium *S. alterniflora* are highly mixed with mud areas. Unfortunately, I did not have many ground control points in these areas due to the difficulty of assessing these low-lying parts of the marsh, so I was unable to quantify improvements in accuracy. Had validation data been available in these areas, I believe that the application of the decision tree would have resulted in larger gains in classification accuracy.

In Chapter 4, I evaluated the effectiveness of remote sensing-derived variables in comparison to edaphic parameters for the classification of salt marsh vegetation, using two different analytical approaches (LDA and CART). LDA and CART achieved comparable accuracies for all models. In cases such as this where both LDA and CART give similar results, the LDA approach is recommended for the prediction of new observations. However, I recommend a workflow that uses CART for variable reduction and selection prior to training by LDA. More importantly, I found that the remote sensing-derived variables were more effective predictors of salt marsh plant distribution compared to edaphic variables, regardless of which classification technique was used. Remote sensing models had accuracies of 0.78 and 0.79, whereas the edaphic models had accuracies of 0.63 and 0.72 for LDA and CART, respectively. The most important remote sensing variables were DEM elevation in relation to mean high water (DEM-MHW), slope and distance to mean high water line, whereas the most important edaphic variables were soil organic matter (SOM) and water content. Although the addition of SOM content to the remote sensing variables generated the most accurate classifications (0.82 and 0.83 for LDA and CART, respectively), these represented only small improvements over the remote sensing model, suggesting that remote sensing-derived variables alone are adequate for classifying marsh vegetation.

It should be noted that the remote sensing-derived variables used in Chapter 4 were generated using the unmodified DEM, as not all of the ground survey sites included in these analyses were located within the domain of the modified DEM produced for Chapter 3. This means that my models would be directly applicable to most situations where there is not enough information available to modify DEMs based on plant classification. Where plant classifications are available, then models describing current plant distributions become less useful. However, I did conduct LDA and CART analyses to develop models that used remote sensing variables derived from the modified DEM (Appendix B). These models could be used in conjunction with predicted changes in slope, elevation, and the other remote sensing variables to evaluate the response of marsh vegetation to sea level rise or other perturbations and is something that should be pursued in the future.

As a whole, this dissertation provides guidance on the use of remote sensing data for mapping salt marsh plant distributions and elevations. The analytical approaches and workflows developed here can be applied elsewhere to correct LIDAR-derived DEMs, classify vegetation based on elevation and HSI, and develop models for predicting vegetation distribution using landscape metrics. An important application of this work will be the use of remote sensing data to assess current plant zonation patterns, as well as to make landscape level predictions of how plant distributions will change in the future. Additionally, given that bathymetry is necessary to set up hydrodynamic models, a corrected DEM is important for accurate simulations of tidal flooding as well as for projecting the effects of storms and sea level rise. This work highlights the value of the remote sensing approach and shows great promise for landscape level analyses of salt marsh habitats.

APPENDIX A

RTK ELEVATIONS IN RELATION TO TIDAL DATUMS

Table A1. Real time kinematic (RTK) elevations in relation to various tidal datums for mean, minimum and maximum observed RTK elevations of each cover class. Shown are elevations relative to the North American Vertical Datum 1988 (NAVD 88), mean low water (MLW), mean sea level (MSL) and mean high water (MHW) tidal datums. Values were determined based on data from the NOAA tide gauge station at St. Simon's Island, Georgia (station ID 8677344) referenced on the 1983-2001 Epoch. The tide station was used to convert the RTK elevations from the NAVD 88 vertical datum to heights above or below MLW, MSL and MHW tidal datums.

Cover Class	NAVD 88	MLW	MSL	MHW
Mean Elevation				
Tall *S. alterniflora*	0.36	1.58	0.56	-0.44
Medium *S. alterniflora*	0.77	1.99	0.98	-0.02
Short *S. alterniflora*	0.87	2.09	1.07	0.07
Intertidal Mud	0.89	2.11	1.10	0.10
S. virginica	0.95	2.17	1.15	0.16
D. spicata	0.96	2.17	1.16	0.16
B. maritima	0.99	2.21	1.20	0.20
Salt pan	1.01	2.23	1.22	0.22
J. roemerianus	1.02	2.23	1.22	0.22
B. frutescens	1.23	2.44	1.43	0.43
Minimum Elevation				
Tall *S. alterniflora*	-0.67	0.55	-0.46	-1.46
Medium *S. alterniflora*	0.24	1.46	0.45	-0.55
Short *S. alterniflora*	0.59	1.81	0.79	-0.20
Intertidal Mud	0.52	1.74	0.73	-0.27
S. virginica	0.75	1.97	0.96	-0.04
D. spicata	0.78	2.00	0.98	-0.02
B. maritima	0.84	2.06	1.04	0.05
Salt pan	0.87	2.09	1.08	0.08
J. roemerianus	0.67	1.88	0.87	-0.13
B. frutescens	0.94	2.16	1.15	0.15

Table A1 (continued).

Cover Class	NAVD 88	MLW	MSL	MHW
<u>*Maximum Elevation*</u>				
Tall *S. alterniflora*	0.85	2.07	1.05	0.05
Medium *S. alterniflora*	1.09	2.31	1.30	0.30
Short *S. alterniflora*	1.14	2.35	1.34	0.34
Intertidal Mud	1.09	2.31	1.30	0.30
S. virginica	1.28	2.50	1.49	0.49
D. spicata	1.10	2.31	1.30	0.30
B. maritima	1.29	2.51	1.50	0.50
Salt pan	1.16	2.38	1.36	0.36
J. roemerianus	1.46	2.68	1.66	0.67
B. frutescens	1.49	2.71	1.70	0.70

APPENDIX B

MULTIVARIATE ANALYSES OF REMOTE SENSING-DERIVED VARIABLES USING MODIFIED DEM ELEVATIONS

In Chapter 4, we evaluated the effectiveness of remote sensing-derived variables in comparison to edaphic parameters for the classification of salt marsh vegetation using linear discriminant analysis (LDA) and classification and regression trees (CART). Although the two classification techniques had similar overall accuracies, we recommended a workflow wherein CART is used for variable reduction and selection prior to training and subsequent prediction of new observations by LDA. More importantly, in Chapter 4 we found that the remote sensing-derived variables were more effective predictors of salt marsh plant distribution compared to edaphic variables, regardless of which classification technique was used. When the remote sensing variables DEM elevation in relation to mean high water (DEM-MHW), slope, distance to mean high water (MHW) line and distance to upland area were used, classification accuracies were 0.78 for LDA and 0.79 for CART (Table 4.2).

The remote sensing-derived variables used for Chapter 4 analyses were generated using unmodified digital elevation models (DEMs) derived from Light Detection and Ranging (LIDAR) data for Sapelo Island and Blackbeard Island, GA (Figure 4.1). Not all the ground survey sites (where edaphic parameters were measured) included in those analyses were located within the domain of the modified DEM produced in Chapter 3 (Sapelo Island marshes, Figure 3.1). However, the results of Chapter 4 suggest that edaphic variables are not necessary for predicting plant distributions, which allows us to expand our analysis to include sampling locations where edaphic data was not available. More importantly, this allows us to examine the use of the modified DEM created in Chapter 3 for CART and LDA models.

In this Appendix, we evaluated the use of remote sensing variables derived from the modified DEM for the classification of a larger data set of plant observations for the Duplin River salt marshes. The sampling locations used here were the same as used in Chapters 2 and 3 and were collected as part of a survey of salt marsh ground control point (GCP) elevations carried out in 2009 to validate and correct the LIDAR-derived DEM (Tables 2.2 and 3.2). At each sampling location the plant species present were recorded and the ground elevation was surveyed using a real time kinematic (RTK) GPS receiver. Additional details can be found in Chapters 2 and 3. Note that only remote sensing-derived variables for these sampling locations (N = 1380) are used in the current analysis; edaphic variables were not measured at these locations.

The remote sensing variables were derived from the modified DEM following the same methods used in Chapter 4. However, for direct comparison of unmodified and modified DEM models, only those remote sensing variables identified as important in Chapter 4 are used here (Figure 4.2B). These included DEM-MHW, slope, and distances to MHW and upland area. The same four vegetation classes were classified using both CART (using rpart) and LDA: tall *S. alterniflora* (ST), short and medium *S. alterniflora* (SS-SM), marsh meadow (MM) and *B. frutescens*/*J. roemerianus* (BF-JR). Once variables were derived from the modified DEM, models were generated using rpart and LDA. We compared rpart and LDA results for the modified DEM to those obtained using the unmodified DEM in Chapter 4 to determine if corrected elevations affected models. Rpart results were examined based on tree structure and variable importance, whereas LDA results were evaluated based on scaled discriminant functions and discriminant function correlations with predictor variables. We also examined the cross-validated confusion matrices for both rpart and LDA to determine model accuracy.

The overall cross-validation accuracy for the rpart tree generated from the modified DEM was 0.79, the same as attained using the unmodified DEM (Table B1 and 4.2). However, there were differences in the tree structure of rpart models based on the modified versus unmodified DEMs (Figures B1 and 4.2B). The modified DEM root node was based on DEM-MHW as opposed to MHW in the unmodified DEM. Although DEM-MHW was still the most important variable, followed by slope, the model based on the modified DEM had a much larger contribution to class discrimination. Class errors using the modified DEM followed the same trend as in the unmodified DEM, but errors for MM and ST were reduced whereas BF-JR and SS-SM errors were larger in the modified DEM (Tables B1, B3, 4.2 and 4.3).

There were few differences in the LDA models produced using the modified as compared to the unmodified DEMs (Figures B2 and Figure 4.3B). However, the overall accuracy slightly decreased from 0.78 using the unmodified DEM to 0.76 for the modified DEM (Tables B1 and 4.2). Using the modified DEM the first discriminant function explained slightly more of the variance between vegetation classes than the unmodified DEM (75% versus 71%), but it was again strongly correlated with DEM-MHW (Tables B3 and 4.4). The second discriminant function explained an additional 20% of the variance and was correlated with slope, similar to results for the unmodified DEM. In the modified DEM, however, the second discriminant function was also strongly correlated with distance to uplands, contrary to the unmodified DEM results (Spearman's correlation coefficients of -0.7 and -0.17 in the modified and unmodified models, respectively) (Tables B3 and 4.4). Most notably, class errors were reduced for all classes when using the modified DEM with the exception of BF-JR for which errors increased from 0.33 to 0.51 (Tables B1 and 4.2). BF-JR errors were mostly due to larger misclassifications of BF-JR observations as SS-SM using the modified DEM (Table B3 and 4.6).

These results indicate that the use of the modified DEM did not greatly affect rpart and LDA classifications in comparison to the unmodified DEM (Chapter 4). In a comparison of the sampling points located used here that were also included in the Chapter 4 study, I found that neither the distance metrics nor the slope were significantly different in the unmodified versus the modified DEM (Wilcoxon rank sum test, p-value > 0.05, data not shown). DEM-MHW was the only remote sensing-derived variable that was significantly different in the two DEMs, which is to be expected based on the fact that the DEM required correction. We therefore believe the models presented in Chapter 4 are robust and could be used in situations where DEMs have not been modified. However, the CART and LDA models developed in this Appendix, which are based on the modified DEM, are the ones that would be most appropriate to use for predicting how plant distributions in the Duplin marshes might change under future conditions.

Table B1. Summary of rpart and LDA errors and overall cross-validation accuracy for the remote sensing models. Rpart values are for the pruned tree. In order of decreasing importance, the variables used in the remote sensing model were DEM-MHW, slope, distance to uplands and distance to MHW.

	Rpart	LDA
Remote Sensing Model		
B. frutescens/*J. roemerianus*	0.44	0.51
Marsh Meadow	0.12	0.25
Short/Medium *S. alterniflora*	0.20	0.13
Tall *S. alterniflora*	0.18	0.27
Overall Accuracy	0.79	0.76

Table B2. Rpart and LDA confusion matrices for the remote sensing models. Rows represent the reference data (what the observation actually was based on validation data) and rows represent the classified data (what the observation was classified as). Shaded cells are those where the classification was accurate and show the proportion of correctly classified observations for each class.

	B. frutescens/J. roemerianus (BF JR)	Marsh Meadow (MM)	Short/Medium *S. alterniflora* (SS SM)	Tall *S. alterniflora* (ST)	Total
Rpart					
B. frutescens/J. roemerianus (BF JR)	**0.56**	0.29	0.13	0.02	1
Marsh Meadow (MM)	0.05	**0.88**	0.06	0.01	1
Short/Medium *S. alterniflora* (SS SM)	0.02	0.11	**0.80**	0.07	1
Tall *S. alterniflora* (ST)	0.00	0.00	0.17	**0.82**	1
LDA					
B. frutescens/J. roemerianus (BF JR)	**0.49**	0.20	0.30	0.00	1
Marsh Meadow (MM)	0.05	**0.75**	0.20	0.00	1
Short/Medium *S. alterniflora* (SS SM)	0.01	0.08	**0.87**	0.04	1
Tall *S. alterniflora* (ST)	0.00	0.00	0.27	**0.73**	1

Table B3. Linear discriminant function scalings and proportion of variance explained for linear discriminant one (LD 1), two (LD 2) and three (LD 3). Values in parentheses are Spearman's correlation coefficients, rho, for correlations between each linear discriminant function corresponding predictor variables.

	LD 1	LD 2	LD 3
Remote Sensing Model			
Variance Explained	0.75	0.16	0.08
DEM-MHW	-4.18 (-0.90)	0.55 (0.15)	-3.51 (-0.10)
Slope	1.08 (0.52)	2.34 (0.7)	-0.82 (-0.3)
MHW	-0.06 (-0.59)	-0.05 (-0.16)	0.27 (0.73)
Uplands	-0.06 (0.68)	-0.09 (-0.70)	0.27 (-0.24)

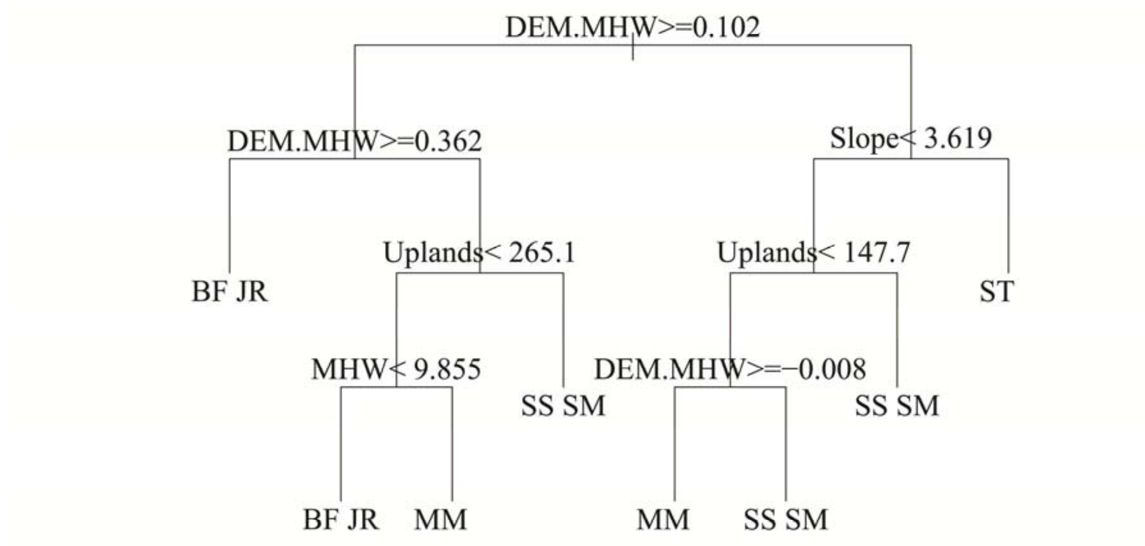

Figure B1. Rpart classification tree using the remote sensing-derived predictor variables (DEM elevation in relation to MHW (DEM-MHW), slope and distances to mean high water (MHW) and uplands) derived from the modified DEM. ST: tall *S. alterniflora*; SS-SM: short and medium *S. alterniflora*; MM: marsh meadow; and BF-JR: *B. frutescens* and *J. roemerianus*.

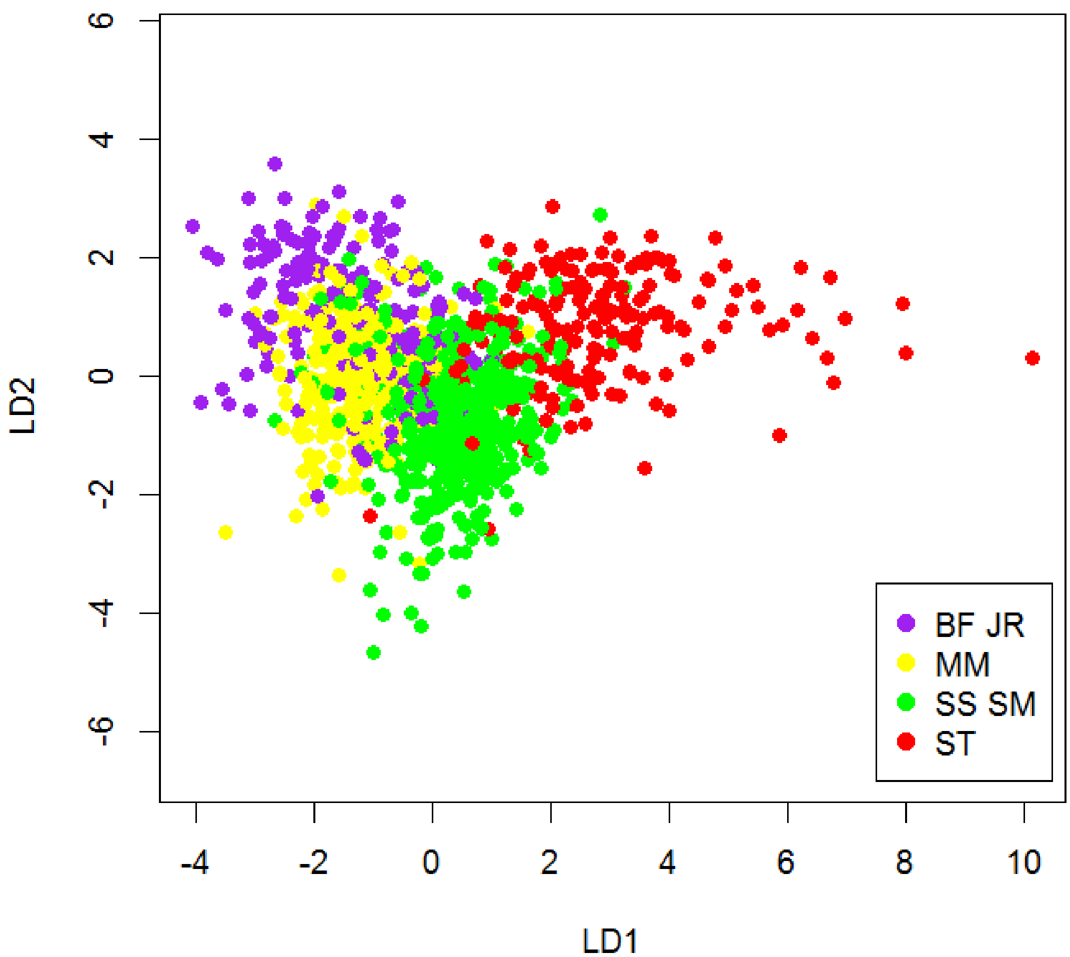

Figure B2. Biplot of linear discriminant function one (LD1) and two (LD2) for remote sensing-derived predictor variables (DEM elevation in relation to MHW (DEM-MHW), slope and distances to mean high water (MHW) and uplands) derived from the modified DEM. ST: tall *S. alterniflora*; SS-SM: short and medium *S. alterniflora*; MM: marsh meadow; and BF-JR: *B. frutescens* and *J. roemerianus*.